PREDICTION OF THE EFFECTS OF LOWER-EXTREMITY MUSCLE FORCES ON KNEE, THIGH, AND HIP INJURIES IN FRONTAL MOTOR VEHICLE CRASHES

by

Chia-Yuan Chang

A dissertation submitted in partial fulfillment
of the requirements for the degree of
Doctor of Philosophy
(Mechanical Engineering)
in The University of Michigan
2009

Doctoral Committee:

Professor Lawrence W. Schneider, Co-Chair
Professor Noboru Kikuchi, Co-Chair
Professor James A. Ashton-Miller
Associate Professor Richard E. Hughes
Assistant Research Professor Jonathan D. Rupp

DEDICATION

To the best mom and dad, for all your love and support

to make my dream come true.

ACKNOWLEDGEMENTS

I would like to gratefully thank Dr. Lawrence W. Schneider and Dr. Jonathan D. Rupp for giving me the opportunity to explore the research topic of this dissertation at the University of Michigan Transportation Research Institute (UMTRI), and to work with such a talented and special group of people in UMTRI's Biosciences Division. Their insight and advice has provided me with valuable guidance and direction for the past four years.

I would also like to thank my committee members, Professors Noboru Kikuchi, James Ashton-Miller, and Richard Hughes, for their input throughout all phases of this study. Their review and critique of this work has improved the value and application of the concepts and ideas presented in this dissertation.

The assistance of my colleagues in UMTRI's Biosciences Division are also gratefully acknowledged, particularly the contributions of Dr. Matthew P. Reed, Sheila Ebert, Laura Malik, Brian Eby, Nathaniel Madura, and Carl Miller.

My sincere thanks to Leda Ricci for her thorough review of this manuscript and for her encouragement during my study at UMTRI. I would also like to express special thanks to Stephanie Huang for her daily support and friendship.

The work reported in this dissertation was supported and made possible by the Doctoral Studies Program at the University of Michigan Transportation Research Institute (DSP-UMTRI) and The University of Michigan's Office of the Vice-President of Research (OVPR). This work was also funded by the National Highway Traffic Safety Administration under contract number DTNH-22-05-H-01020.

TABLE OF CONTENTS

LIST OF FIGURES

Figure

LIST OF TABLES

Table

LIST OF APPENDICES

ABSTRACT

Recent experimental and computational studies of knee-thigh-hip (KTH) tolerance and response to dynamic knee loading suggest that most AIS 2+ KTH injuries due to knee-bolster loading in frontal crashes should occur at the hip. This is in contrast to data from real-world frontal crashes in the Crash Injury Research Engineering Center (CIREN) and National Automotive Sampling System (NASS) databases, which indicate that approximately 40% of AIS 2+ KTH injuries from knee-bolster loading are to the thigh (i.e., the femoral shaft). One hypothesis for this difference is that muscle tension is often present in the lower extremities of vehicle occupants involved in frontal crashes due to braking and/or bracing, but was not present in the cadaver subjects used to characterize KTH tolerance and response. In particular, muscle tension is thought to alter the stress and strain distributions in the KTH complex produced during knee-impact loading by increasing the axial compressive forces in the KTH complex and by affecting the bending moments in the curved shaft of the femur. In addition, muscle tension may affect the force transmitted through the KTH by increasing the coupling of soft-tissue mass distal or proximal to the hip.

In this study, computational modeling was used to study the effects of muscle tension on KTH injury in frontal motor-vehicle crashes. Major tasks included: (1) developing a lower-extremity finite element model (LX FE Model) of a midsize male with realistic lower-extremity skeletal and muscle geometry, mass distribution, and material properties, (2) collecting surface electromyography (EMG) from lower-extremity muscles of midsize male subjects during experimentally simulated braking and bracing, (3) using the data from subject testing to tune and validate a commercial musculoskeletal model, (4) using the tuned and validated musculoskeletal model to estimate force activation levels in all lower-extremity muscles during braking/bracing, and (5) using the validated LX FE Model to simulate knee impacts with and without the

muscle forces predicted by the musculoskeletal model to estimate the effects of muscle forces on KTH injuries during knee-to-knee-bolster loading in frontal impacts.

The LX FE Model was developed by remeshing the MADYMO human finite element model to account for regional differences in cortical bone thickness and to incorporate articular cartilage, trabecular bone, and cortical bone with directionally dependent material properties and Tsai-Wu failure criteria. This resulted in improvements in the prediction of stress, strain, and bone fracture prediction over previous models. The LX FE Model also includes 35 Hill-type force-generating muscle elements that represent the individual muscles in each side of the lower extremities. Each of these muscle models includes mass in proportion to the muscle volume so that the model can predict the effects of muscle tension on changes in coupling of muscle mass distal and proximal to the hip joint.

The dynamic response of the LX FE Model without muscle tension was validated by simulating cadaver-segment biomechanical tests documented in the literature as well as tests in which seated cadavers were impacted using knee-loading conditions similar to those produced in frontal motor-vehicle crash testing. A parameter sensitivity study of the LX FE Model showed that cortical bone stresses and fracture prediction are sensitive to changes in cortical bone thickness. However, changes in bone stiffness and cortical bone thickness have relatively small effects on the forces produced by knee impacts or the forces transmitted from the knee to the hip. In addition, a model mesh-density sensitivity study showed that simulations constructed using a finer mesh size reduced force required to produce fracture.

A commercial three-dimensional musculoskeletal modeling system called the AnyBody Model was used to estimate the muscle forces produced by the muscles in the lower extremities during maximum braking/bracing. This model was validated by simulating tests in which 12 midsize male subjects performed simulated one-foot braking and two-foot bracing at 50% and 100% of maximum braking/bracing in a vehicle laboratory buck and compared measured muscle activations to predicted muscle activations. Results of these simulations indicated that the AnyBody Model is able to

reasonably predict agonistic muscle activations during isometric braking/bracing but is not able to predict antagonistic muscle activations.

Simulations of knee impacts using the validated LX FE Model with and without muscle forces predicted by the musculoskeletal model for maximal braking indicate that muscle tension increases knee impact forces by increasing the effective mass of the KTH complex due to tighter coupling of muscle mass to bone. Muscle tension was also found to preferentially couple mass distal to the hip and thereby increase the decrease in force between the knee and the hip. The magnitude of this increase of force decrease is such that force transmitted to the hip without muscle tension is similar to force transmitted to the hip with muscle tension despite the higher knee-impact forces with muscle tension. Simulation results also indicate that muscle tension has the potential to shift fracture location from the hip to the shaft of the femur by increasing bending moments in the femoral shaft. This explains why previous cadaver testing did not produce femoral shaft fracture and suggests that femoral shaft fractures in real-world frontal crashes may require muscle activation.

CHAPTER 1
INTRODUCTION

1.1 BACKGROUND

With increased seatbelt usage rates and the implementation of frontal-impact airbags in all vehicles, the likelihood of front-seat occupants sustaining AIS 2+ lower-extremity injuries is now greater than the likelihood of sustaining AIS 2+ injuries to any of the other Abbreviated Injury Scale (AIS) body regions (i.e., the head, the neck, and the chest; Kuppa and Fessahaie 2003). Many lower-extremity injuries, especially those involving the ankle and hip joints, are associated with a high potential for long-term disability and are therefore of substantial concern to clinicians, vehicle designers, and federal regulators. It has been estimated that the total annual cost of lower-extremity injuries from frontal crashes is over $7.5 billion, and that injuries to the knee-thigh-hip (KTH) complex account for approximately half of this cost (Kuppa and Fessahaie 2003).

Rupp et al. (2002) analyzed real-world frontal-crash data in the National Automotive Sampling System (NASS) database from calendar years 1995-2000 and found that the incidence of AIS 2+ hip injuries in frontal crashes is higher than the incidence of knee or thigh injuries. In particular, the NASS data indicate that approximately 30,000 occupants sustain AIS 2+ injuries to the KTH complex annually in frontal crashes, and that approximately 47% of these are to the hip. For this analysis, and for the remainder of this document, the knee, thigh, and hip are defined as illustrated in Figure 1-1, such that the knee includes the patella and femoral condyles, the thigh includes the supracondylar region, the shaft, and the subtrochanteric region of the femur, and the hip includes the femoral head and neck and acetabulim.

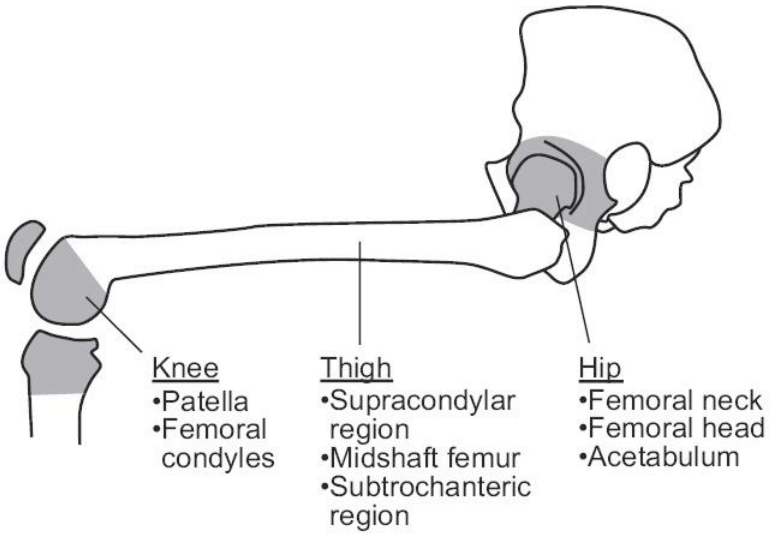

Figure 1-1. Illustration of anatomic components that comprise the knee, thigh, and hip (adapted from Rupp et al. 2002).

Figure 1-2 illustrates the loading scenario associated with knee, thigh, and hip injuries in frontal crashes. When a vehicle decelerates during contact between the front end of the vehicle and another vehicle or an object, such as a tree or pole, the vehicle occupants continue to move forward relative to the vehicle interior into vehicle restraint systems, such as seatbelts and airbags, and/or the vehicle interior. Contact between the knees of front-seat occupants and the energy-absorbing knee bolster applies force to the patella and femoral condyles. This force is transmitted along the shaft of the femur and into the femoral head where it is, in turn, transmitted to the posterior surface of the acetabulum of the pelvic bone (i.e., the socket of the hip joint). However, the force that is transmitted to the hip joint is lower than the force applied at the knees due to inertial factors (i.e., deceleration of mass between the knee and the hip). At any point in time during impact loading, this decrease in force is determined by the ratio of the effective (dynamic) mass distal to the hip to the total effective mass of the body to knee-impact loading (Rupp et al. 2008). Because much of the mass in the lower extremities is comprised of soft tissue, the coupling of this soft-tissue mass distal and proximal to the KTH complex can be expected to play an important role in the transmission of force between the knee and the hip. Since muscle tension in the lower extremities during

emergency braking or bracing is likely to affect the coupling of soft-tissue mass, the effects of muscle tension may affect the force transmitted while also increasing the compressive loads throughout the KTH complex (Rupp 2006).

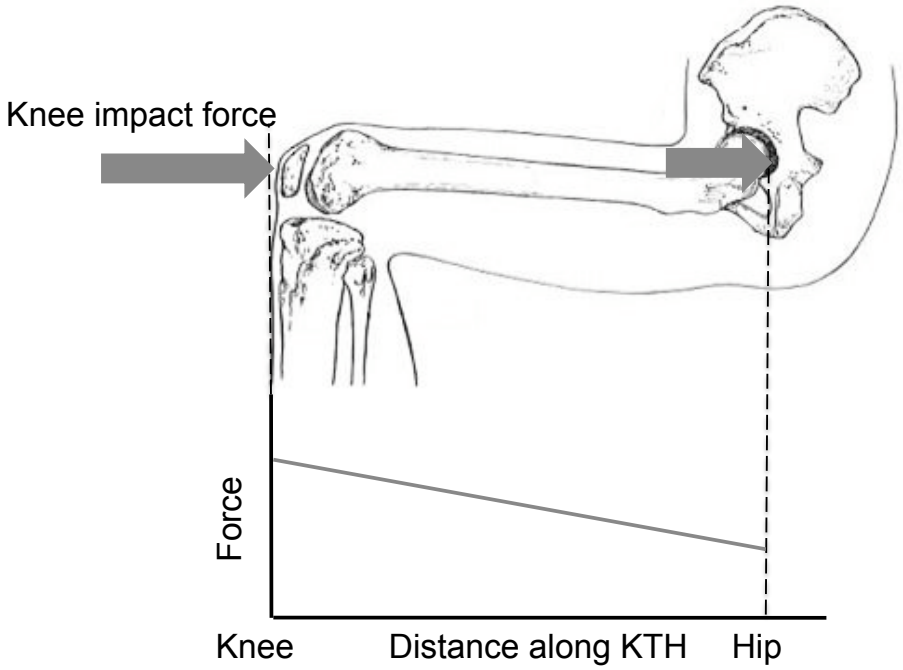

Figure 1-2. Illustration of KTH injury scenario and force decrease along the KTH in frontal motor-vehicle crashes.

Designing occupant restraint systems to reduce the risk of KTH injuries requires an understanding of the tolerance of the KTH complex to knee impact. Many biomechanical tests have been performed with cadavers to determine biomechanical responses and injury tolerances of the KTH in frontal knee impacts. The response and injury of the KTH complex due to loading of the anterior aspect of the flexed knee were studied extensively in the 1960s and 1970s (Patrick et al. 1965, 1967; Melvin et al. 1975, 1976, 1980; Powell et al. 1974, 1975). In these studies, tests were conducted by impacting the knees of whole cadavers with a rigid or lightly padded impactor, as well as by directing the knees of unrestrained whole cadavers into padded knee stops in sled impact tests.

To test the biofidelity of the Hybrid III KTH complex of the midsize-male Hybrid III Anthropomorphic Test Device (ATD)[1], or crash-test dummy, Donnelly and Roberts (1987) impacted the flexed knees of unembalmed cadavers and Hybrid III midsize-male ATD using a rigid flat-faced pendulum. Forces applied to cadaver and Hybrid III knees were measured and compared, as was the axial force near the mid shaft of the cadaver femur, which is similar to the location of the Hybrid III femur load cell. It was found that, on average, 53% of the peak force applied to the cadaver knees was transmitted to the mid shaft of the cadaver femur, compared to 68% of the peak force applied to the Hybrid III knee being transmitted to the Hybrid III femur. Also, because of the greater stiffness of the Hybrid III KTH complex, the Hybrid III produced peak knee-impact forces that were almost two times greater than those produced by similar sized cadavers under similar knee loading conditions.

The results of these early cadaver knee-impact tests conducted at high loading rates, along with the higher forces produced by the Hybrid III ATDs and the greater decrease in force between the knee and the middle of the femur, led to the adoption of a KTH injury criterion for the Hybrid III of 10 kN peak force measured at mid femur. In 1984, this force level was implemented in Federal Motor Vehicle Safety Standard 208 Occupant Crash Protection (FMVSS 208; NHTSA 2008), which states that the force at mid femur of a mid-size-male Hybrid III ATD shall not exceed 10 kN in a 13.4 m/s (48 kph) frontal impact of the vehicle into a rigid barrier.

However, the biomechanical tests performed in the 1960s through the 1980s used much higher knee-loading rates (between 2000 and 3000 N/ms) than those produced by knee-to-knee-bolster loading in frontal crashes of newer-model vehicles equipped with energy-absorbing knee bolsters. As stated by Rupp et al. (2002), the higher loading rates used in previous biomechanical studies resulted in fractures to the distal femur and knee before significant forces reached the hip due to laxity along the KTH complex. Specifically, data from knee impacts performed on seated whole cadavers with denuded

[1] The Hybrid III ATDs are the crash-test dummies used in federal motor vehicle safety standard frontal crash tests. There is a "family" of Hybrid III ATDs from a 3-year-old child to a large adult male. The midsize-male Hybrid III ATD represents a U.S. male who is about 175cm tall with a total body mass of about 77kg.

femurs by Viano and Stalnaker (1980) indicated that there is a 2-to-5 ms time lag between the application of force at the knee and the development of a reaction force at the hip due to laxity in the hip joint. In addition, because these early biomechanical tests used free-back conditions, KTH fracture forces were reported in terms of force applied to the knee and force at the hip was unknown.

For these reasons, Rupp et al. (2002) performed KTH tolerance tests using loading rates similar to those measured by the femur load cell of the Hybrid III midsize male ATD in FMVSS 208 compliance testing of late-model airbag/knee-bolster equipped vehicles, which are less than 300 N/ms. In these tests, force was applied in the direction of the long axis of the femur using a setup in which the pelvis was fixed to ensure that the force applied at the knee was the same as the force transmitted to the hip. In addition, the surface of the impactor was molded to fit the cadaver knee to reduce concentrated loads on the patella and reduce the likelihood of producing distal knee fractures. In contrast to earlier biomechanical tests, all of these fixed pelvis tests produced fractures of the posterior acetabulum (i.e., the hip-joint socket), with an average acetabular fracture force of 6.1 kN.

Rupp et al. also measured the fracture tolerance of the uninjured knee/femur specimens that were used in the fixed pelvis tests by removing the pelvic bone and supporting the femoral head in an "acetabular cup." All of these knee/femur tolerance tests produced femoral neck fractures, and the average fracture tolerance from these tests was 8.1 kN. When considered together, the injury patterns and fracture forces measured in the fixed pelvis and fixed femoral head tests demonstrate that the acetabulum is the weakest part of the KTH complex when impact forces are delivered to the anterior flexed knee, and that the femoral neck, which is also considered part of the hip joint, has the next lowest tolerance. Fracture forces from these tests were used to develop injury risk curves for the hip as a function of force applied to the hip (Rupp et al. 2008).

To apply these hip injury risk curves and the knee injury risk curves reported by Rupp and Flannagan (2009), it is necessary to know the relationships between force histories at specific locations in the KTH produced by knee impacts. Toward this end, Rupp et al. (2008) developed a one-dimensional mathematical spring-mass-damper

model of a cadaver based on a series of tests in which the knees of whole, seated midsize-male cadavers were symmetrically impacted using a high-mass padded impactor. To determine the contributions of different body components and soft-tissue mass coupling to knee-impact response, the knee impacts were also repeated after sequentially (1) cutting the thigh flesh, (2) removing the thigh flesh, and (3) removing the torso. From the simulations with this model, Rupp et al. reported that, for the majority of knee-bolster-like loading conditions that are capable of producing KTH injury, forces at the hip exceed the hip tolerance before force at the knee and distal femur exceed the knee and distal femur tolerance levels. The outputs of the model were also compared to the responses of the Hybrid III and THOR-NT ATDs with the goal of developing new injury assessment reference values (IARVs) for assessing KTH injury risk in staged crash tests with current frontal-impact crash dummies. These IARVs are based on quantities measured by instrumentation in ATDs that are associated with known probabilities of injuries in a similar sized human.

While the tolerance data and simulations by Rupp et al. represent a significant improvement in our understanding and ability to predict knee, thigh, and hip injuries, a primary limitation of model developed by Rupp et al. is that it is one dimensional and is therefore not able to simulate three-dimensional failure mechanisms, such as fracture of the femoral shaft in bending, which is a mode of femoral shaft fracture in many frontal impacts (Viano and Staknaker 1980). Also, this model does not account for the effects of coupling of soft-tissue mass to the skeletal components of the KTH on the force transmitted through the KTH due to muscle activation during braking and bracing by live occupants.

As described above, based strictly on the level of force required to cause a KTH fracture, the hip, including the acetabulum and the femoral neck, is the weakest part of the KTH complex (Rupp et al. 2002, 2003, and 2008). This finding explains the relatively high frequency of hip injuries to front-seat occupants in frontal crashes of airbag/knee-bolster-equipped vehicles in which lower knee loading rates allow transmission of significant force to the hip before the higher force tolerances at the knee and distal femur are exceeded. However, the fact that Rupp et al. (2002) always

produced a hip fracture in the fixed-pelvis and fixed-acetabular-cup KTH tolerance tests is in significant contrast to the relatively high frequencies of knee and thigh injuries observed in frontal crashes, as indicated by analyses of crash/injury databases. For example, Rupp (2006) analyzed the UM Crash Injury Research Engineering Center (CIREN) database for the distribution of AIS 2+ injuries to the knee, thigh, and hip in frontal crashes of airbag-equipped vehicles. As shown in Figure 1-3, although the hip is the most frequently injured part of the KTH complex, constituting about 45% of all KTH injuries, approximately 40% of KTH injuries are to the thigh and most of these injuries are to the shaft of the femur.

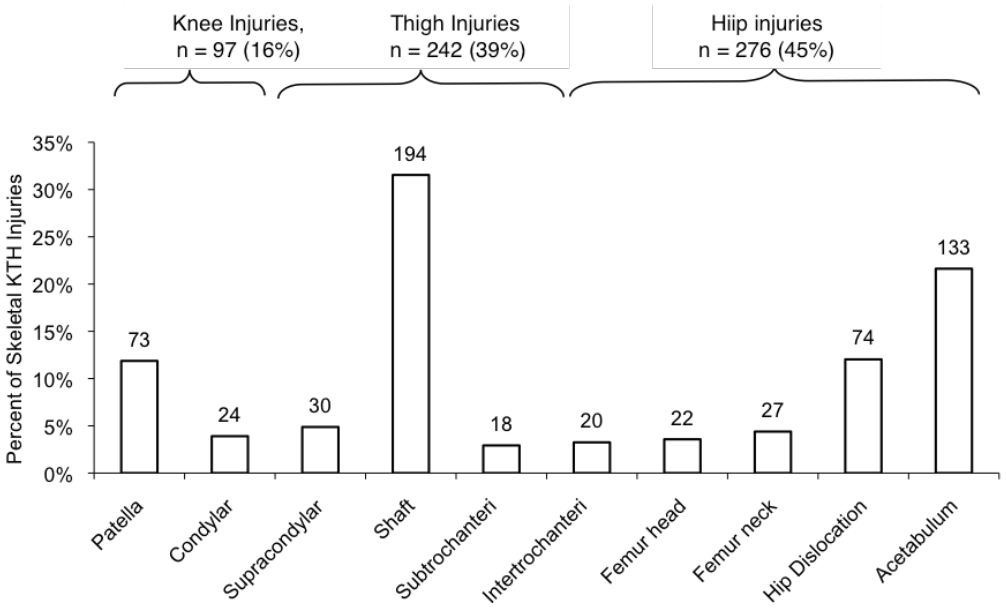

Figure 1-3. Percent of AIS 2+ injuries to different parts of the knee, thigh, and hip in UM CIREN frontal crashes from 1997 to 2003 (adapted from Rupp 2006).

There are several possible reasons for the differences in the distribution of KTH injuries produced in the fixed-specimen KTH tolerance tests and in the simulations conducted by Rupp et al. (2008) compared to the distribution of KTH injuries in real-world frontal crashes. One is the difference in the angle of impact loads to the axis of the femur. However, another potentially important factor is the effects of muscle activation

in the lower extremities of vehicle occupants during braking and/or bracing prior to an imminent crash. This muscle tension has the potential to alter the bone stress and strain distributions in the KTH complex produced during knee impact loading by increasing the axial compressive forces in the KTH complex and by increasing or decreasing the bending moments in the curved shaft of the femur. Muscle tension may also affect the force transmitted through the KTH by differentially altering the soft-tissue coupling distal and proximal to the hip.

Since anthropomorphic crash-test dummies and cadavers lack active musculature, it is not possible to characterize the effects of muscle tension on free-back knee-impact response and injury using physical testing. Although some researchers have attempted to simulate muscle tension in cadaver subjects by pulling on a single tendon (e.g., Kitagawa et al. 1998; Funk et al. 2002; Meyer and Haut 2003), this technique is limited and is not feasible when it is necessary to replicate tension in a large number of muscles in the KTH complex during whole-body free-back testing. In addition, the devices used to apply muscle tension and the surgery needed to install these devices undoubtedly affect knee impact response.

A more reasonable approach to study muscle tension effects would be to use a rigid-body model that replicates skeletal geometry along with simplified one-dimensional muscles (e.g., Chancey et al. 2003; Oi et al. 2004; Van Ee et al. 2000; Kitagawa et al. 1998). However, such an approach is limited by the fact that rigid-body models cannot predict the stresses, strains, and skeletal deformations that are necessary to fully represent different mechanisms of injury (e.g., compression, bending, etc.) along the KTH complex.

Therefore, the only reasonable approach for studying the effects of muscle tension during braking and bracing on KTH injuries is human-body finite-element (FE) modeling. This approach allows for prediction of both skeletal and soft-tissue stresses and strains, and the use of failure models to assess the potential for skeletal fractures.

1.2 LIMITATIONS OF PREVIOUS FINITE-ELEMENT HUMAN MODELS

In recent years, several human finite-element (FE) models have been developed and used for automotive crash safety research and design. Three of the most recent models are the Wayne State University (WSU) model (Lee and Yang 2001; Shah et al. 2001 and 2004; Beillas et al. 2001; Kim et al. 2005) and the Total Human Model for Safety, or THUMS (Iwamoto et al. 2000), and the Human Model for Safety, or HUMOS (Robin 2001). In general, these models include detailed representations of bones, skin, flesh, muscles, and internal organs.

In addition, several anatomically detailed lower-extremity FE models have been developed. Most of these models have focused on pedestrian injuries (Schuster et al. 2000; Takahashi et al. 2000; Beillas et al. 2001; Snedeker et al. 2003; Untaroiu et al. 2005) and foot and ankle injuries in frontal impacts (Beillas et al. 2001; Iwamoto et al. 2005). Only a few models have been developed to study knee, thigh, and hip injuries in frontal knee loading conditions. Detailed FE models of the knee were developed by Hayashi et al. (1996) and Atkinson et al. (1998), and Kim et al. (2005) developed a KTH model to study knee impact response and injury in frontal crashes.

Several of these whole-body FE models incorporate simplified musculature in the lower extremities (Beillas et al. 2001; Iwamoto et al. 2005; Kim et al. 2005), but none of these models can be used to study the effects of muscle tension on KTH injuries in frontal impacts for several reasons. First, although the response of the lower extremities of many of these models have been validated on a component level, none of these models have been validated on a whole-body level because of a paucity of sufficient data on whole-body knee impact response to predict the decrease in force between the knee and the hip. Second, none of the previous models include complete representation of muscles in the lower extremities, and are therefore not able to fully represent muscle activations in the lower extremities during braking or bracing. Third, no models have assigned mass to the different muscle groups. This limitation may be particularly important if muscle tension differentially increases the coupling of muscle mass to skeletal components distal and proximal to the hip, thereby affecting both the force applied to the knees and the transmission of force from the knee to the hip (Rupp 2006).

1.3 THE NEED FOR A NEW HUMAN FE MODEL AND DATA ON MUSCLE FORCES DURING BRAKING AND/OR BRACING

Investigating and understanding the effects of muscle forces during braking and/or bracing on KTH injury using human modeling requires both a model that can simulate the direct effects of muscle forces on tissue stresses as well as the effects of muscle forces on coupling of soft tissue mass to the applied force at the knees and the transmission of force along the KTH complex. The development and successful implementation of such a model requires information on the activation levels of the primary muscles within the KTH complex. To date, only a few researchers have attempted to use either electromyography (EMG) or mathematical musculoskeletal models to estimate lower-extremity muscle forces during driver braking (Behr et al. 2006; Choi et al. 2005; Hardin et al. 2004). However, these models were simplified representations of the lower-extremity muscular and only included a few of the major muscle groups.

Numerical musculoskeletal models have been used for decades to estimate muscle forces of people performing various tasks since it is not feasible in a clinical setting to measure muscle forces from live subjects. However, the analysis of musculoskeletal systems usually leads to a mathematical indeterminate problem because the number of unknown muscle forces is greater than the degrees of freedom of the system. Inverse dynamic optimization analysis is one way to resolve this problem. This approach minimizes an objective function subject to constraints of equilibrium equations and upper limits on individual muscle strength (i.e., the maximum force-generating capacity of a muscle). This mathematical approach has been used in many studies, and particularly for estimating *in vivo* muscle forces during gait (Crowninshield and Brand 1981; Patriarco et al. 1981; Pedersen et al. 1987). Several commercially available programs, such as AnyBody (AnyBody Technology A/S, Denmark), SIMM (Musculographics, Inc., Chicago, IL, USA), and LifeMOD (LifeModeler, Inc. San Clemente, CA, USA) have been developed using the optimization approach to simulate human kinematics and the corresponding muscle reactions. Predicted muscle forces are typically validated by comparing them to forces based on electromyography (EMG) measurements

(Crowninshield and Brand 1981; Glitsch and Baumann 1997) obtained during volunteer testing.

Even though optimization methods have often been used to predict muscle forces associated with specific tasks, no efforts have been made to determine forces developed in the hip and lower extremities during emergency braking and bracing in frontal collisions.

1.4 RESEARCH OBJECTIVES AND PLAN

The objective of this research was to explore the effects of muscle tension on KTH injury in frontal motor-vehicle crashes using a validated human FE model and muscle forces predicted by a numerical musculoskeletal model. In particular, it was hypothesized that muscle tension has the potential to alter the stress and strain distributions in the KTH complex produced during knee impact loading by increasing the axial compressive forces in the KTH complex and by increasing or decreasing the bending moments in the curved shaft of the femur. Muscle tension may also affect the force transmitted through the KTH by altering the muscle mass coupling distal or proximal to the hip.

Figure 1-4 shows a flowchart of the research effort and indicates the relationship between the primary research tasks, which include:

Task 1 - Develop an anatomically detailed human pelvis and lower-extremity finite-element model (LX FE Model) for the midsize male, which includes 35 force-generating muscle elements that represent the individual muscle masses in the pelvis and lower extremities on each side of the body.

Task 2 - Use surface EMG electrodes to measure activation levels of 12 muscle groups on each side of the body produced by midsize-male volunteers during simulated one-foot braking and two-foot bracing in a laboratory test buck.

Task 3 - Use the results of Task 2 to tune and validate a numerical musculoskeletal

model and use this model to predict complete muscle forces in the lower extremities during emergency braking and bracing.

Task 4 - Apply the muscle forces from Task 3 to the LX FE Model developed in Task 1 to study the effects of muscle forces in the lower extremities during braking and bracing on KTH injuries during knee-bolster-like loading to midsize-male front-seat occupants in frontal impacts.

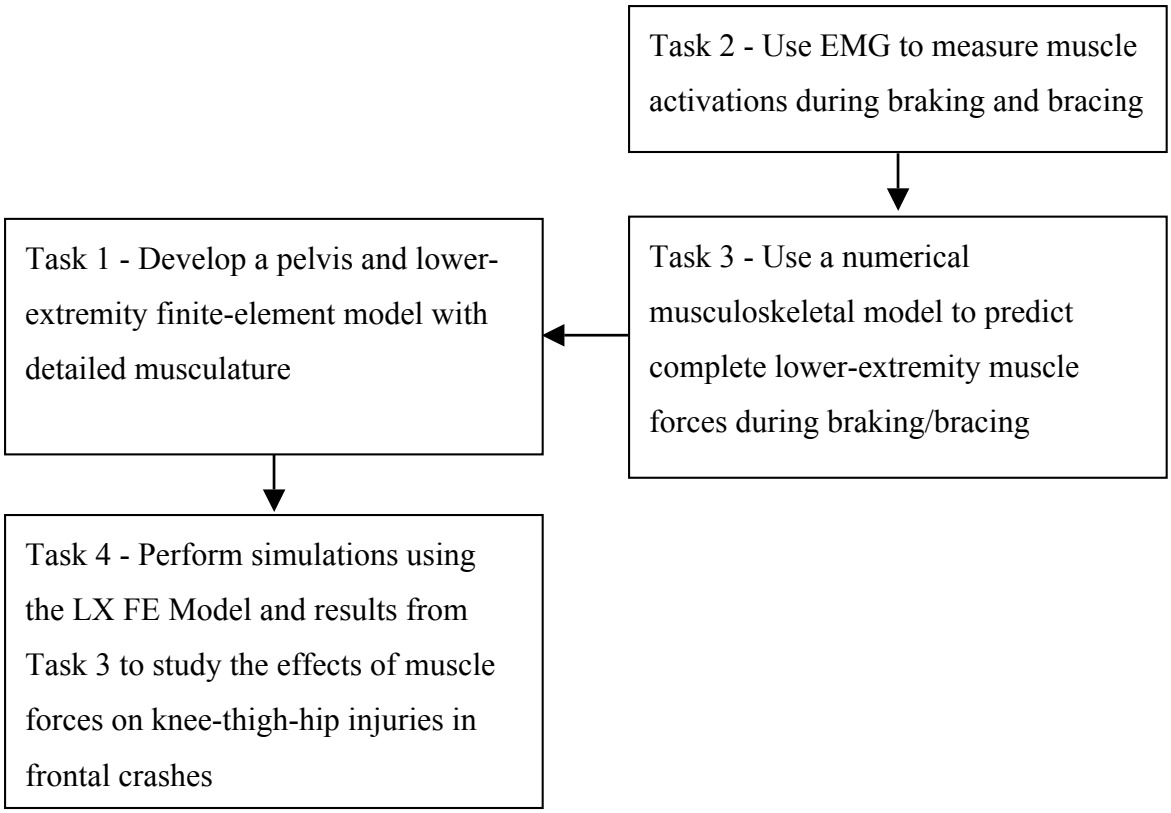

Figure 1-4. Flow chart of research plan.

1.5 ORGANIZATION OF DISSERTATION

Development of the LX FE Model of the midsize male is described in Chapter 2. Subject testing to measure muscle activation levels using surface EMG electrodes and load cells to measure reaction forces produced by volunteers during one-foot braking and two-foot bracing in a laboratory test buck is described in Chapter 3. The use of these EMG data along with measured reaction forces and subject posture to ensure the fidelity of muscle forces predicted from a commercial musculoskeletal model, and the use of this

musculoskeletal model to predict muscle forces throughout the lower extremities during emergency braking/bracing are described in Chapter 4. Frontal knee impact simulations with the LX FE Model to study the effects of muscle forces in the lower extremities on KTH injuries during knee-bolster-like loading are described in Chapter 5. Chapter 6 is a discussion of the results and limitations of the study and includes recommendations for future research. Chapter 7 provides a brief summary of the accomplishments and conclusions from this research.

CHAPTER 2
DEVELOPMENT OF A LOWER-EXTREMITY FINITE-ELEMENT MODEL

2.1 OVERVIEW

As discussed in Chapter 1, several midsize male lower-extremity finite-element (FE) models have been developed in recent years. However, the frontal knee impact responses of these models were only validated with regard to force at the knees and no efforts have been made to validate the force transmitted to the hip. In addition, mass was not assigned to muscles in any of these models, which further decreases the potential for these models to accurately predict the decrease in force between the knee and the pelvis. To achieve better predictions of the responses of the KTH complex in frontal crashes, a more detailed and anatomically accurate lower-extremity FE model is required.

This chapter describes the development and validation of an anatomically detailed pelvis and lower-extremity FE model (LX FE Model) that includes 35 Hill-type muscles in each lower extremity with masses assigned to account for the coupling of muscle mass to the skeletal regions of the KTH complex. This model also accounts for regional differences in cortical bone thickness, incorporates articular cartilage, trabecular bone, cortical bone with directionally dependent mechanical properties, and Tsai-Wu failure criteria (Tsai and Wu 1971) for better prediction of stress, strain, and fracture of bone. The skeletal response of the model was validated by simulating biomechanical tests without muscle tension, including cadaver skeletal segment impact tests documented in the literature as well as recent tests of seated whole cadavers that were impacted using knee loading conditions similar to those produced in FMVSS 208 testing (NHTSA 2008). A parameter sensitivity study was performed using the validated LX FE Model to examine how variations in cortical bone thickness, cortical and trabecular bone stiffness,

acetabular cartilage stiffness, and element mesh density affect the forces along the KTH and the stress distributions in the femur and acetabulum during knee impact loading.

2.2 MODEL DEVELOPMENT

2.2.1 Geometry

The geometry of skeletal components and soft tissue of the LX FE Model of the midsize male are from the MADYMO finite-element lower-extremity model (TASS, Delft, the Netherlands). This model is coupled with a torso based on the MADYMO finite-element occupant model. The external geometry and anatomy of the MADYMO lower extremities and torso are based on the Human Model for Safety (HUMOS) (Robin, 2001), which is similar in size to a 50th-percentile adult male. Table 2-1 demonstrates that the relevant whole bone geometry of the MADYMO lower-extremity model is close to the midsize male reported by Schneider et al. (1983) and Reynolds et al. (1981). The model was converted to LS-DYNA code, Version 971 (Livermore Software Technology Corporation, CA) using the HyperMesh version 8.0 (Altair Engineering, INC., Troy, MI).

Table 2-1. Comparisons of Distances Between Skeletal Landmarks of the Midsize-Male MADYMO Model with the Midsize Male Dimensions Reported by Schneider et al. (1983) and Reynolds et al. (1981)

Measurement	Definition	MADYMO	Schneider et al. (1983)	Reynolds et al. (1981)
Pelvis width	Bi ASIS* breadth	239.7 mm	232 mm	234 ± 11.3 mm
	Inter iliocristale distance	236.6 mm	238 mm	238 ± 14.1 mm
	Inter H-point distance	152.0 mm	164 mm	166 ± 7.1 mm
Pelvis height	Length of a line perpendicular to the inter-ASIS line to the pubic symphysis	74.3 mm	78 mm	78 ± 12.7 mm
Pelvis depth	Distance between the ASIS and the PSIS**	151.8 mm	NA	159 ± 22.9 mm
Femoral condyle width	Distance between lateral and medial femoral epicondyles	85.8 mm	93 mm	NA
Femur length	Distance between the center of the femoral head and the middle of the lateral and medial femoral epicondyles	422.2 mm	431.3 mm	NA

*ASIS: Anterior-superior iliac spine.
**PSIS: Posterior-superior iliac spine.

Since KTH injuries are the primary focus of this study, all of the skeletal components of the upper body (ribs, neck, head, vertebral bodies, and upper extremities) and legs were modeled as rigid bodies using the original MADMO model element mesh and the feet were modeled with lumped-mass nodal elements located at the centers of mass of the left and right feet. These simplifications served to reduce computational run times. Since the KTH complex in frontal knee impact is the primary focus of this study, these simplifications should have minimum effects on the KTH response. The LS-DYNA keyword card CONSTRAINED_JOINT_SPHERICAL was used to define the joints between rigid components in the upper body and a high elastic stiffness was applied to these joints (i.e. ES = 1000.0 N/rad) to prevent relative rotation of these rigid components during knee impact simulations.

Lower-extremity muscles were constructed using one-dimensional beam elements. The origins, insertions, and paths of muscles were derived from data on 35 muscles in the lower extremities reported by Delp (1990), and are the same as those used in the AnyBody musculoskeletal model (AnyBody Technology A/S, Denmark). The mass of each muscle was determined by multiplying the cross-sectional area and density of the muscle by its length. Muscle density was assumed to be 1056 kg/m^3 based on data from Wickiewicz et al. (1983). The cross-sectional area of each muscle was determined by multiplying the physiologic cross-sectional area (PCSA) by the cosine of its pennation angle both of which were obtained from Delp (1990) and are based on the reports by Wickiewicz et al. (1983) and Friederich et al. (1990). These values are contained in Appendix A and applied for all 35 muscles in the lower extremities. Total muscle mass connected to both sides of the hip and lower extremities is 17.75 kg, which is similar to the mass of 18.1±3.1 kg reported by Janssen et al. (2000) who used magnetic resonance imaging (MRI) to examine the skeletal muscle mass of the male lower body.

For reference, Table 2-2 compares the body segment masses of the LX FE Model to those reported by McConville et al. (1980) for the midsize male, and shows that total body mass and the masses of all body segments in the model are close to those provided by McConville et al. Figure 2-1 shows a side view of the LX FE Model with lower-extremity musculature included.

Table 2-2. Body Segment Masses and Total Body Mass for the Midsize Male from the LX FE Model and McConville et al. (1980)

Region	Mass (kg)	
	Model	McConville et al. (1980)
Upper Body	37.61	37.93
Pelvis and Flaps	16.05	17.35
Thigh	14.86	12.15
Leg	8.23	7.34
Foot	1.95	1.84
Total	78.70	76.61

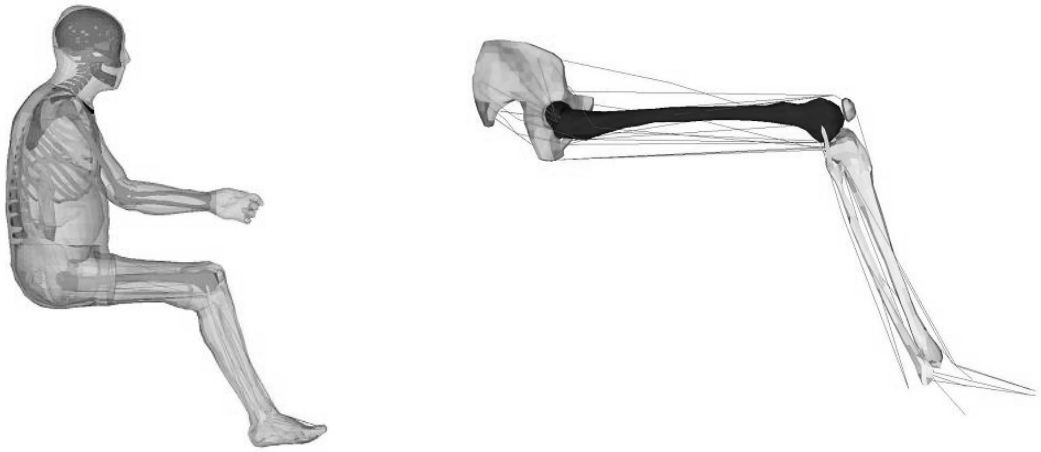

Figure 2-1. Side views of the LX FE Model with rigid-body torso and lower extremities (left) and the muscles included in the lower extremities (right).

2.2.2 Musculoskeletal Structure and Material Properties

As part of the development of the LX FE Model, many modifications to the MADYMO lower-extremity model were made, especially to the pelvis, femur, and patella shown in Figure 2-2. The cortical bone in the MADYMO model was remeshed using shell elements (ELFORM=1). Trabecular bone was added to the pelvis, femoral head, and femoral condyles, and was modeled using 4-node tetrahedral elements that were produced by the Hypermesh automatic mesh generator. Trabecular bone was

modeled using the constant-stress solid element (ELFORM=1). Models of the articular cartilage of the knee and hip were created using 8-node hexahedral elements (ELFORM=1).

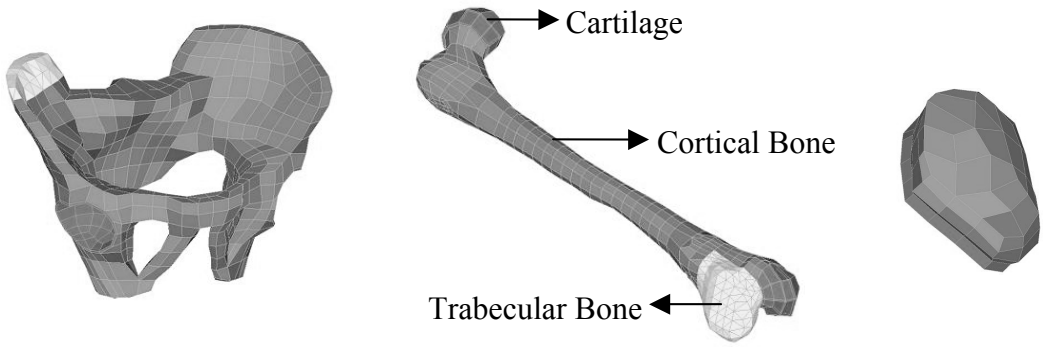

Figure 2-2. FE models of the pelvis (left), femur (middle), and patella (right).

Table 2-3 lists the thicknesses of cortical bone and cartilage used in the LX FE Model relative to ranges of femur and pelvis cortical bone thickness reported in the literature. The cortical bone thicknesses used in the femur and pelvis of the model are based on data reported by Looker et al. (2004) and Anderson et al. (2005). These cortical bone thicknesses were also selected because they produced model responses that most closely approximated the experimental data used for model validations. Uniform cortical and cartilage thickness values were used over the listed regions and transition elements between the diaphysis, and epiphysis of the femur were developed to connect two regions with different thicknesses. The cross-sectional areas of cortical bone in the femoral mid shaft and femoral neck are 445 mm^2 and 271 mm^2, respectively. These values are close to the values of 481±81 mm^2 calculated by Kennedy et al. (2004) for the femoral shaft and to the values of 292 ± 47 mm^2 for the femoral neck reported by Riggs et al. (2004). The moments of area of the femoral mid shaft and femoral neck cortical bone are approximately 37,534 mm^4 and 4,3007 mm^4, respectively. Since cortical bone thickness in the patella is not well documented in the literature, a thickness of 1 mm from the MADYMO model was retained in the current model. Because the cortical bone and

cartilage thicknesses differ from those used in the MADYMO model, it was necessary to slightly adjust some nodal positions, particularly in the outer surfaces of the cartilage of the knee and hip joints, to prevent penetration between the components prior knee-impact loading.

Table 2-3. Cortical Bone and Cartilage Thickness Values Used to Develop the LX FE Model Relative to Ranges of Femur and Pelvis Cortical-Bone Thickness Values Reported in the Literature

		Ranges	Model
Cortical bone	Patella	N/A	1.0 mm (Robin 2001)
	Femur	Diaphysis: 3 to 10mm Epiphysis: 1 to 3mm (Gomberg, et al. 2005; Hogler et al., 2003; Looker et al. 2004; Peacock et al., 1998)	Diaphysis: 6.81mm; Epiphysis: 1.71mm (Looker et al. 2004)
	Pelvis	0.0 to 4.0 mm (Anderson et al., 2005)	1.41mm (Anderson et al. 2005)
Cartilage	Patella	1.9 to 3.2 mm (Cohen et al. 1999; Faber et al. 2001; Hudelmaier et al. 2001)	3.05mm (Cohen et al. 1999)
	Femur	Head: 2.5 to 3.3 mm; Condyle: 1.6 to 2.2 mm (Cohen et al. 1999; Faber et al. 2001; Ferguson et al. 2000; Hudelmaier et al. 2001; Wyler et al. 2007)	Head: 3.0mm (Ferguson et al. 2000); Condyle: 2.08 mm (Cohen et al. 1999)
	Acetabulum	0.95 to 3.13 mm (Anderson et al. 2005; Wyler et al. 2007)	2.0mm (Anderson et al. 2005)

Table 2-4 shows the material properties used in the LX FE Model relative to the ranges of cortical bone, trabecular bone, and cartilage stiffness reported in the literature. Cortical bone of the femur and pelvis are described by a linear elastic orthotropic material model with a Tsai-Wu fracture criterion (Tsai and Wu, 1971) (Material type 55, MAT_ENHANCED_COMPOSITE_DAMAGE). This material model is accepted as one of the better methods for predicting failure of cortical bone (Gomez-Benito et al. 2005; Dejak et al. 2007). Since data on the material axes of the cortical bone in the pelvis are not available, cortical bone in the pelvis was modeled as isotropic with a Tsai-Wu fracture criterion. Cortical bone of the patella was modeled using an isotropic elastic material model (Material type 1, MAT_ELASTIC).

Table 2-4. Material Properties Used to Develop the LX FE Model Compared to Ranges of Cortical Bone, Trabecular Bone, and Cartilage Stiffness Values Reported in the Literature

		Ranges	Model
Cortical	Patella		E=16.0GPa, n=0.25, r=6000kg/m3 (Robin 2001)
	Femur	Longitudinal: 17.0-27.4 GPa Circumferential: 8.51-18.8 GPa Radial: 6.91-18.8 GPa (Athanasiou et al., 2000; Ciarlet, 1990; Cowin, 2001; Kim et al., 2005)	E11=20.0GPa, E22=13.4GPa, E33=12.0GPa, G12=6.23GPa, G13=5.61GPa, G23=4.53GPa, n12=0.235, n13=0.222, n23=0.375, (Ashman et al. 1984), r=1500kg/m3 (Robin 2001) Stension=151MPa, Scompression=224MPa Sshear=70MPa (Yaszemski et al. 1996)
	Pelvis	5.26-20 GPa (Athanasiou et al., 2000; Ciarlet, 1990,	E=17.0GPa, S=121MPa, n=0.3 (Anderson et al. 2005), r=1500kg/m3 (Robin 2001)
Trabecular	Femur	20 to 345 MPa (Athanasiou et al., 2000, Ciarlet, 1990; Goldstein, 1987)	E=58.8MPa, S=14.7MPa, n=0.3 (Lindahl et al. 1976), r=1000kg/m3, C=0, P=0
	Pelvis	5 to 282 MPa (Athanasiou et al., 2000, Ciarlet, 1990; Goldstein, 1987)	E=58.9MPa, S=12.3MPa, n=0.3 (Dalstra et al. 1993), r=1000kg/m3, C=0, P=0
Cartilage	Knee/ Femoral Head		C1=4.1MPa, C2=0.41MPa r=3600kg/m3 (Anderson et al. 2005)
	Acetabulum	0.45 to 1.90 MPa (Athanasiou et al. 1995; Magnussen et al. 2005)	E=1.2MPa (Yamada 1970) n=0.46 r=3600kg/m3 (Anderson et al. 2005)
Soft Tissues	Skin		E=1.5 MPa, n=0.46 r=1000kg/m3 (Robin 2001)
	Flesh		K=250kPa, G∞=155kPa, G0=69kPa r=1000kg/m3 (Robin 2001)
	Organs		K=250kPa, G∞=155kPa, G0=69kPa r=1000kg/m3 (Robin 2001)
	Medial Collateral Ligament		E=250 MPa, S=35MPa, n=0.46 r=1000kg/m3 (Robin 2001)
	Lateral Collateral Ligament		E=400 MPa, S=35MPa, n=0.46 r=1000kg/m3 (Robin 2001)
	Posterior Cruciate Ligament		E=200 MPa, S=35MPa, n=0.46 r=1000kg/m3 (Robin 2001)
	Anterior Cruciate Ligament		E=300 MPa, S=35MPa, n=0.46 r=1000kg/m3 (Robin 2001)

Trabecular bone was modeled with continuum damage mechanics (CDM) using Material type 105 (MAT_DAMAGE_2). Cartilage in the knee joint and femoral head was modeled with a transversely isotropic Mooney-Rivlin model (Material type 91, MAT_SOFT_TISSUE), which is appropriate to describe the hyperelastic characteristics of materials like biological soft tissues. However, there is no fracture formulation in the

Mooney-Rivlin model. To simulate failure of cartilage in the acetabulum, an elastic-viscoplastic material (Material Type 105, MAT_DAMAGE_2) was used to model this cartilage. Mechanical properties of other soft tissues such as ligaments, skin, flesh, and internal organs in the torso were modeled as either visco elastic or elastic materials using original MADYMO material properties as shown in Table 2-4.

The muscles of the lower extremity were modeled using Hill-type muscle elements (Material type 156, MAT_MUSCLE). Characteristic curves used in this model, including the relationship between muscle force and muscle strain and strain rate, are based on those reported by Delp (1990) and are provided in Appendix A. In this material model, activated muscle force can be determined by multiplying the muscle strength by its activation level at each point in time. Individual muscle strengths are from the report by Delp (1990), as well as those from the studies by Friederich and Brand (1990) and Wickiewicz et al. (1983). A summary of individual muscle strengths is provided in Appendix A.

The LX FE Model consists of 12,612 elements and 5,974 nodes in the KTH and 45,860 elements and 37,850 nodes in the entire model. The elements of the patella are the same size as those in the original MADYMO model at approximately 10 mm in length, but the elements in the femur and pelvis were refined by splitting elements at the mid point of each edge from the original MADYMO model lengths of 4.0 to 7.0 mm. The elements of the soft tissues in the KTH were maintained at the original mesh size from the MADYMO model of 10.0 to 15.0 mm. A three-dimensional contact algorithm, CONTACT_AUTOMATIC_ SURFACE_TO_SURFACE, was implemented to establish the contact interface of all components. All the resultant time-history outputs from the model were filtered using a CFC 600 low-pass filter (SAE J211, 1994). Simulations were performed using LS-DYNA 3-D explicit Finite Element Analysis software (LSTC Livermore Software Technology Corporation, CA) in Linux (64-bit) running on an Intel Xeon 2.8 GHz processor in a Mac Pro 8 core computer. The minimum time step was 0.12 μs and the computational time was less than 3 hours for each simulation.

2.3 MODEL VALIDATION

Validation of the LX FE Model was performed in two parts. The first part focused on validating the skeletal response of the model against data from skeletal component tests in the biomechanical literature. The second part focused on validating the model's free-back knee impact response using data from knee impacts to stationary seated whole cadavers and tests in which the knees of seated cadavers were impacted with flesh and body segments removed.

2.3.1 Skeletal Component Validation

Femur Three-Point-Bending Tests. The ability of the LX FE Model to predict bone fracture and skeletal impact response was first validated using response and injury results from medial-lateral (M-L) and anterior-posterior (A-P) 3-point femur bending tests conducted by Kennedy et al. (2004). Figure 2-3 illustrates the test facility and the configuration of the model. To simulate these tests, soft tissue was removed from the distal and proximal femur and the most medial points on the femoral head, and the femoral condyles were constrained so that they could rotate but not translate. Similar to the Kennedy et al. tests, the specimen was impacted at mid shaft in a medial-to-lateral direction by a cylindrical impactor with a mass of 9.8 kg and an initial velocity at impact of 5 m/s. To simulate the A-P bending tests performed by Kennedy et al., the most posterior points on the femur were supported and the mid-shaft of the femur was loaded in a similar manner. Predicted peak femur bending moments at the impacted cross section were compared to peak bending moments reported by Kennedy et al. Strain histories predicted by the model on the cortical bone surface of the femur opposite to the impacted side were also compared to strain-gage data measured by Kennedy et al. at a similar location.

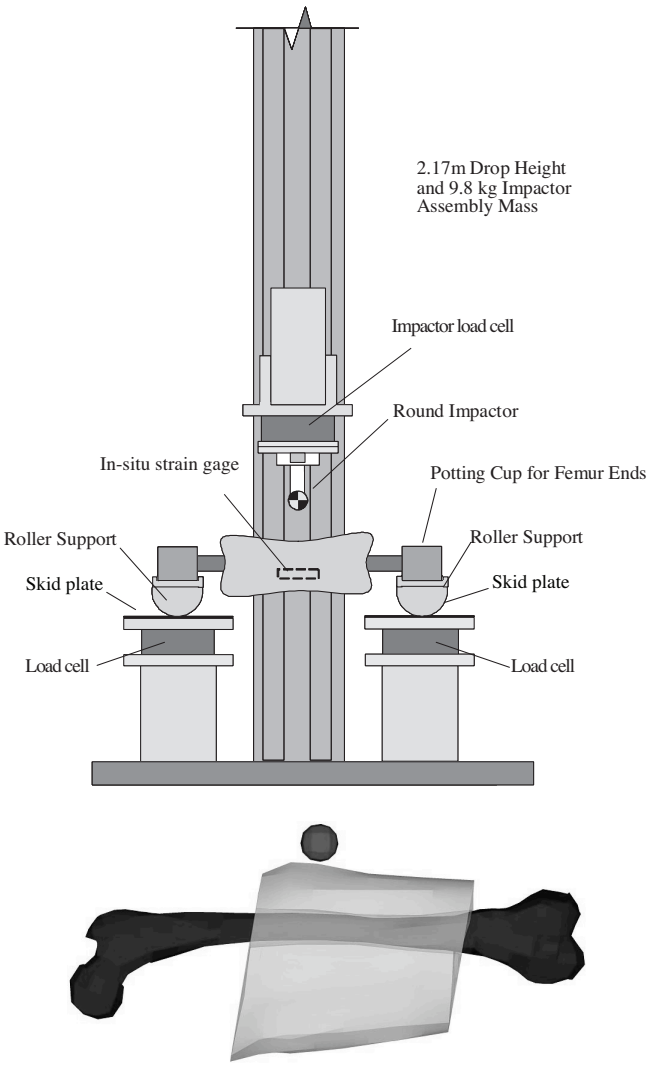

Figure 2-3. Illustration of experimental setup (top) used by Kennedy et al. (2004) in femur three-point-bending test (adapted from Kennedy et al. 2004) and model (bottom) of femur configured to simulate these tests.

Figure 2-4 shows that the predicted bending moments at the time of fracture in the cross section of the femur shaft at the impact location for the A-P and M-L simulations are 346 Nm and 385 Nm, respectively. These values are similar to those obtained by Kennedy et al. (2004), who estimated the failure bending moment of the femur at 348 ± 96 Nm for A-P bending and 352 ± 83 Nm for M-L bending.

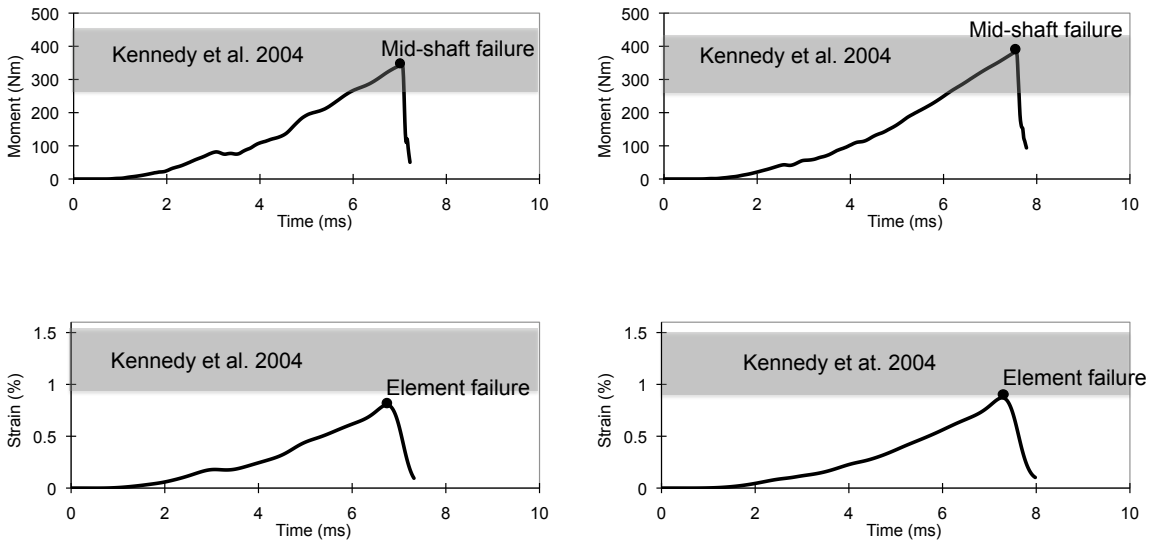

Figure 2-4. Strain and bending moment histories from simulations of femur three-point bending tests for A-P bending (left) and M-L bending (right) compared to failure moments from Kennedy et al. (2004).

Figure 2-4 also shows the predicted strain histories at the element opposite the impact site for simulated A-P and M-L three-point bending tests compared to failure strains measured by Kennedy et al. The predicted tensile strains at failure for this element are 0.81% for A-P bending and 0.87% for M-L bending. These values are lower than the tensile failure strain of 1.2 ± 0.3% for A-P bending and 1.3 ± 0.3% for M-L bending measured in a similar location by Kennedy et al. (2004). These differences may be explained by differences in the manner by which failure strain was determined and measured. Kennedy et al. measured failure strain at the outer surface of the femur immediately opposite the site of impact at the time of "whole-bone" failure. In the simulations reported in this paper, failure strain history was from the first produced failure a "single element" of cortical bone, which is lower than the strain at which whole bone fracture would occur.

Fixed-Pelvis and Fixed-Femoral-Head Tests. The LX FE Model was further validated by simulating the fixed-specimen hip-tolerance and femur-tolerance tests

performed by Rupp et al. (2002). Figure 2-5 illustrates the test facilities and the simulations used to model the loading and boundary conditions applied in the hip and femur tolerance tests. In the hip tolerance tests, one knee of a section of the body consisting of the pelvis and both lower extremities was loaded through a rigid material that was molded to the shape of the anterior knee. This molded interface was initially in contact with the knee and distributed applied forces across the patella and femoral condyles. To eliminate the inertially induced decrease in force between the knee and the hip, the pelvis was fixed in the hip tolerance tests by gripping the iliac wings. In the femur tolerance tests, the femoral head was supported by an "acetabular cup" and force was applied to the knee by the same molded knee interface. In both hip tolerance and femur tolerance tests, knee loading was directed along the long axis of the femur.

To simulate the fixed pelvis hip tolerance tests, eight nodes at the edges of the iliac wing were constrained in the x, y and z directions to represent the iliac wing fixation. The knee was loaded by a rigid interface with a contour that exactly matched the anterior contours of the patella and femoral condyles. Impactor movement in the model was prescribed by applying a representative ram acceleration history from a hip tolerance test. To simulate the femur tolerance tests, a representative ram acceleration history was used and the femoral head was supported by a rigid hemispherical cup that allowed it to rotate freely. In all simulations, knee angle was set so that the position of the patella on the femoral condyles matched that observed in lateral view x-rays taken during a subset of the Rupp et al. (2003) femur tolerance tests. Predicted and measured knee impact force histories were compared. Force at the knee at the time that the model predicted fracture was also compared to experimentally measured fracture forces.

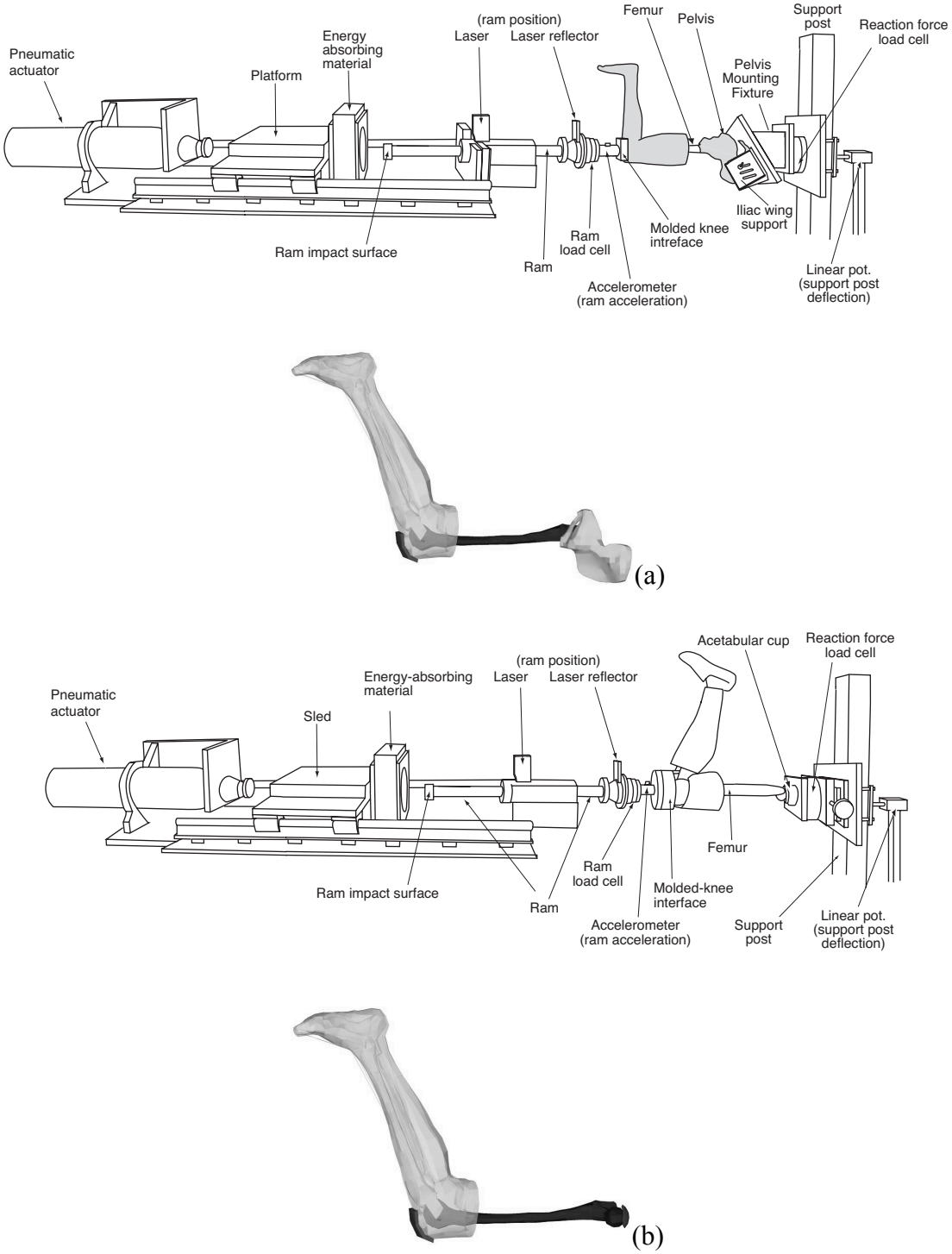

Figure 2-5. Illustrations of test fixtures and setup and LX FE Model configurations for hip (a) and femur tolerance tests (b) performed by Rupp et al. (2002).

The LX FE Model was also validated by simulating fixed pelvis tests that were performed using hip postures that were 15° abducted and 10° adducted from the neutral posture reported by Rupp et al. (2003). For these simulations, the LX FE Model was configured as shown in Figure 2-5a. Hip abduction and adduction were simulated by rotating the pelvis about the hip joint center similar to in the experimental tests. Predicted and experimentally measured knee impact force histories and forces at the times of hip fracture were compared.

Figure 2-6 shows the simulated fractures at the acetabulum and femoral neck for simulations of the hip and femur tolerance tests, respectively, and compares predicted knee impact force histories (black lines) to those obtained experimentally (gray lines) by Rupp et al. (2002). The predicted force histories for fixed pelvis and fixed femoral head tests compare favorably to experimentally measured force histories. In addition, the fracture forces predicted by the model are 7.55 kN and 6.09 kN for the femur and hip tolerances tests, respectively, which are very similar to the experimentally measured average femur and hip fracture tolerances of 8.1 ±1.7 kN and 6.1±1.4 kN, respectively.

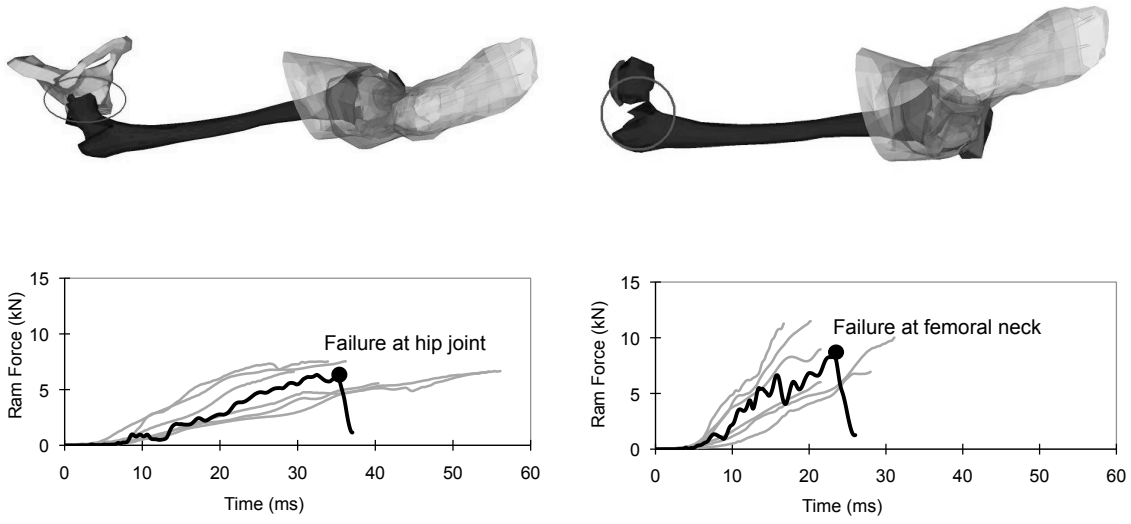

Figure 2-6. Simulated fractures and comparisons of predicted (black lines) and experimental measured (gray lines) knee impact force histories from hip tolerance tests (left) and femur tolerance tests (right).

When the model was used to simulate fixed pelvis tests with the hip abducted 15˚ and adducted 10˚ from the midsize-male seated automotive neutral posture, acetabular fracture was predicted at forces of 7.24 kN and 5.42 kN, respectively. The first of these values represents a 19% increase in fracture force from the neutral posture value, which compares favorably to the 15% increase reported by Rupp et al. (2003). Similarly, the second value represents a 14% decrease in fracture force from the neutral posture value, which also compares well to the reported 11% decrease reported by Rupp et al.

2.3.2 Free-Back Knee Impact Response

The coupling and contributions of soft-tissue mass and body segments to knee impact response were validated by simulating symmetric free-back knee-impact tests performed by Rupp et al. (2008). An illustration of the test setup and an image of the model configured to simulate the loading and boundary conditions applied by the test apparatus are shown in Figure 2-7. In these tests, the knees of whole, seated midsize-male cadavers were symmetrically impacted at 1.2 m/s, 3.5 m/s and 4.9 m/s using a high-mass padded impactor. To quantify the contributions of the thigh flesh and the torso to knee impact response, the symmetric knee impacts were repeated after sequentially cutting the thigh flesh, removing the thigh flesh, and removing the torso.

In the simulations of these tests, impactor motion was prescribed to be the average of the impactor displacement histories from all subjects tested at each condition. The average friction force history reported by Rupp et al. for each test condition was applied to the elements of the pelvis flesh over the ischia for that test condition. The validity of the model was assessed by comparing experimentally measured and predicted knee impact force and femur and pelvis velocity histories in all subject conditions. The femur and pelvis velocity histories were recorded in the local x-axis direction, which was initially normal to the frontal plane (same direction of the impactor motion). In addition, model predictions of force transmitted to the acetabulum were compared to forces experimentally measured by the implanted load cell in thigh-flesh-removed and torso-removed conditions.

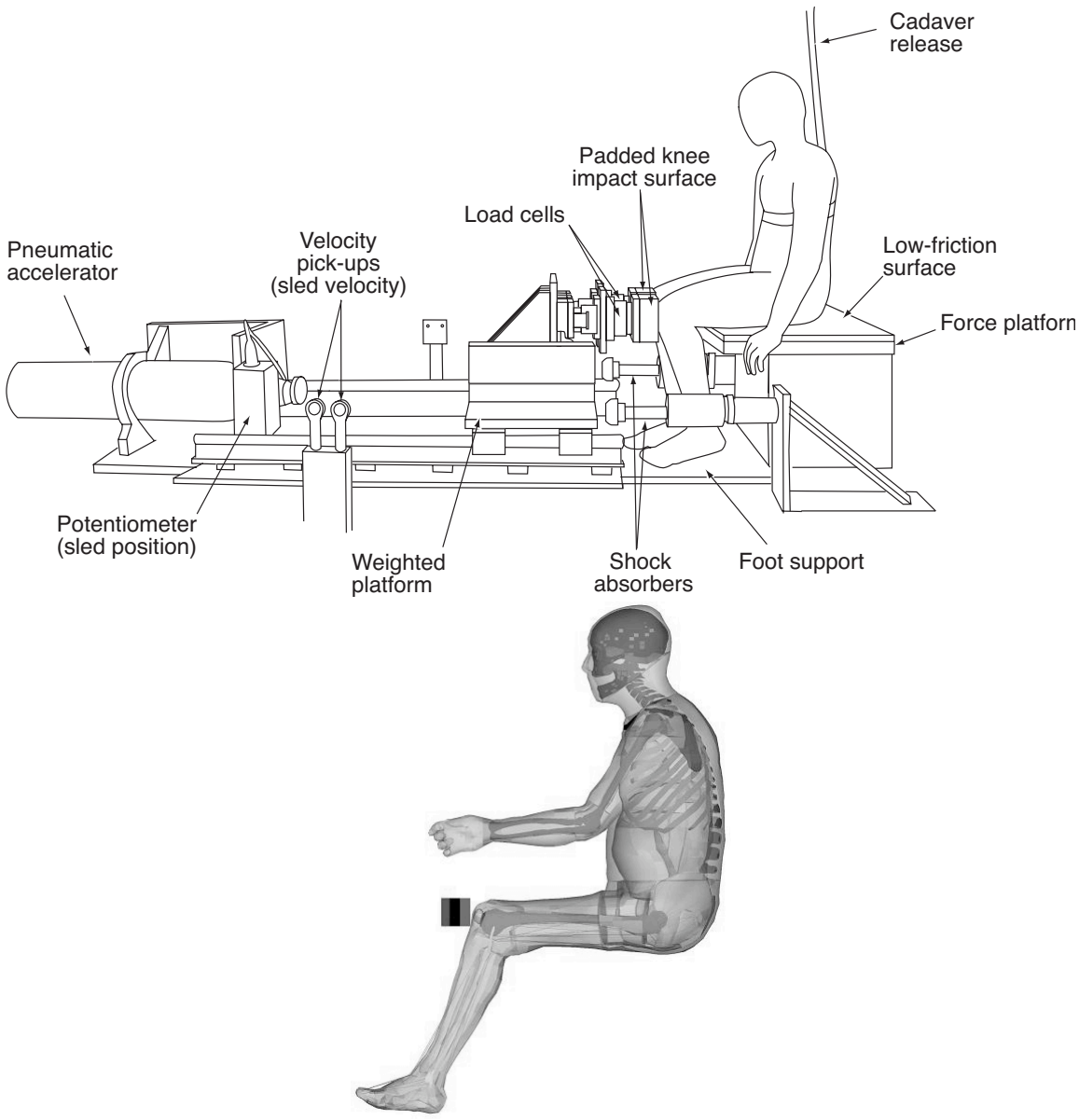

Figure 2-7. Illustration of experimental setup for whole-body symmetric knee impact tests conducted by Rupp et al. (2008) and LX FE Model with rigid-body torso and lower-extremity configuration to simulate these tests.

Figures 2-8 through 2-11 and Table 2-5 compare the simulation results with the experimental results reported by Rupp et al. (2008) at an impact speed of 4.9 m/s. Comparisons of the simulation results with the experimental results at 3.5 m/s and 1.2 m/s are provided in Appendix B. In general, model predictions are within the range of experimental data for applied and femur forces and femur velocities at all impact velocities. Predicted pelvis velocity is within the range of experimentally measured

pelvis velocity for whole-body tests, tests with the thigh flesh cut, and tests with the thigh flesh and muscle removed. However, the pelvis velocities predicted by the simulations with the torso removed differ from the experimentally measured values at all three impact velocities.

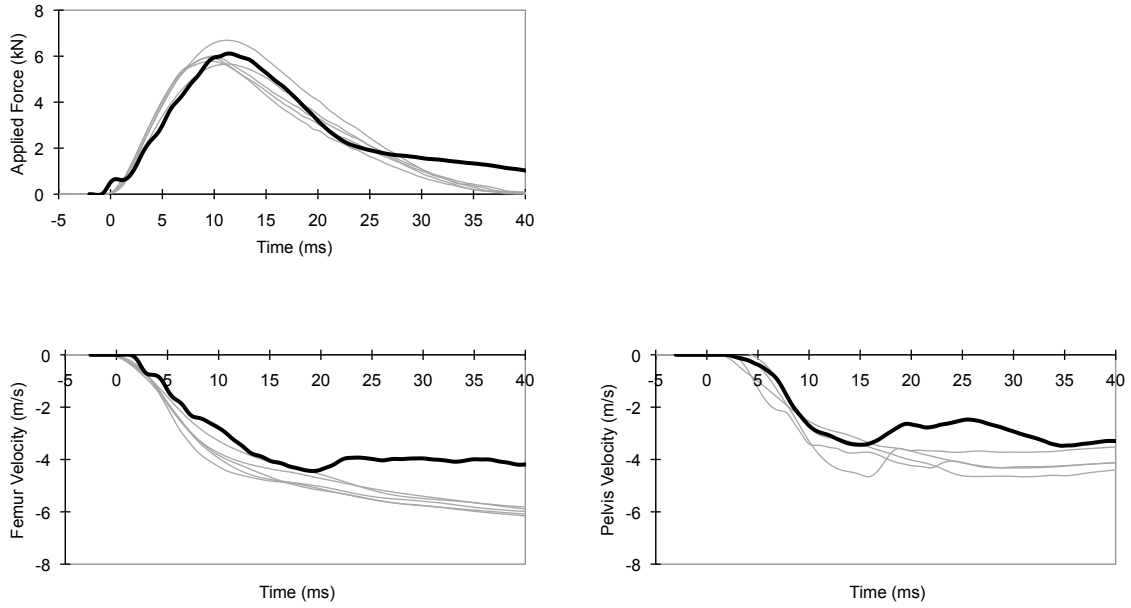

Figure 2-8. Comparison of applied force (top), femur velocity (bottom left), and pelvis velocity (bottom right) histories from experimental tests (gray lines) and KTH FE simulations (black lines) of whole-body 4.9 m/s tests.

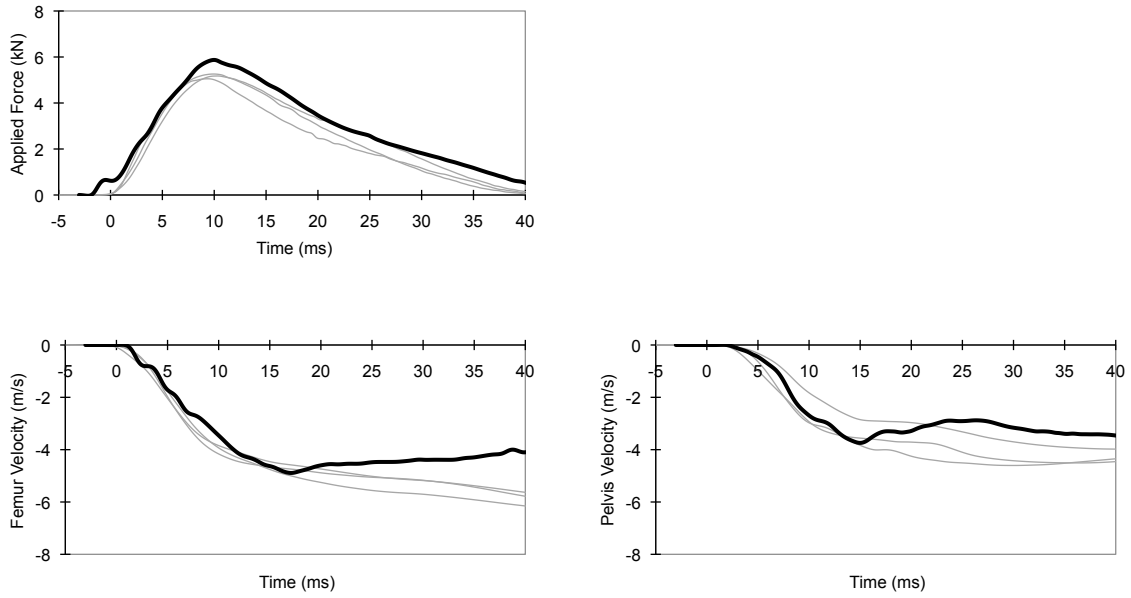

Figure 2-9. Comparison of applied force (top), femur velocity (bottom left), and pelvis velocity (bottom right) histories from experimental tests (gray lines) and KTH FE simulations (black lines) of thigh-flesh-cut 4.9 m/s tests.

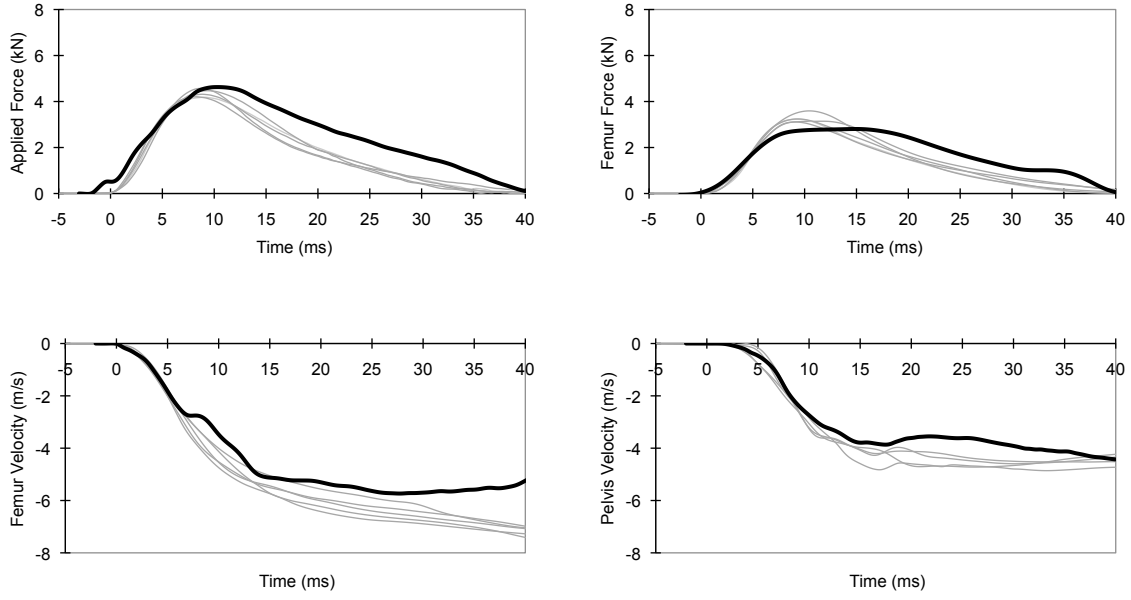

Figure 2-10. Comparison of applied force (top), femur velocity (bottom left), and pelvis velocity (bottom right) histories from experimental tests (gray lines) and KTH FE simulations (black lines) of thigh-flesh-removed 4.9 m/s tests.

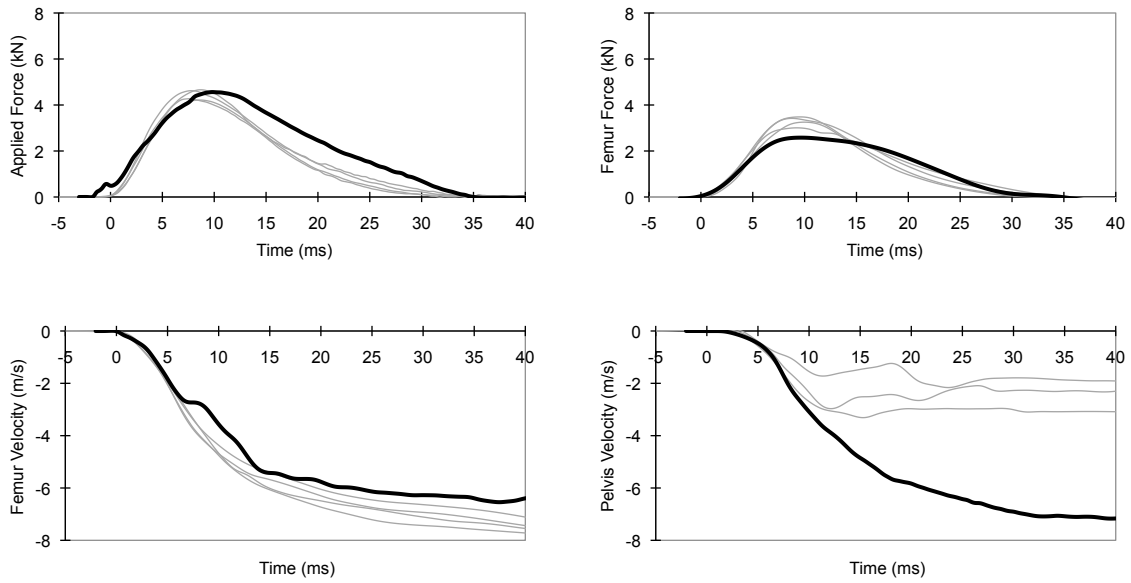

Figure 2-11. Comparison of applied force (top), femur velocity (bottom left), and pelvis velocity (bottom right) histories from experimental tests (gray lines) and KTH FE simulations (black lines) of torso-removed 4.9 m/s tests.

Table 2-5. Comparisons of Average (and Ranges) of Experimental and Simulation Results on Applied Force, Femur Force, Femur Velocity, and Pelvis Velocity at Time of Peak Applied Force of 4.9 m/s Tests.

	Time of Peak Applied Force (ms)	Applied Force (kN)	Femur Force (kN)	Femur Velocity (m/s)	Pelvis Velocity (m/s)
Whole-Body					
Experiment	10.3 (9.5 to 11.3)	6.01 (5.66 to 6.69)	NA	-3.89 (-3.36 to -4.33)	-3.10 (-2.60 to -3.47)
Simulation	10.4	6.11	NA	-3.06	-2.85
Error	0.97 %	1.66 %		21.34 %	8.06 %
Thigh-Flesh-Cut					
Experiment	9.9 (9.4 to 10.3)	5.16 (5.05 to 5.26)	NA	-3.96 (-3.83 to -4.14)	-2.55 (-1.80 to -2.95)
Simulation	10.0	5.87	NA	-3.45	-2.69
Error (%)	1.01 %	13.76 %		12.88 %	5.49 %
Thigh-Flesh-Removed					
Experiment	8.8 (8.2 to 9.3)	4.35 (4.18 to 4.56)	3.22 (3.04 to 3.51)	-3.94 (-3.60 to -4.29)	-2.46 (-2.37 to -2.54)
Simulation	10.3	4.63	2.79	-3.95	-3.14
Error (%)	17.05 %	6.44 %	13.35 %	0.25 %	27.64 %
Torso-Removed					
Experiment	8.2 (7.7 to 8.7)	4.44 (4.22 to 4.66)	3.23 (2.93 to 3.46)	-3.88 (-3.72 to -4.06)	-1.55 (-1.04 to -1.99)
Simulation	9.8	4.56	2.56	-3.91	-3.44
Error (%)	19.51 %	2.70 %	20.74 %	0.77 %	121.94 %

2.4 MATERIAL PROPERTIES AND PARAMETER SENSITIVITY STUDY

A parameter sensitivity study was performed to examine how variations in pelvis and femur cortical bone thickness and cortical bone, trabecular bone, and acetabulum cartilage stiffness affect the predicted forces and stress distributions in the femur and acetabulum during knee impact loading. In this study, the target model parameters were decreased and increased 50% from the original settings listed in Table 2-6. In simulations in which cortical bone thickness was varied, the density of the cortical bone was adjusted to maintain the same mass as the original model. All simulations were performed using the impact conditions from the simulations of 4.9 m/s whole-body knee impact tests described in the model validation. All the fracture functions were turned off to prevent element failure, which would alter stress distributions and force transmitted through the KTH. Maximum principal stresses in the femoral neck, the femoral shaft, and the acetabulum were used to evaluate the sensitivity of model response to variations in parameters. The sensitivity of the model to variations in each parameter, S, was defined as the percent change in output value divided by the percent change in input parameter value, or:

$$S = \frac{\%\ change\ in\ output\ value}{\%\ change\ in\ input\ parameter}.$$

In all simulations, the maximum principal stress in each region of the femoral neck, femoral shaft, and acetabulum occurred at the middle of the posterior surface of the femoral neck, the lateral surface of the femur mid-shaft, and the lateral edge of the acetabulum, respectively. Table 2-7 summarizes the predicted peak knee impact forces and maximum principal stresses at the femoral neck, femoral shaft, and acetabulum from simulations where the stiffness and thickness of femur and pelvis cortical bone, stiffness of femur and pelvis trabecular bone, and stiffness of acetabular cartilage were varied. In general, the maximum principal stress of the cortical bone at each region was increased by increasing cortical-bone stiffness and by decreasing cortical-bone thickness. Changes in peak impact forces due to variations in all of the parameters are lower than 5% in most of the conditions.

Table 2-6. Model Parameters Varied in Parameter-Sensitivity Study

Type	Model Parameter	Changes
Femur cortical bone stiffness	Original: E_{11}=20.0GPa, E_{22}=13.4GPa, E_{33}=12.0GPa Case 1: E_{11}=10.0GPa, E_{22}=6.7GPa, E_{33}=6.0GPa Case 2: E_{11}=30.0GPa, E_{22}=20.1GPa, E_{33}=18.0GPa	 -50% +50%
Femur trabecular bone stiffness	Original: 58.8MPa Case 1: 29.4MPa Case 2: 88.2MPa	 -50% +50%
Femur cortical bone thickness	Original: Diaphysis:6.81mm; epiphysis: 1.71mm Case 1: Diaphysis:3.41mm; epiphysis: 0.86mm Case 2: Diaphysis:10.22mm; epiphysis: 2.57mm	 -50% +50%
Pelvis cortical bone stiffness	Original: 17.0GPa Case 1: 8.5GPa Case 2: 25.5GPa	 -50% +50%
Pelvis trabecular bone stiffness	Original: 58.9 MPa Case 1: 29.45 MPa Case 2: 88.35 MPa	 -50% +50%
Pelvis cortical bone thickness	Original: 1.5 mm Case 1: 0.75 mm Case 2: 2.25 mm	 -50% +50%
Acetabulum cartilage stiffness	Original: C1=4.1MPa, C2=0.41MPa Case 1: C1=2.05MPa, C2=0.205MPa Case 2: C1=8.2MPa, C2=0.82MPa	 -50% +50%

Table 2-7. Results from the Parameter-Sensitivity Study of the LX FE Model

		Impact Force		Femoral Neck		Femoral Shaft		Acetabulum	
		Max Force (kN)	Sensitivity (%)	Max Principle Stress (MPa)	Sensitivity (%)	Max Principle Stress (MPa)	Sensitivity (%)	Max Principle Stress (MPa)	Sensitivity (%)
	Original	6.1		66.8		36.2		60.4	
Femur	Cortical Stiffness -50%	5.8	11.1%	59.7	21.1%	33.6	14.5%	58.1	7.7%
Femur	Cortical Stiffness +50%	6.0	-3.6%	91.4	73.9%	38.4	11.9%	65.9	18.2%
Femur	Cortical Thickness -50%	5.7	13.8%	**138.2**	**-214.0%**	**77.5**	**-227.8%**	58.6	5.7%
Femur	Cortical Thickness +50%	6.1	0.0%	**48.3**	**-55.2%**	**21.5**	**-81.6%**	64.4	13.4%
Femur	Trabecular Stiffness -50%	6.1	1.8%	74.1	-21.8%	37.0	-4.4%	58.7	5.4%
Femur	Trabecular Stiffness +50%	6.0	-3.3%	60.0	-20.2%	35.7	-2.9%	59.0	-4.6%
Pelvis	Cortical Stiffness -50%	6.0	4.8%	64.6	6.6%	34.9	7.6%	43.3	56.7%
Pelvis	Cortical Stiffness +50%	6.1	-0.9%	68.8	6.0%	36.7	2.7%	64.3	13.1%
Pelvis	Cortical Thickness -50%	6.0	4.5%	74.2	-22.2%	34.8	7.9%	**103.0**	**-141.3%**
Pelvis	Cortical Thickness +50%	6.1	-0.3%	79.6	38.5%	39.0	15.2%	**40.5**	**-66.0%**
Pelvis	Trabecular Stiffness -50%	6.0	3.3%	64.1	7.9%	36.1	0.6%	54.7	18.7%
Pelvis	Trabecular Stiffness +50%	6.0	-2.4%	67.0	0.6%	36.5	1.4%	60.3	-0.1%
Hip Joint	Cartilage Stiffness -50%	6.1	1.8%	80.4	-40.9%	38.1	-10.5%	68.4	-26.6%
Hip Joint	Cartilage Stiffness +50%	6.0	-3.0%	63.7	-9.3%	35.6	-3.4%	58.7	-5.4%

Figure 2-12 compares sensitivity of cortical bone thickness and cortical bone and trabecular stiffness to the principal stresses at femoral neck, femoral shaft, and acetabulum in frontal knee impacts. As can be seen, cortical bone stresses are very sensitive to changes in cortical bone thickness, especially when cortical bone thickness is reduced. The increases in peak cortical bone stresses at the femoral neck and femoral shaft are more than 210% when femur cortical bone thickness is decreased by 50%. Also, cortical bone stress at the acetabulum is increased by more than 140% when pelvis cortical bone thickness is decreased by 50%. Pelvis and femur stresses are decreased by more than 50% when cortical bone thickness is increased by 50%.

Interestingly, it was found in this parameter sensitivity study that changing the stiffness of the acetabulum cartilage did not produce significant changes in the stresses in the underlying cortical bone. This is probably because there are relatively large lateral displacements in the cartilage during compressive loading due to its high Poisson's ratio. These lateral displacements reduce the effects of cartilage stiffness on the stresses of the underlying bone.

2.5 MESH-SIZE SENSITIVITY STUDY

To evaluate the sensitivity of element mesh size on fracture prediction, simulations of femur M-L and P-A three-point-bending tests and hip and femur tolerance tests were performed after splitting the elements at the mid point of each edge (i.e., dividing each element into quarters). All the simulation conditions with the finer mesh elements were identical to the simulation conditions used with original model. Comparisons of the failure moments in the M-L and P-A three-point-bending tests and failure force in the hip and femur tolerance were made between the simulations using the original model and the model with finer mesh.

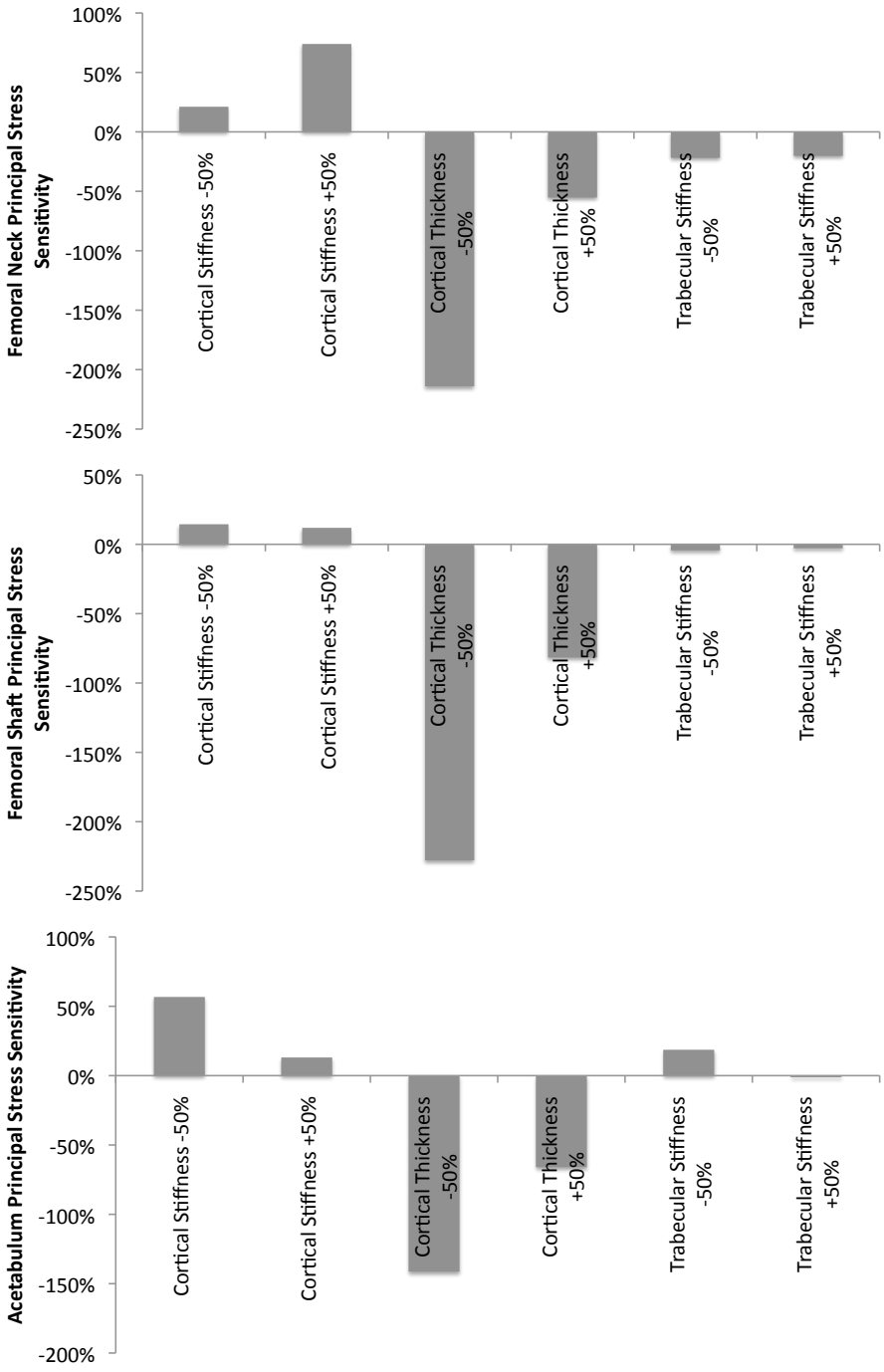

Figure 2-12. Sensitivities of cortical bone and trabecular bone stiffness and cortical bone thickness to the principal stress at the femoral neck (top), femoral shaft (middle), and acetabulum (bottom) in frontal knee impacts.

Table 2-8 compares the fracture moments and fracture forces in the simulations of femur M-L and A-P three-point-bending tests and femur and hip tolerance tests using the original model and the model with the finer mesh size. When a finer mesh size model was used, the predicted moment at the time of fracture for the A-P and M-L bending simulations was reduced by approximately 8%, and the predicted fracture forces for the femur and hip tolerance tests were reduced from 13 to 25%. The higher failure moments and forces with the larger mesh size are thought to be due to combining and averaging of regions of high and low stress into one element. That is, the larger mesh size smoothes the stress fields and reduces the magnitude of peak stress. In contrast, the finer mesh size increases the magnitude of peak stress in an element and cause the element to reach the failure criterion at lower applied forces.

Table 2-8. Comparisons of Fracture Moments and Fracture Forces in Simulations with Original LX FE Model and Finer-Mesh Model

Test Simulated	Fracture moment or force with original model	Fracture moment or force with finer-mesh model
Femur M-L three-point-bending	385.0 Nm	354.2 Nm
Femur A-P three-point-bending	345.6 Nm	328.1 Nm
Femur tolerance	7.6 kN	5.8 kN
Hip tolerance	6.1 kN	5.3 kN

2.6 SUMMARY AND DISCUSSION

This chapter describes the development and validation of the LX FE Model, which represents an advance over other lower-extremity models in two primary ways. The first is that the model has been validated using knee impact response data from free-back cadaver tests in which force applied along the long axis of the femur and dynamic responses (i.e., velocitiess) of the femur and pelvis were measured. These validations ensure that the model correctly predicts the decrease in force along the KTH for knee-bolster-like knee impacts in the absence of lower-extremity muscle forces. The second is that the model includes a complete set of lower-extremity muscles that offers the

potential to accurately simulate the effects of muscle activation on KTH response and the decrease in force along the KTH during occupant braking and bracing.

The primary reason cortical bone was modeled using shell elements is because shell elements allow the use of a Tsai-Wu failure criterion in LS-DYNA, which is accepted as one of the better methods for predicting bone fracture. Previous modelers have used only one or two layers of solid elements to model cortical bone (e.g., Untaroiu et al. 2005 and Takahashi et al. 2000). As a result, responses of these models using solid elements with single-point integration should be similar to those of the LX FE Model using the shell element. In addition, the use of shell elements avoids calculations in errors associate with the large aspect ratio of the elements in the thin cortical-bone regions.

The LX FE Model was validated by simulating fixed pelvis and fixed femoral head tests, femur three-point-bending tests, free-back whole-body knee-impact tests, and free-back knee-impact tests with body segments and flesh removed. As shown in Figures 2-8 through 2-11, predicted responses fall within the ranges of experimentally measured data, with the exception of pelvis velocity in simulations of free-back knee-impact tests with the torso removed. The hypothesized reason for the difference in predicted and measured pelvis velocity is that the pelvis was initially oriented in an upright posture in the simulations so that the sacrum was nearly vertical, but pre-test photos indicate that it was rotated rearward from this posture in torso-removed tests by 30˚to 60˚. As a result, pelvis velocity in the local x-axis, which was determined by integrating the component of pelvis acceleration normal to the sacrum, was aligned with the A-P direction of pelvis motion in the simulations, but was rotated by between 30 and 60 degrees from this direction in the torso removed tests.

To examine this hypothesis to explain the differences in pelvis velocity between experiments and simulations, the model was reconfigured to simulate a 4.9 m/s torso-removed test with the greatest initial pelvis rearward rotation of approximately 60 degrees. Figure 2-13 compares the femur and pelvis velocity histories from the experiment and simulation for this subject. As can be seen, due to the initial rearward rotation of the pelvis, pelvis velocity in the local x-axis is much smaller than femur

velocity in both the experiment and the simulation. Most importantly, the close match of the experimental and simulation results for pelvis velocity confirms that the hypothesized explanation is correct.

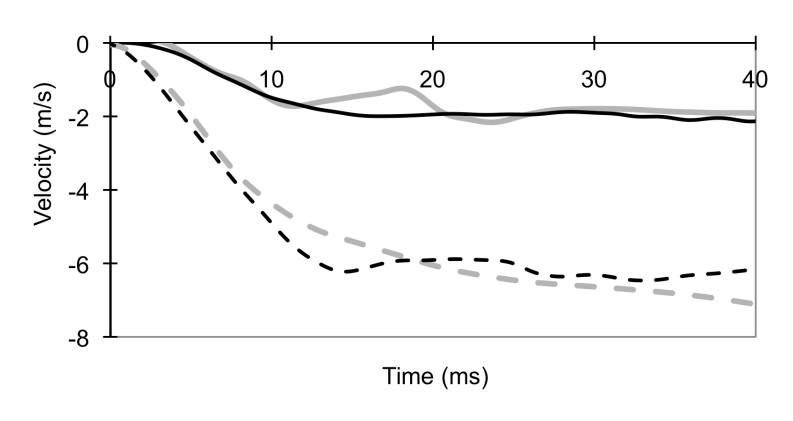

Figure 2-13. Comparisons of femur (dashes lines) and pelvis (solid lines) x-axis velocities from the experiment (gray lines) and simulation (black lines) for a torso-removed 4.9 m/s test.

CHAPTER 3
MEASUREMENT OF LOWER-EXTREMITY MUSCLE ACTIVATIONS DURING SIMULATED ONE-FOOT BRAKING AND TWO-FOOT BRACING

3.1 OVERVIEW

This chapter describes an experiment to characterize muscle activation patterns produced by midsize male volunteers during simulated one-foot braking and two-foot bracing in a laboratory seating buck. The levels of muscle activations were recorded for twelve major muscles in the lower extremities using surface EMG electrodes during subjects exerted maximum and 50% maximum one-foot braking or two-foot bracing forces on a foot plate. Testing was conducted using three target knee angles while reaction forces on the seat and footplate were measured. EMG voltages corresponding to maximum voluntary muscle contractions were obtained for the different muscle groups used to estimate the percent muscle activation levels from EMGs recorded during simulated one-foot braking and two-foot bracing. Data from these simulated braking and bracing tests were used to validate and adjust the fidelity of muscle activation forces and patterns predicted by the numerical musculoskeletal model described in the Chapter 4.

3.2 METHODS

3.2.1 Subjects

Muscle activation data were collected during simulated braking and bracing from twelve male subjects who were approximately 50^{th} %ile by U.S. stature and weight (Schneider et al. 1983) and ranged in age from 21 to 34 years. Table 3-1 lists the characteristics of each subject. All subjects were screened for injuries or diseases that could affect lower extremity neuromuscular performance or their potential to perform

moderately stressful physical activity. All test protocol and procedures were approved by the University of Michigan Institutional Review Board and an informed consent form was signed by each subject before testing.

Table 3-1. Characteristics of Test Subjects

Subject Number	Age	Stature (cm)	Weight (kg)	Knee Height (cm)*	Buttock-Knee Length (cm)**	Hip Breadth (cm)***
1	33	178.2	73.3	49.6	56.0	35.4
2	34	183.2	76.4	51.8	55.6	32.8
3	29	180.6	66.2	50.5	54.8	31.8
4	26	179.5	85.0	49.9	54.9	39.8
5	26	174.7	62.8	49.8	56.0	30.1
6	30	174.2	81.9	48.2	51.9	37.6
7	20	174.2	68.5	50.6	55.0	34.1
8	21	181.1	68.3	51.6	61.4	31.8
9	25	173.8	73.9	49.3	57.2	38.1
10	24	175.5	85.7	50.3	62.1	38.7
11	32	186.4	73.9	52.8	60.3	37.5
12	24	179.2	77.3	51.7	59.7	37.2
Mean	27.0	178.4	74.4	50.5	57.1	35.4
sd	4.6	4.0	7.3	1.3	3.1	3.2

* Measured as vertical distance from the floor to the top of the patella with the subject seated and hip and knees at 90 degrees.
** Measured horizontally from the back of buttocks to the front of the knee with the subject seated and hips and knees at 90 degrees.
*** Measured as distance between the most lateral aspects of the left and right hips with the subject seated.

3.2.2 Subject Preparation for Testing

To reduce the potential for musculoskeletal injury, all subjects were required to warm up their muscles prior to testing by pedaling on a stationary bicycle for a minimum of 10 minutes. Following warm-up cycling, twenty-three retro-reflective markers (plastic spheres approximately 10 mm in diameter) were attached to body landmarks on the torso, pelvis, and lower extremities as illustrated and listed in Figure 3-1. These markers provided for tracking of the subject's posture during testing using a 13-camera Vicon 524 Motion Capture System (Vicon Motion Systems, Inc., Lake Forest, CA).

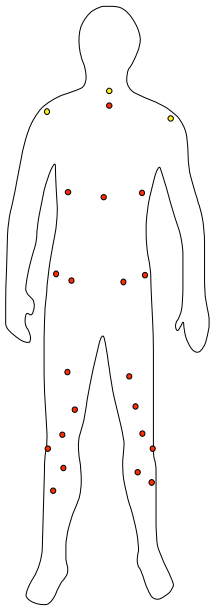

Marker Location		Numbers of targets
Torso	C7	1
	Clavicle	1
	Left Shoulder	1
	Right Shoulder	1
	Sternum	3
Pelvis	Left Pelvis	2
	Right Pelvis	2
Left Lower Limb	Thigh	2
	Knee	2
	Leg	2
Right Lower Limb	Thigh	2
	Knee	2
	Leg	2
Total number of targets		23

Figure 3-1. Locations of subject markers.

Silver-silver chloride pre-gelled duotrode surface EMG electrodes with 10-mm diameter electrode tips and an inter-electrode distance of 20 mm (Stens Corporation, San Rafael, CA) were placed over the palpated bellies of twelve major muscles in the right side of the lower extremity as listed in Table 3-2. Specific placements of these electrodes on the palpated bellies were based on standard locations reported in the literature (Cram and Kasman 1998, Delagi et al. 1975, Leis and Trapani 2000). Each electrode site was shaved and cleaned with alcoholic pads prior to electrode placement. The recorded EMG signals were pre-amplified with a gain of 100 and band-pass filtered at 10-500 Hz. The root mean square (RMS) of the signal was determined using a time step of 55 ms. Processed EMG data were input to the Vicon 524 Motion Capture Data Acquisition System that synchronized EMG data with load cell signals and occupant posture data.

Table 3-2. List of Muscles Measured in the Test

	Muscles
Leg	Medial gastrocnemius (MG)
	Lateral gastrocnemius (LG)
	Soleus (SOL)
	Tibialis anterior (TA)
Femur	Rectus femoris (RF)
	Vastus lateralis (VL)
	Vastus medialis (VM)
	Adductor longus (AL)
	Biceps femoris long head (BFLH)
	Biceps femoris short head (BFSH)
Hip	Gluteus medius (GMED)
	Gluteus maximus (GMAX)

3.2.3 Subject Tests

Maximum-Voluntary Contraction (MVC) Tests. When using EMG signals to estimate the level of muscle activity, it is common to normalize the muscle activation level to the percent of maximum voluntary contraction (MVC) based on EMG measurements. Therefore, prior to the bracing and braking tests, participants were instructed to exert their maximum voluntary isometric effort in six conditions: (1) knee extension, (2) knee flexion, (3) hip extension, (4) hip flexion, (5) hip adduction, and (6) hip abduction, as illustrated in Figure 3-2. In these tests, subjects sat on a padded horizontal seat with their hips secured by an adjustable belt and their torso against the seatback. The angle between the seat and the seatback was 100˚.

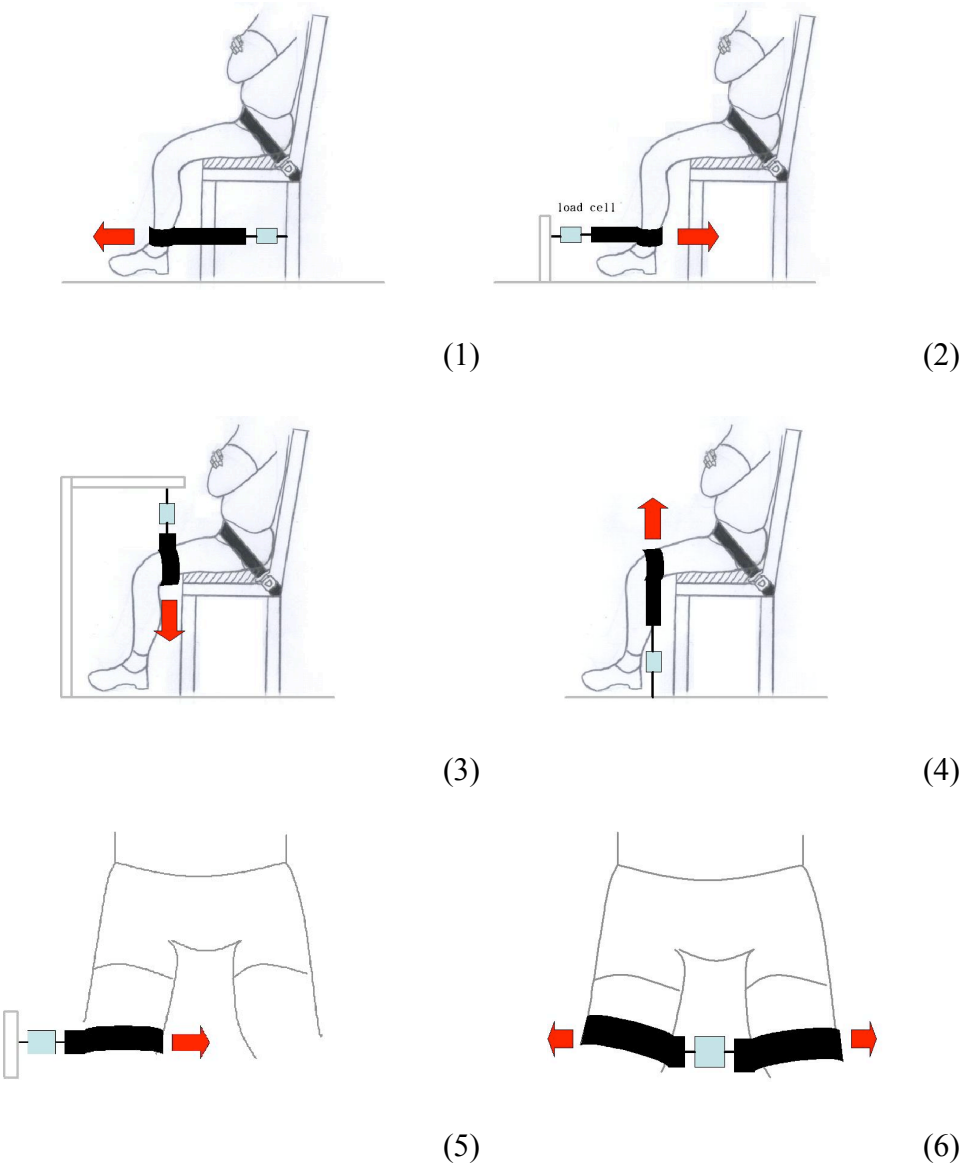

Figure 3-2. Schematic of MVC tests: (1) knee extension, (2) knee flexion, (3) hip extension, (4) hip flexion, (5) hip adduction and (6) hip abduction.

Subject posture was maintained constant for all MVC tests with the knees at approximately 90 degrees, the angle between the thigh and torso (hip flexion angle) at approximately 90 degrees, and the thigh abduction angle at approximately 0 degrees (i.e., no thigh splay). As illustrated in Figure 3-2, forces were applied by each subject through belt webbing wrapped around the appropriate portion of the lower extremity and were measured by a load cell that connected the belt to a fixed structure on the test fixture.

The subjects were instructed to perform each MVC test by reaching maximum voluntary exertion within about 2 seconds and to hold their maximum effort for three seconds. In the knee extension and flexion tests, subjects' legs were wrapped by a belt above the right ankle. Subjects were asked to exert maximum force on pulling the belt forward or backward without abducting/adducting or extending/flexing their hip. In the hip extension and flexion tests, subjects' thigh were wrapped by a belt near the right knee. Subjects were asked to exert maximum force on pulling the belt downward or upward without abducting/adducting the hip or extending/flexing the knee. In the hip adduction and abduction tests, subjects' right thigh or both thighs were wrapped by belts near the knees. Subjects were asked to exert maximum force on pulling the belt inward or outward without extending/flexing the hip or knee. Each MVC tests was repeated three times with a rest period of two minutes between tests to prevent muscle fatigue.

One-Foot Braking and Two-Foot Bracing Tests. Figure 3-3 shows a side-view photo and schematic drawing of the test apparatus for one-foot braking and two-foot bracing tests. In these tests, subjects sat on a horizontal seat and their torso against the seatback. The same rigid seat was used in the subject MVC tests. A six-axis force platform in front of the seat measured the reaction forces and moments applied by one or both feet (depending on the tests), and another six-axis force platform under the seat was used to measure the combined reaction forces at the subject's buttock and back. The distance between the seat and footplate and the angle of footplate were adjusted between test conditions to vary subject posture as described below.

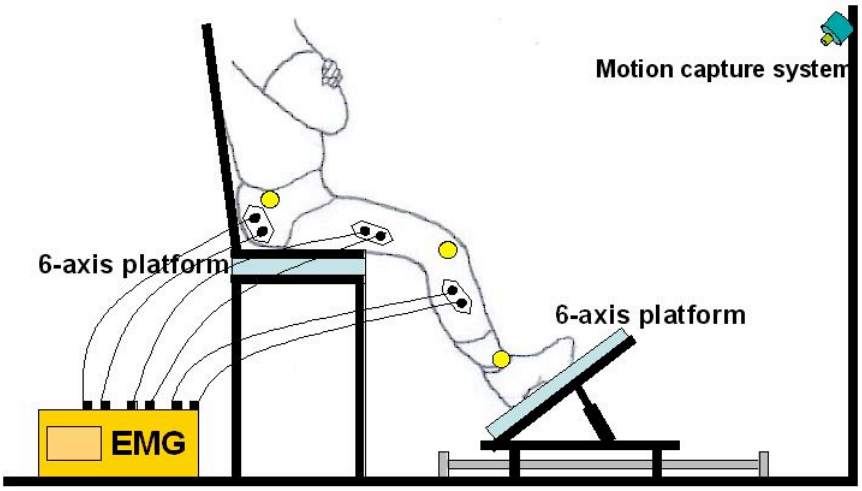

Figure 3-3. Test apparatus used to measure muscle activations and subject reaction forces during simulated one-foot braking and two-foot bracing.

Subjects were tested for one-foot braking and two-foot bracing in the twelve conditions listed in Table 3-3. Each of the twelve conditions represents all combinations of three postures (knee angles), two applied force levels of maximum effort and 50% of maximum, and one-foot braking and two-foot bracing. The included knee angles for the three postures were 120°, 105°, and 90°. These angles were chosen based on estimates of knee angles during normal driving (approximately 120 degree) to knee angles during knee contact with the knee bolster (approximately 90 degree) in a frontal collision (Rupp et al., 2007). As shown in Figure 3-4, an electronic numeric display was used to provide

subjects with feedback on the amount of force being exerted so and the level of force corresponding to 50% of their maximum force attained in previous testing.

Table 3-3. Processes of the One-Foot Braking and Two-Foot Bracing Tests

One-Foot Braking Tests			
Knee angle / Bracing force	120°	105°	90°
Maximum	Condition 1	Condition 5	Condition 9
50% Maximum	Condition 2	Condition 6	Condition 10
Two-Foot Bracing Tests			
Knee angle / Braking force	120°	105°	90°
Maximum	Condition 3	Condition 7	Condition 11
50% Maximum	Condition 4	Condition 8	Condition 12

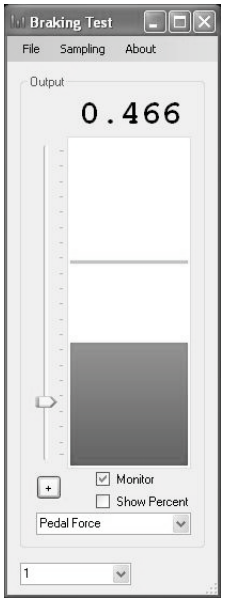

Figure 3-4. The electronic numeric display used to provide subjects with feedback on the amount of force being exerted and the force level corresponding to 50% of maximum force exertion (horizontal bar).

Each one-foot braking and two-foot bracing trial lasted approximately seven seconds, including two seconds to reach the target force, three seconds of sustained hold at the target force, and two seconds to return to the relaxed condition. Each test condition was repeated three times. At least a two-minute rest period was provided between all efforts.

3.2.4 Data Processing

The locations of joint centers for the ankle, the knee, and the hip were calculated from exterior body landmarks tracked by the VICON system during subject testing using methods reported by Reed et al. (1999). As illustrated in Figure 3-5, the middle second of the hold phase of each braking or bracing test was used to determine the force values, posture, and muscle activation levels. The middle second was calculated by computing the middle data point between the time of 80% peak of maximum force applied to the foot plate during the rise and fall to maximum force, and averaging data points form 0.5-seconds before and 0.5 seconds after the middle data point. A total of 60 data points were included from the 60 HZ sampling rate in one second. Mean values from the same period of the EMG data and hip, knee, and ankle joint angle data in each trial were then calculated as illustrated in Figure 3-6. Three repetitions of each MVC and braking/bracing trial were conducted and the average of the values calculated from these trials were computed.

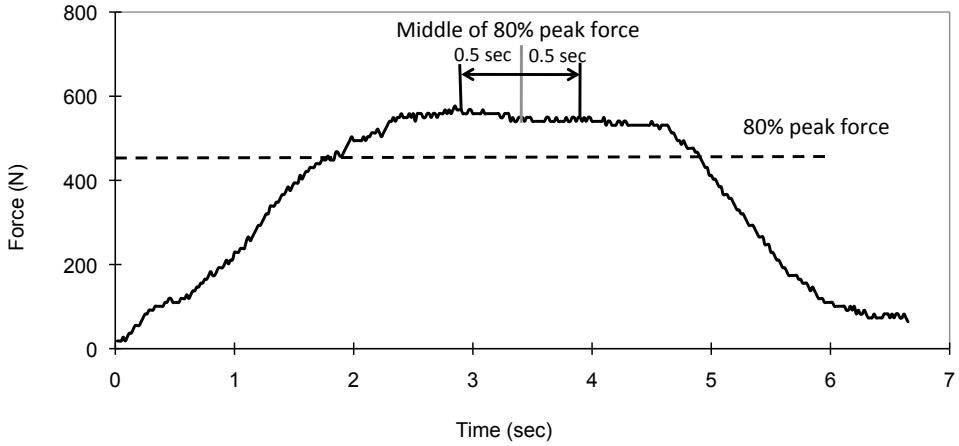

Figure 3-5. Typical footplate force exertion history illustrating the period used to calculate the force exertion level.

Maximum EMG activity measured for each muscle group across all tests was considered to represent 100% activation level for that muscle group. EMG data from the MVC and braking/bracing tests were then normalized with respect to the largest muscle activation level measured in the MVC and braking/bracing trials to determine the percentage activation of each muscle (i.e., %MVC) produced by each subject in each test.

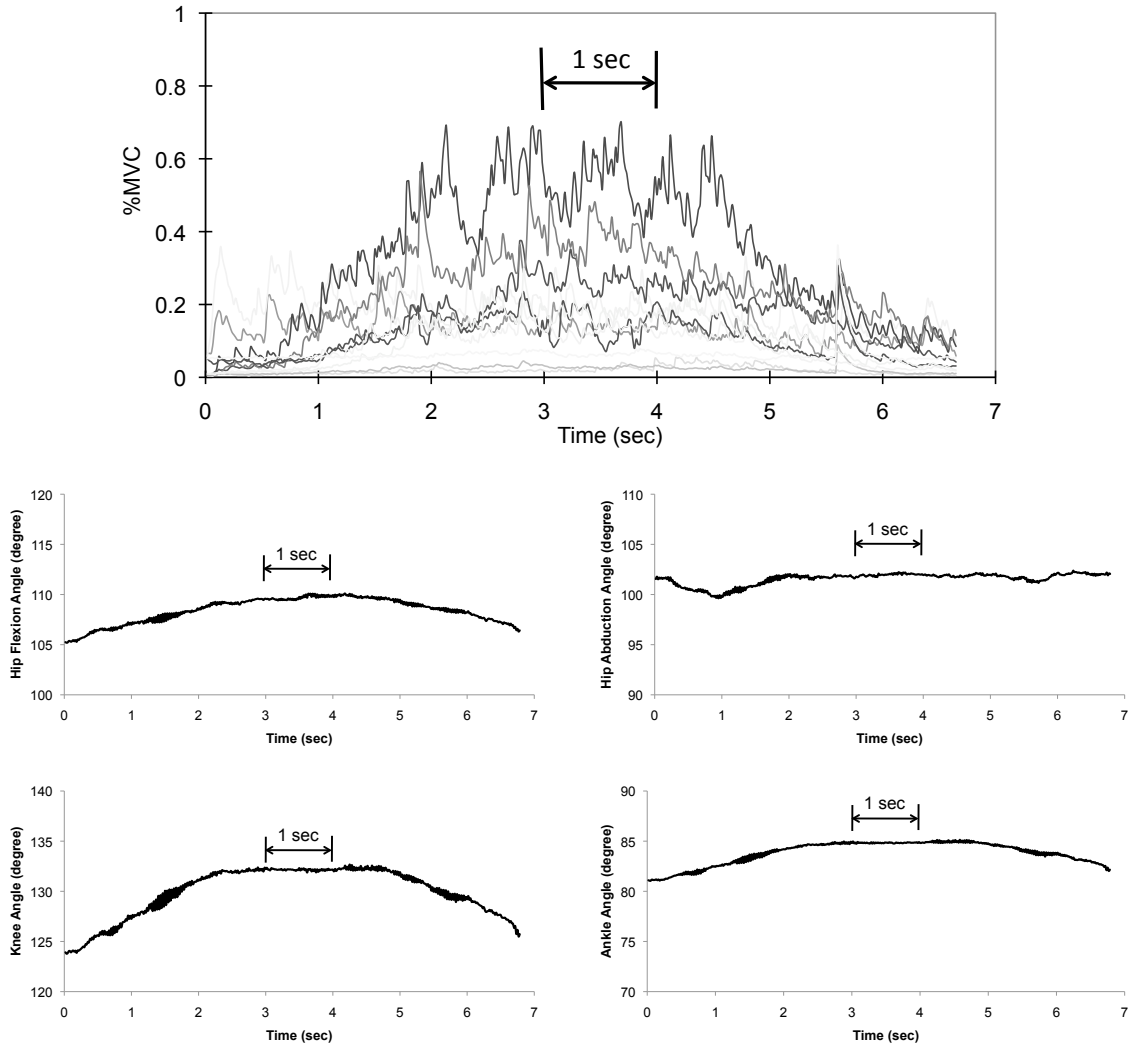

Figure 3-6. Typical EMG (top), hip flexion angle (middle left), hip abduction angle (middle right), knee angle (bottom left), and ankle angle (bottom right) histories illustrating the period used in the study.

3.3 RESULTS

Table 3-4 summarizes the subjects' skeletal segment dimensions calculated from the distances between joint centers. The distance between left and right hip joint centers, femur length, and leg length were calculated from the hip, knee, and ankle joint coordinates determined using methods developed by Reed et al. (1999). The average inter values for inter hip joint distance, femur length, and leg length are 16.7±1.4 cm, 42.8±2.2 cm, and 41.2±1.7 cm, respectively. These skeletal dimensions are very close to

the values of 16.4 cm, 43.2 cm, and 41.5 cm, respectively, reported by Schneider et al. (1983) for the midsized male.

Table 3-4. Summary of Subject Lower-Extremity Skeletal Dimensions

Subject #	Inter H-point distance (cm)	Femur Length (cm)	Leg Length (cm)
1	16.3	41.1	41.3
2	19.0	42.7	43.5
3	14.7	43.1	43.5
4	16.5	38.9	41.7
5	15.2	42.3	40.4
6	18.1	41.6	37.9
7	14.7	42.3	39.4
8	17.2	48.0	41.7
9	17.3	43.2	40.6
10	16.7	42.4	40.1
11	16.9	45.3	43.5
12	17.5	42.8	41.0
Mean	16.7	42.8	41.2
sd	1.4	2.2	1.7

The subjects' postures (i.e., hip, knee, and ankle angles) calculated from the detected marker locations at the body landmarks in all one-foot braking and two-foot bracing test are summarized in Appendix C. Figure 3-7 shows the average hip extension, hip abduction, knee extension, and ankle extension angles from the initial posture to the postures at maximum one-foot braking and two-foot bracing with initial knee angles of 120, 105, and 90 degrees. As can be seen, hip, knee, and ankle angles were increased (i.e., extension) with similar magnitudes for maximum one-foot braking and two-foot bracing tests. In particular, knee angles increased more than 10 degrees in all test conditions at maximum force exertion. Hip abduction angles were slightly reduced (i.e., thigh moved inward) in all test conditions but the hip tended to adduct more during two-foot bracing than during one–foot braking.

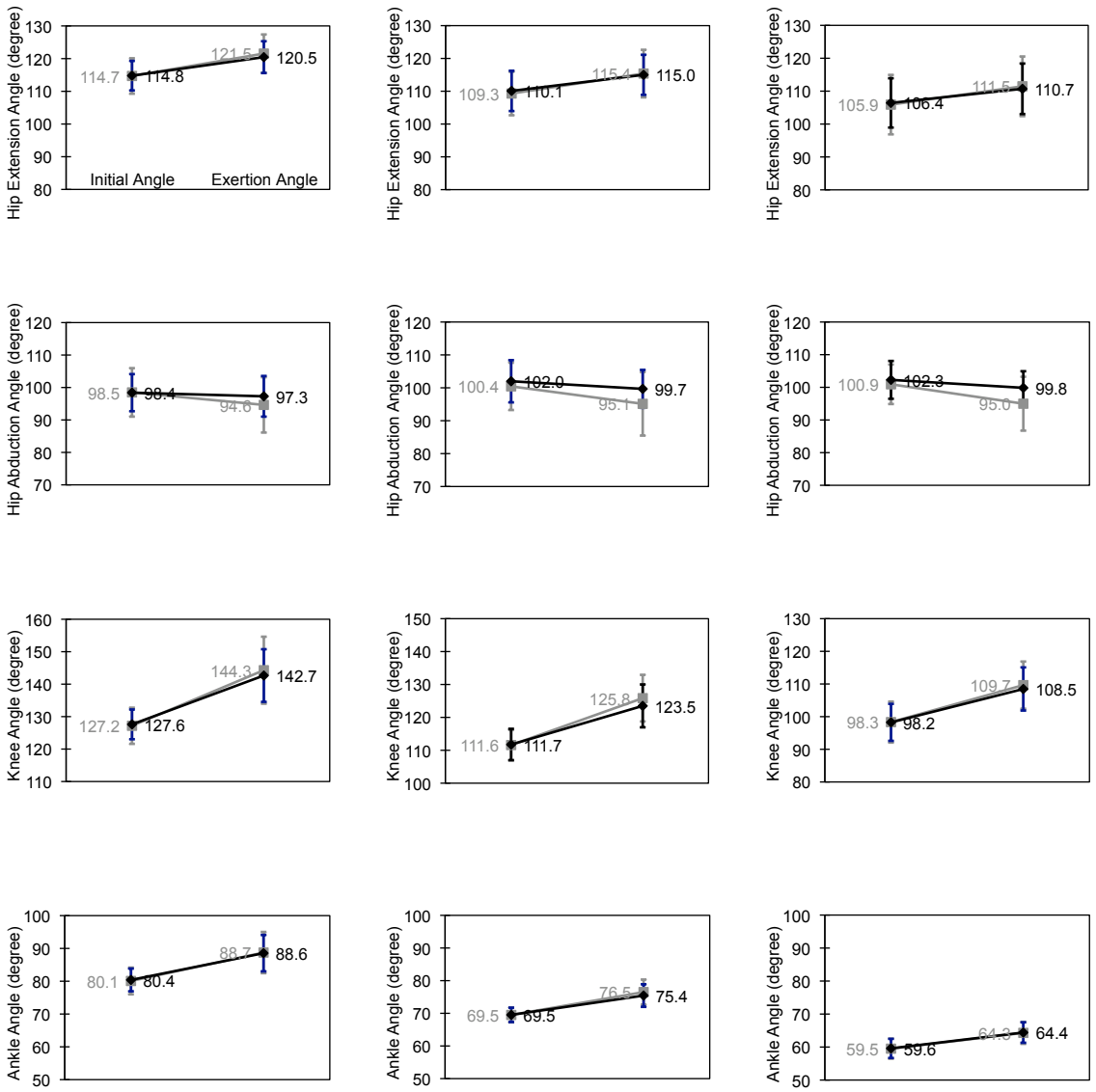

Figure 3-7. Changes in hip, knee, and ankle angles from initial positions to maximum exertion positions during one-foot braking tests (black lines) and two-foot bracing tests (gray lines).

Table 3-5 summarizes the results for maximum forces exerted in the MVC isometric tests. In general, the maximum force for any particular test condition varied widely across subjects. The maximum force exertion was greater in performing knee extension than in performing knee flexion for all subjects. Maximum force exertion for

hip abduction and hip adduction were similar, but forces in hip flexion and hip extension were different for most of the subjects.

Table 3-5. Summary of Peak Forces in Subject MVC Tests (Unit:N)

Subject #	Knee		Hip			
	Flexion	Extension	Flexion	Extension	Abduction	Adduction
1	471	828	449	1226	492	370
2	198	510	515	230	395	476
3	124	207	247	170	228	271
4	196	348	304	464	280	326
5	119	278	201	107	126	196
6	170	253	260	214	251	240
7	278	433	410	389	435	477
8	346	539	369	603	440	536
9	269	280	285	190	288	204
10	274	369	330	643	315	371
11	225	356	470	287	457	536
12	475	608	535	464	510	557
Mean	262	417	365	416	351	380
sd	119	178	111	309	120	134

The results for maximum force during one-foot maximum braking and two-foot maximum bracing tests are summarized in Table 3-6. The maximum braking and bracing forces varied widely across subjects. In general, the maximum force was slightly reduced with decreases in initial knee angle, both in braking and bracing tests. The average one-foot braking forces are 698±280 N, 675± 269 N, and 597±211 N for initial knee angles of 120°, 105° and 90°, respectively. The average two-foot bracing forces are 880±355 N, 859±334 N, and 768±220 N for initial knee angles of 120°, 105° and 90°, respectively. Maximum one-foot braking forces are similar to ~700N reported by other researchers who studied subjects performing maximum voluntary braking tests in a vehicle buck (Manning et al. 1998; Hardin et al. 2004).

Table 3-6. Summary of Peak Resultant Forces on Foot Plate During Maximum Braking and Bracing Tests

Subject #	One-Foot Braking Force (N)			Two-Foot Bracing Force (N)		
	Knee 120˚	Knee 105˚	Knee 90˚	Knee 120˚	Knee 105˚	Knee 90˚
1	847	743	732	945	943	880
2	805	701	664	1018	857	751
3	454	379	415	593	579	563
4	688	642	541	886	899	838
5	428	388	320	500	507	464
6	318	325	318	458	429	502
7	772	731	755	839	974	909
8	827	800	952	1305	1290	1146
9	412	458	347	406	523	481
10	799	933	679	943	987	917
11	668	724	611	1076	753	806
12	1359	1279	833	1592	1562	960
Mean	698	675	597	880	859	768
sd	280	269	211	355	334	220

Table 3-7 summarizes the average muscle activation levels in the MVC tests. As expected, most muscles showed significantly greater activation levels for direction of joint movement for which muscle activation has primary control. For example, the knee flexors, MG, LG, BFLH, and BFSH, had significant greater activation levels in knee flexion tests, and the knee extensors, RF, VL, and VM, produced greater activation levels in knee extension tests. Also, the hip adductor, AL, and hip abductors, GMED and GMAX, reached activation levels of more than 80% during hip-adduction and hip-abduction, respectively. Since ankle flexion and extension MVC tests were not performed, the activation levels for ankle flexor and extensor muscles (i.e., SOL and TA) in the MVC tests were all less than 50%. Maximum activation levels (i.e., 100%) of these muscles were taken from the maximum braking or bracing tests.

Table 3-7. Summary of Average Percentage of Maximum Muscle Activation in MVC Tests

Muscle Group	Knee		Hip			
	Flexion	Extension	Flexion	Extension	Abduction	Adduction
MG	95%	14%	24%	14%	16%	17%
LG	94%	10%	16%	6%	4%	7%
SOL	43%	26%	15%	18%	8%	8%
TA	26%	43%	35%	10%	9%	7%
RF	5%	84%	59%	9%	17%	11%
VL	7%	75%	13%	15%	6%	10%
VM	8%	69%	10%	21%	5%	10%
AL	81%	17%	77%	16%	8%	82%
BFLH	100%	14%	19%	26%	18%	22%
BFSH	83%	30%	45%	15%	34%	18%
GMED	21%	21%	39%	44%	93%	27%
GMAX	19%	15%	38%	44%	81%	21%

Figure 3-8 compares the average muscle activation levels during maximum one-foot braking and two-foot bracing tests for all subjects in all three postures. Individual subject muscle activation levels for all the braking and bracing tests are summarized in Appendix C. As can be seen in Figure 3-8, AL and BFLH were barely activated in the braking/bracing tests. Activation levels of the leg muscles (i.e., MG, LG, SOL, and TA) were slightly greater in maximum braking tests than in maximum bracing tests. However, for the thigh knee extensor muscles (i.e., RF, VL, and VM) and hip extensor muscles (i.e., GMED and GMAX), activation levels were approximately 25-30% greater in maximum one-foot braking tests than in maximum two-foot bracing tests. In addition, activation levels of TA, RF, VL, and VM increased with decreases in knee angle for all maximum and 50% maximum braking and bracing tests. All muscle activation levels in 50% maximum braking/bracing tests were approximately half the levels produced in the activation levels in maximum braking/bracing tests.

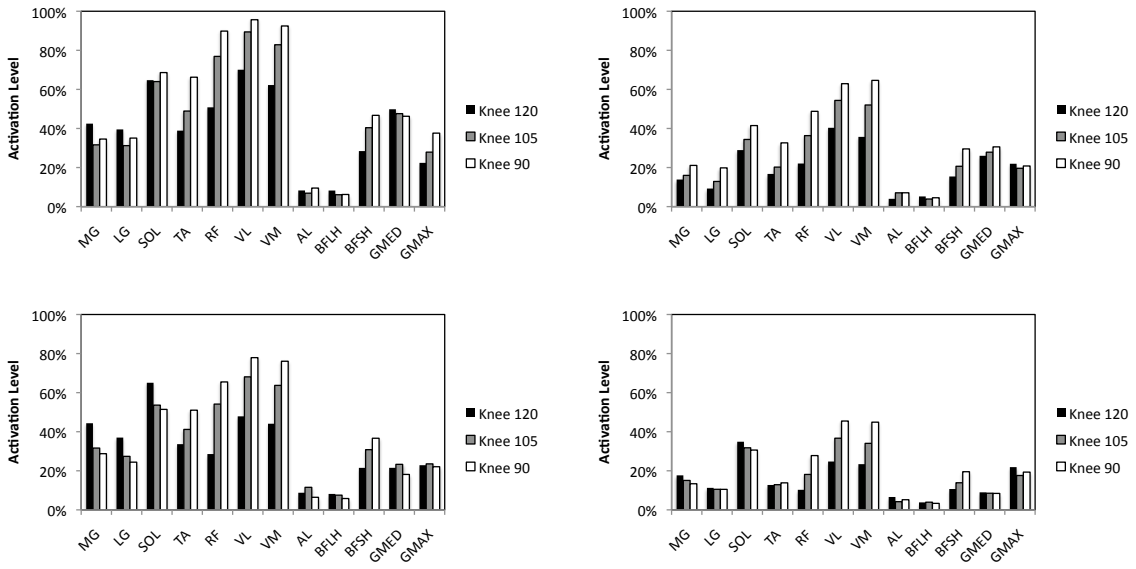

Figure 3-8. Comparisons of average muscle activation levels with knee angles 120, 105, and 90 degrees for maximum and 50% maximum one-foot braking tests (top left and right) and maximum and 50% maximum two-foot bracing tests (bottom left and right).

3.4 SUMMARY AND DISCUSSION

Activation levels of twelve major muscles in the hip and lower extremities for twelve midsize male subjects were recorded during isometric maximum and 50% of maximum force exertions on a foot plate during simulated one-foot braking and two-foot bracing using surface EMG electrodes. A motion capture system was used to determine and monitor subjects' postures during the tests. Six MVC tests were conducted to normalize the muscle activation levels of each muscle group obtained during braking and bracing tests. For both braking and bracing tests, the maximum force exerted on the force plate decreased with the decreasing knee angles. The average maximum one-foot braking forces are 698±280 N, 675± 269 N, and 597±211 N for initial knee angles of 120°, 105°, and 90°, respectively. Muscle activation levels were 25-30% greater in maximum one-foot braking tests than in maximum two-foot bracing tests, especially for the muscles in the thigh and hip.

From the testing results shown in Table 3-6, the maximum normal force exerted on the foot plate in braking and bracing tests varied widely across subjects, with the force

for the strongest subject being two to three times that for the weakest subject for the same task. There is no meaningful correlation between forces exerted on the footplate and subjects' stature or body weight for the sample of midsize male subjects of this study. The large differences in maximum braking and bracing force between subjects are therefore thought to be due to the differences of muscle strength between subjects of similar stature and weight and differences in subject's perception of maximum voluntary effort. These factors are supported by the results shown in Figure 3-9 that compares the maximum one-foot braking forces produced in the MVC tests for the twelve subjects. As indicated, there is a good correlation between the forces exerted in the braking and MVC tests (R^2 = 0.55-0.68), even for those MVC tests that have little relationship to the act of braking. A similar relationship was also found between forces in two-foot bracing tests and MVC tests. These results suggest that a subject who has greater muscle strength and/or a greater willingness to exert a maximum force will produce larger forces in both MVC tests and in braking and bracing tests.

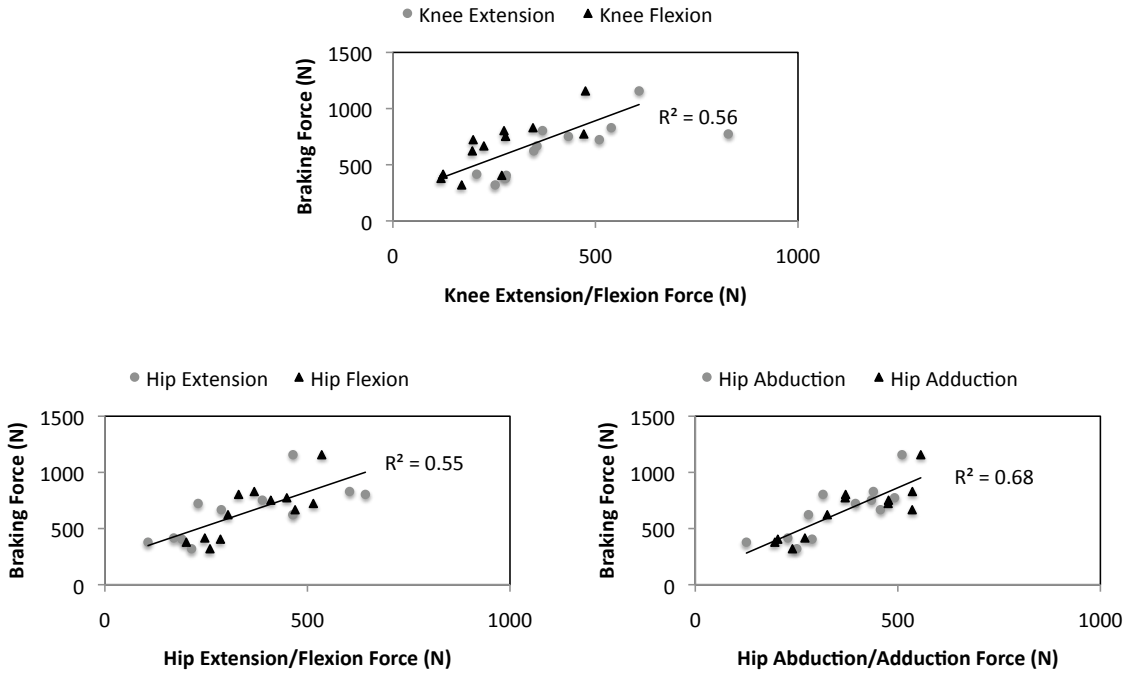

Figure 3-9. Comparisons of subject maximum braking forces with forces in MVC tests.

Since force is exerted by both feet, two-foot bracing might be expected to produce twice the force on the footplate as in one-foot braking. However, as shown in Figure 3-10, the average maximum two-foot bracing forces are only 26.1%, 27.1%, and 28.6% more than the average maximum one-foot braking forces with knee angles of 120°, 105° and 90°, respectively. This finding is agreed with observations of muscle activation levels, particularly for the muscles in the thigh. Table 3-8 compares the muscle activation levels of major muscles in the thigh during the maximum one-foot braking tests and the maximum two-foot bracing tests. As can be seen, thigh muscles were about 25-30% less activated during two-foot bracing than in one-foot braking. This decrease in thigh muscle activation levels during maximum two-foot bracing compared with maximum one-foot braking is probably from a neural mechanism, called "bilateral deficit", which has been associated with inhibition of the expression of maximum strength during two leg extensions (Howard and Enoka 1991; Koh et al. 1993; Schantz et al. 1989; Vandervoort et al. 1984) or two-foot jumps (van Soest et al. 1985; Vint and Hinrichs 1996). The cause of bilateral deficit is thought to be an inability of the central nervous system (CNS) to produce bilateral maximum activation of a large number of muscles simultaneously.

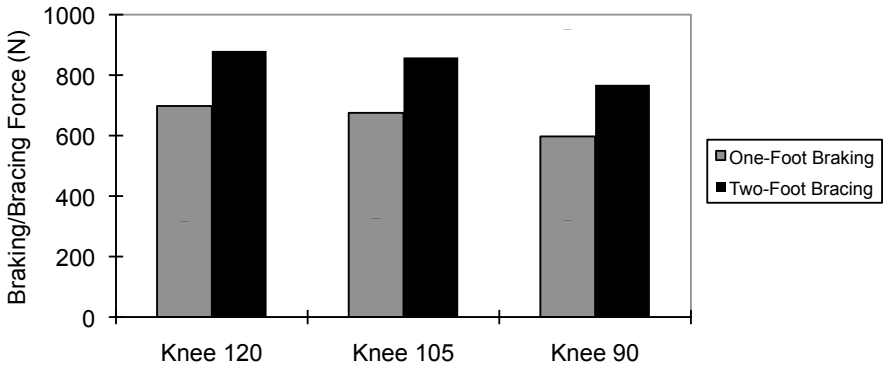

Figure 3-10. Average maximum one-foot braking and two-foot bracing forces from subject tests.

Table 3-8. RF, VL, and VM Muscle Activation Levels in Maximum One-Foot Braking and Two-Foot Bracing Tests

	RF		VL		VM	
	One-foot	Two-foot	One-foot	Two-foot	One-foot	Two-foot
Knee 120°	0.51	0.29	0.70	0.48	0.62	0.44
Knee 105°	0.77	0.54	0.89	0.68	0.83	0.64
Knee 90°	0.90	0.65	0.96	0.78	0.92	0.76

The results in Figure 3-7 show that subjects tended to extend hip, knee, and ankle joints during braking and bracing. As a result, and as expected, the hip, knee, and ankle extensors (i.e., MG, LG, SOL, RF, VL, and VM) were significantly activated during braking and bracing. However, as shown in Figure 3-8, muscles that produce knee, hip, and ankle flexion (the ankle flexor, TA, and knee flexor, BFSH) were also substantially activated, or co-contracted. However, co-contractions of TA and BFSH were not observed in all the subjects. Figure 3-11 compares numbers of subject TA and BFSH in different activation level groups in the braking and bracing tests. Three of the twelve subjects had activation levels of TA below 0.2 in maximum braking and bracing tests. However, four subjects produced activation levels in these muscles greater than 0.6 in maximum braking and bracing tests. More than half of the subjects produced low activation levels in TA and BFSH in 50% maximum braking and bracing tests. The differences of activations of antagonistic muscles between subjects suggest that the occurrence of muscle co-contraction is likely depended on the strategy that subjects used to perform braking and bracing.

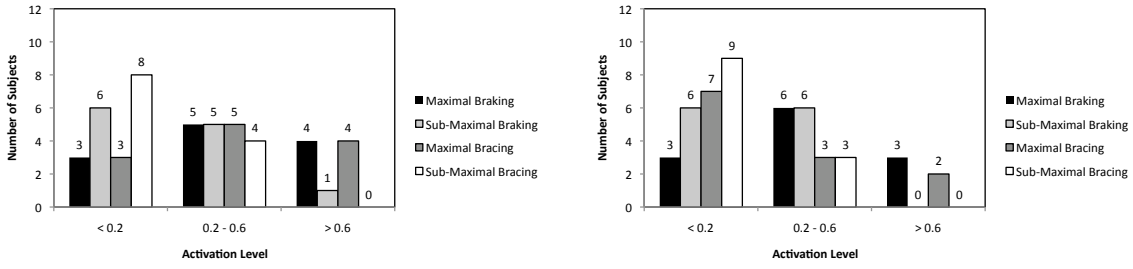

Figure 3-11. Numbers of subject TA (left) and BFSH (right) in different groups of activation levels in the braking and bracing tests.

It has been shown that surface EMG measurements are sensitive to several factors other than muscle activation level. For example, muscle fatigue, electrode placement, muscle crosstalk, and anatomical differences between subjects (Cram and Kasman 1998) can affect muscle EMG measurements. One of the most common methods to minimize the effects of these factors is to normalize the muscle activations using the EMG signals from the MVC tests. In this study, MVC tests for six different isometric exertions of the hip and knee joints were conducted. However, several factors might influence the accuracy of the MVC test results. For example, it is possible that different subjects may have different levels of willingness to exert maximum efforts. Also, since each MVC test was performed for a single posture for each test, the potential of each muscle to show greatest muscle strength might not have been obtained from the MVC tests performed in this study.

CHAPTER 4
ESTIMATING HIP AND LOWER-EXTREMITY MUSCLE FORCES DURING ONE-FOOT BRAKING AND TWO-FOOT BRACING

4.1 OVERVIEW AND APPROACH

Figure 4-1 shows the process that was used to estimate forces in all 35 muscles in each lower extremity during simulated emergency one-foot braking and two-foot bracing. A three-dimensional musculoskeletal modeling system, called the AnyBody Model (AnyBody Technology A/S, Aalborg, Denmark), was used to predict muscle forces. This model uses an inverse dynamics approach combined with an optimization scheme that is based on minimizing maximal muscle activation (i.e., normalized muscle force).

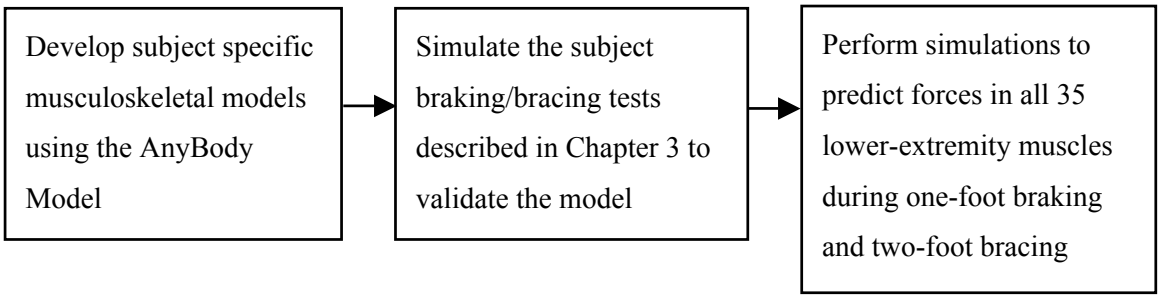

Figure 4-1. Process used to estimate lower-extremity muscle forces while emergency braking/bracing.

Because subject muscle and body segment lengths differ from the baseline values used in the AnyBody Model, inter H-point distance, femur length, and leg length in the AnyBody Model were scaled to match experimental measurements for each subject being simulated. For a similar reason, the maximum force-generating capacities of the lower-

extremity muscles in the AnyBody Model were also scaled to match values derived from the maximum voluntary contraction (MVC) EMG data based on the muscle activation data measured in the MVC tests as described in Chapter 3. After the model was adjusted and validated, it was used to predict complete lower-extremity muscle forces of the midsize male during emergency braking and bracing in different postures (i.e., different knee angles).

To ensure the muscle forces predicted by the model are appropriate for braking or bracing, it was necessary to validate the ability of the AnyBody Model to predict muscle activation during braking and bracing. To do this, the model was used to simulate each of the experimental braking and bracing tasks described in Chapter 3, and the percentage muscle activations predicted for 12 muscles in these simulations were compared to muscle activation levels for these muscles based on experimental EMG data. Each one-foot braking or two-foot bracing task performed by each subject was simulated separately.

4.2 ANYBODY MODEL BACKGROUND

The AnyBody Model is a commercial software package that combines a solver for the multi-body inverse dynamics problem with optimization algorithms to solve the muscle-recruitment problem (Rasmussen et al. 2003). Figure 4-2 shows the whole-body musculoskeletal model used in this study. Each lower extremity contains four rigid bodies, including the pelvis, the femur, the leg, and the foot. These rigid bodies are connected by the hip, knee, and ankle joints, which are modeled with three degrees of freedom (DOF) (external/internal rotation, abduction/adduction, and extension/flexion), one DOF (extension/flexion), and two DOF (plantar/dosiflexion and eversion/inversion), respectively.

This model is equipped with 35 Hill-type muscles in each lower extremity with muscle geometry, strength (i.e., the maximum force generating capacities), and passive/active force-stretch characteristics obtained from Delp (1990). The model uses

the same muscle geometry (i.e., origins, insertions, and muscle path) that was used in the development of the LX FE Model described in Chapter 2.

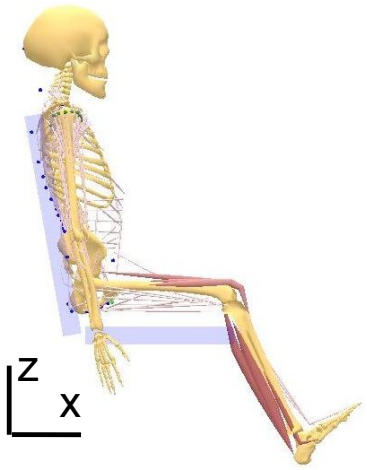

Figure 4-2. Side view of the AnyBody Model as configured for use in this study.

Muscle forces for a given task are calculated using a min/max optimization procedure in AnyBody (Rasmussen et al. 2001), where the overall activation of muscles for a given task is minimized. Physiologically, this optimization function that minimizes normalized muscle forces is similar to minimizing muscle fatigue (Dul et al., 1984). This is because the largest relative load on any muscle in the system is minimized, thereby postponing fatigue of any muscle. A solution to the optimization problem is achieved through an iterative technique, and a Numerical Recipe (NR) Simplex approach (Press et al. 2002). The optimization function is:

Minimize Max (f_i/N_i) equation 4-1

Subject to:

$C\boldsymbol{f}=d$ equation 4-2

$0 \leq f_i/N_i \leq 1,\ i=1,\ \ldots,\ 35$ equation 4-3

where f_i and N_i are the muscle force and muscle strength for the *ith* muscle, respectively. Equation 4-2 is the equilibrium equation, where C is the coefficient matrix for the unknown muscle forces and d is the known applied loads and inertia forces. It serves to balance to exterior loads from the solution of muscle recruitment. Equation 4-3 ensures non-negativity constraints on the muscle forces (i.e., muscles can only pull, not push) and that all muscle forces are less than or equal to their strength.

4.3 DEVELOPMENT OF SUBJECT-SPECIFIC MODELS

The skeletal geometry and the muscle model used in the AnyBody Model are based on data from a single midsize male (Delp 1990). However, the skeletal geometry of different midsize males as well as the force generating capacities (i.e., strengths) of each individual's muscles will differ from those used in the baseline AnyBody Model. Therefore, to use the baseline AnyBody Model to simulate the braking and bracing performed by subjects tested in this study, it is necessary to adjust the model geometry and the muscle strengths to match those of the subjects. To do this, twelve different configurations of the Anybody Model were developed by adjusting the lower-extremity dimensions of the AnyBody Model to match each subject. This was accomplished by first adjusting the dimensions of the model so that the distances between right and left hip joints, between the hip and knee joints, and between the knee and ankle joints matched the measured individual subject's inter H-point distance, femur length, and leg length, respectively. These values are summarized in Table 3-4 for each subject. Locations of the origin and insertion sites of the muscles were then scaled in proportion to the changes in model geometry.

The maximum force generating capacities of the lower-extremity muscles in these subject-specific musculoskeletal models were then "tuned" for each subject by equating the maximum force generating capacity of a muscle to the force predicted in the simulation of the subject's 100% MVC test for that muscle. This was done by simulating those tests that produced the maximum EMG level for each MVC-tested muscle using the baseline Anybody Model. For each simulation that produced 100% activation of each

muscle in the test, the muscle activation predicted in the simulation was used to determine the muscle "strength" adjustment ratio. For example, 100% activation of the Adductor Longus (AL) of Subject #1 was obtained from the hip-adduction MVC test. However, simulation of Subject #1 hip-adduction MVC test using the baseline AnyBody Model showed that only 68% of AL activation was required to produce Subject #1's hip-adduction force, so that the muscle "strength" of Subject #1 AL is 68% of that for the AL muscle in the baseline AnyBody Model.

The next step in developing subject specific AnyBody Models was to divide the 35 muscles in the hip and lower extremities into four groups based on the joint motions that the muscles tend to produce, as summarized in Table 4-1. These four groups include knee extensors, knee flexors, hip adductors, and hip abductors. Scale factors for each muscle group were determined by averaging the subject-specific strength ratios determined from the simulations of the 100% MVC tests for that muscle group. For example, a scale factor for the knee flexors was determined by averaging the ratios of the forces in subject-specific simulations of tests that produced 100% MVC of the BFLH and BFSH divided by each muscle's maximum force-generating capacity. These scale factors were then applied to the strengths of all of the muscles in the baseline AnyBody model that are contained in the muscle group associated with the scale factor.

Table 4-1. Muscle Groups Used to Adjust Muscle Strength in the Hip and Lower Extremities

Group	Muscles from AnyBody Model Muscle Group	EMG Name for Muscle Group
Knee Flexors	semitendinosus, semimembranosus, biceps femoris long head, biceps femoris short head, sartorius, gracilis, soleus, gastrocnemius, flexor digitorum longus, flexor hallucis longus, tibialis posterior, peroneus brevis	BFLH, BFSH
Knee Extensors	vastus lateralis, vastus medialis, vastus intermedius, rectus femoris, iliopsoas, tibialis anterior, extensor digitorum longus, extensor hallucis longus	VM, VL, RF
Hip Abductors	all gluteus minimus, all gluteus medius, all gluteus maximus, tensor fasciae latae	GMED, GMAX
Hip Adductors	adductor longus, all adductor magnus	AL

Because EMG-based MVC measurements of subjects tested in this study were not obtained for ankle extension and flexion (i.e., doriflexion and plantar flexion of the foot), muscles that mainly plantar flex or dorsiflex the foot were adjusted using the same scale factor that was used for the knee flexors or extensors in the lower extremities. That is, the strengths of the soleus, gastrocnemius, flexor digitorum longus, flexor hallucis longus, tibialis posterior, and the peroneus brevis (i.e., the muscles that produce foot doriflexion) were adjusted using the same scale factor as for the knee flexor group, and the strengths of the tibialis anterior, extensor digitorum longus, and the extensor hallucis longus (i.e., the muscles that produce plantar flexion) were adjusted using the scale factor for the knee extensors.

Table 4-2 summarizes the ratios used to adjust the muscle strengths from the baseline AnyBody model for each muscle group of each subject. The results of MVC simulations to obtain these adjustment ratios are summarized in Appendix D. In general, the adjustment ratios for the four muscle groups are similar for each subject and the muscle strengths for most subjects are lower than those used in the baseline AnyBody.

Table 4-2. Adjustment Ratio of Subject Muscle Strength

Subject #	Knee Flexor	Knee Extensor	Hip Abductor	Hip Adductor
1	1.18	1.25	0.66	0.68
2	0.54	0.77	0.69	0.76
3	0.37	0.37	0.48	0.53
4	0.51	0.58	0.43	0.51
5	0.23	0.45	0.28	0.31
6	0.31	0.23	0.34	0.35
7	0.68	0.69	0.77	0.81
8	0.82	0.65	0.72	0.88
9	0.60	0.33	0.35	0.34
10	0.61	0.45	0.55	0.59
11	0.52	0.50	0.47	0.47
12	1.10	0.46	0.91	0.89

4.4 MODEL VALIDATION

After subject-specific models were developed, simulations of the maximum and 50% maximum one-foot braking and two-foot bracing tests described in Chapter 3 for each subject were performed to "validate" each of the subject-specific models. A total of 144 simulations were performed using data from the twelve maximum and 50% of maximum braking/bracing conditions (Table 3-3) from each of the twelve subjects. For all of these simulations, nodes at the most posterior points of the spine and pelvis were used to constrain the torso angle to match the seatback angle used in the tests described in Chapter 3. Subject posture in each trial was determined by inputting the hip, knee, and ankle angles measured by the VICON motion-capture system at the time producing peak force as reported in Appendix C. Peak braking and bracing forces and torques on the footplate were applied at the foot-ground joint located at the approximate geometric center of each foot, and included forces along the x-axis (fore-aft) and z-axis (vertical), and torque about the y-axis (lateral), as illustrated in Figure 4-3. It was assumed that the measured forces and torques were evenly split between left and right feet in two-foot bracing tests and were only applied to the right foot in one-foot braking tests.

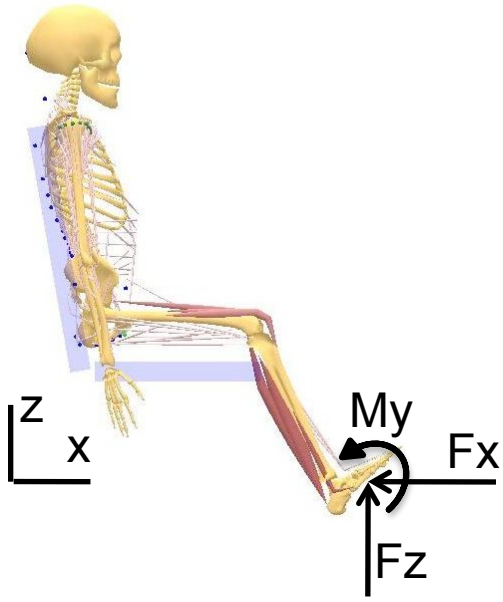

Figure 4-3. Illustration of boundary forces and moment in the subject-specific AnyBody model.

The measured torque about the y-axis was determined by multiplying the measured normal force by the distance between the center of the applied force and the horizontal centerline of the force plate, as shown in Figure 4-4. The distance between the force center and force plate centerline depended on both the foot position and braking/bracing strategies of each subject. For example, some subjects tended to perform braking/bracing with the applied force concentrated near the ball of the foot but other subjects tended to exert force concentrated near the heel. These differences could account for differences in subject strategies and subject strengths. In the AnyBody Model, the braking/bracing forces were applied at the geometric center of the foot (i.e., foot-ground joint in the AnyBody Model). Since the geometric center of the foot was not located at the centerline of the force plate for each subject and each trial, a correction between measured torque and torque at the foot center was applied, as shown in Figure 4-3 and equation 4-4:

$$M_{y'} = M_y - D_{foot} \times F_{normal} \qquad \text{equation 4-4}$$

where $M_{y'}$ is the estimated torque at foot center, M_y is the measured torque at the y-axis, D_{foot} is the distance between the foot center and force plate centerline, and F_{normal} is the measured normal force on the foot plate. D_{foot} is estimated from the marker locations on the force plate and the subject's foot. The exerted forces and adjusted torques for all simulations are summarized in Appendix C.

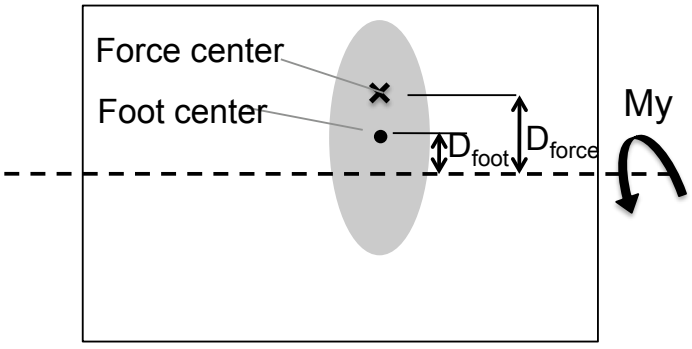

Figure 4-4. Illustration of foot location on the force plate (shaded area), the geometric center of the foot, the center of applied force, and the distances to the horizontal centerline of the force plate.

Predicted muscle-activation levels from the subject specific models were calculated and compared to the activation levels of the twelve major muscles in the hip and lower extremities measured using the surface EMGs described in Chapter 3. The predicted muscle activation level for each muscle was determined by dividing the predicted muscle force by the muscle's maximum force-generating capacity or strength. Figure 4-5 shows the comparisons between the predicted and measured activation levels for the twelve muscles from which EMG data were measured for all maximal and sub-maximal (50% of maximum) braking and bracing trials. Predicted and experimentally measured muscle-activation levels are qualitatively similar for ankle and knee extensors MG, LG, SOL, RF, VL, and VM. However, the antagonistic muscles, TA, BFLH, and BFSH, which are knee dorsiflexion and knee flexion muscles, were barely activated by the AnyBody Model. The model also predicted smaller activations for the hip abductor muscles, GMAX and GMED, than indicated by the experimental EMG measurements. These results suggest that the subject-specific AnyBody models reasonably predict activations of agonist joint extensor muscles but not the antagonistic joint flexor muscles for simulations of braking and bracing.

4.5 ESTIMATE OF MUSCLE FORCES WHILE EMERGENCY BRAKING AND BRACING

To estimate muscle forces in the hip and lower extremities during emergency braking and bracing, simulations were performed using the model geometry set to match the average weight, stature, and lower-extremity dimensions from the twelve subjects that participated in the tests (Table 3-1 and Table 3-4). Muscle strength was tuned using the scale factors averaged from all twelve subjects, as shown in Table 4-2. Simulations performed include the maximal one-foot braking and two-foot bracing at knee angles of 120°, 105°, and 90°. The averaged postures and braking/bracing forces and torques for the twelve subjects were used and are listed in Table 4-3.

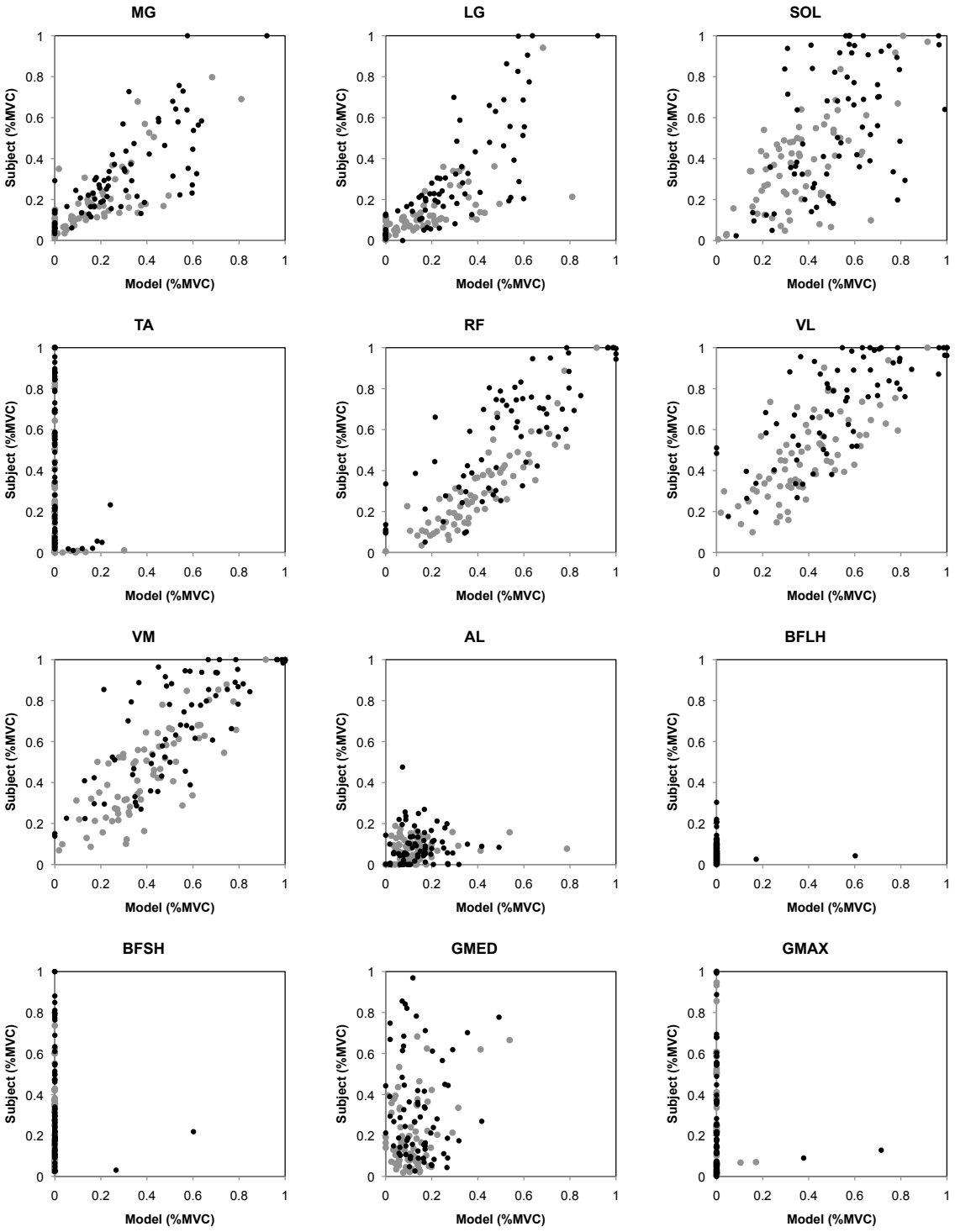

Figure 4-5. Comparisons of measured (vertical-axis) and predicted (horizontal-axis) muscle activations in maximal (black points) and sub-maximal (gray points) one-foot braking and two-foot bracing.

Table 4-3. Average Posture and Exerted Forces and Moments for 12 Subjects in Maximum One-Foot Braking and Two-Foot Bracing Tests

	One-foot braking			Two-foot bracing		
Posture	Knee 120°	Knee 105°	Knee 90°	Knee 120°	Knee 105°	Knee 90°
Hip extension angle	121.5°	115.4°	111.5°	120.5°	115.0°	110.7°
Hip abduction angle	94.6°	95.1°	95.0°	97.3°	99.7°	99.9°
Knee angle	144.3°	125.8°	109.7°	142.7°	123.5°	108.5°
Ankle angle	88.7°	76.5°	64.3°	88.6°	75.4°	64.4°
X-axis force (N)	603.1	564.6	478.3	781.6	733.8	636.5
Y-axis force (N)	347.6	366.9	356.1	398.0	439.5	424.0
Z-axis torque (Nm)	33.6	33.2	28.2	71.6	58.8	46.6

Table 4-4 summarizes the predicted muscle forces in the hip and lower extremities from the simulations of maximal one-foot braking and two-foot bracing for different postures. As can be seen, the antagonistic muscles are not activated in any simulations and muscle forces are greater in one-foot braking than two-foot bracing. This is because the braking forces exerted by the right foot in one-foot braking tests were greater than half of the net braking force produced in the two-foot bracing tests. Forces of the ankle plantar flexors (i.e., soleus, tibialis posterior, and peroneus brevis) and knee extensors (i.e., vastus lateralis, vastus medialis, vastus intermedius, and rectus femoris) increased with decreasing of knee angle. However, forces in both hip adductors (i.e., adductor longus and adductor magnus) and abductors (i.e., gluteus minimus and gluteus medius) decreased with decreasing knee angle.

Table 4-4. Predicted Muscle Forces (N) in Maximum One-Foot Braking and Two-Foot Bracing with Knee Angles of 120°, 105°, and 90°

	One-foot braking			Two-foot bracing		
Muscle	Knee 120°	Knee 105°	Knee 90°	Knee 120°	Knee 105°	Knee 90°
Soleus	787.0	1200.0	1630.0	667.0	853.0	1110.0
Gastrocnemius	446.0	276.0	137.0	378.0	261.0	108.0
Flexor Digitorum Longus	0.0	0.0	0.0	0.0	0.0	0.0
Flexor Hallucis Longus	89.0	135.0	0.0	75.4	96.4	0.0
Tibialis Posterior	85.7	94.7	174.0	24.3	46.2	113.0
Peroneus Brevis	97.3	148.0	201.0	82.5	105.0	138.0
Tibialis Anterior	0.0	0.0	0.0	0.0	0.0	0.0
Extensor Digitorum Longus	0.0	0.0	0.0	0.0	0.0	0.0
Extensor Hallucis Longus	0.0	0.0	0.0	0.0	0.0	0.0
Sartorius	0.0	0.0	0.0	0.0	0.0	0.0
Gracilis	0.0	0.0	0.0	0.0	0.0	0.0
Vastus Lateralis	324.0	713.0	972.0	233.0	509.0	665.0
Vastus Medialis	224.0	494.0	673.0	161.0	353.0	461.0
Vastus Intermedius	214.0	471.0	642.0	154.0	336.0	439.0
Rectus Femoris	135.0	298.0	405.0	97.1	212.0	277.0
Semitendinosus	0.0	0.0	0.0	0.0	0.0	0.0
Semimembranosus	0.0	0.0	0.0	0.0	0.0	0.0
Biceps Femoris Caput Longum	0.0	0.0	0.0	0.0	0.0	0.0
Biceps Femoris Caput Breve	0.0	0.0	0.0	0.0	0.0	0.0
Iliopsoas	84.2	65.3	46.2	100.0	77.1	50.0
Adductor Longus	41.6	32.3	22.8	49.5	38.1	24.7
Adductor Magnus 1	0.0	0.0	0.0	0.0	0.0	0.0
Adductor Magnus 2	30.7	23.8	16.9	36.5	28.1	18.2
Adductor Magnus 3	44.1	34.2	24.2	52.5	40.4	26.2
Gluteus Minimus 1	18.6	14.4	10.2	22.1	17.0	11.0
Gluteus Minimus 2	19.6	15.2	10.8	23.4	18.0	11.7
Gluteus Minimus 3	22.2	17.2	12.2	26.4	20.3	12.2
Gluteus Medius 1	56.9	44.1	31.2	67.6	52.1	33.8
Gluteus Medius 2	39.3	30.5	21.6	46.7	36.0	23.3
Gluteus Medius 3	45.0	34.9	24.7	53.5	41.2	26.7
Gluteus Maximus 1	0.0	0.0	0.0	0.0	0.0	0.0
Gluteus Maximus 2	0.0	0.0	0.0	0.0	0.0	0.0
Gluteus Maximus 3	0.0	0.0	0.0	0.0	0.0	0.0
Tensor Fasciae Latae	0.0	0.0	0.0	0.0	0.0	0.0
Piriformis	0.0	0.0	0.0	0.0	0.0	0.0

4.6 SUMMARY AND DISCUSSION

This chapter describes the validation of the AnyBody model and its use to predict muscle forces in simulations of emergency vehicle one-foot braking and two-foot bracing. Validation of the model was performed using subject specific lower-extremity dimensions and muscle strengths. In general, model predictions show good agreement with the activation data of the agonist muscles measured from the EMG. However, the

model does not predict activations of antagonistic muscles. Estimated muscle forces from 35 muscles in each side of the hip and lower extremities during maximum one-foot braking and two-foot bracing were determined.

Because the maximum force generating capacities of subjects varied and were different from the baseline values used by the AnyBody model, simulations of experimental trials where individual maximum muscle activations in the hip and thigh occurred were used to adjust muscle strengths for each individual. There are several possible reasons why most of the subjects showed lower muscle strengths than those in the baseline AnyBody model. First, peak muscle activations measured experimentally may not actually represent maximum force generating capacity. In other words, the subjects' maximum efforts might have been limited by fear of being injured. Second, the muscle strength values used in the AnyBody are based on Delp (1990) reported by Friederich and Brand (1990) and Wickiewicz et al. (1983). These data are based on experiments performed using a limited number of subjects, which may not produce a reliable estimate of the average midsize male muscle strengths.

Comparisons of predicted and measured muscle activation levels were made in the model validation to ensure that the model can reasonably predict muscle forces during one-foot braking and two-foot bracing. These comparisons are based on the assumption of a linear relationship between muscle force and EMG data, which may or may not be reasonable. Most studies have found that there is a linear relationship between the amplitude of the EMG data and the muscle force during isometric contractions (Bigland and Lippold 1954; Hof 1984; Karlsson and Gerdle 2001; Bogey et al. 2005). However, some researchers report nonlinear relationships between the surface EMG and the tension produced by a muscle (Komi and Buskirk 1970; Bigland 1981). The nonlinear relationship between muscle force and EMG data is likely due to muscle fatigue, which reduces the force produced by individual muscle fibers. Muscle fatigue shifts distribution of frequency spectra lower. This results in more muscle fibers being recruited to perform a task and thereby increases the amplitude of the EMG (Hagg et al. 2000).

CHAPTER 5
SIMULATIONS WITH THE LX FE MODEL TO EVALUATE THE EFFECTS OF MUSCLE FORCES ON KTH INJURIES IN FRONTAL IMPACTS

5.1 OVERVIEW

As described in Chapter 1, it was hypothesized that muscle tension has the potential to alter the stress and strain distributions in the KTH complex produced during knee-impact loading by increasing the axial compressive forces in the KTH complex and by increasing or decreasing the bending moments in the curved shaft of the femur. Muscle tension may also affect the force transmitted through the KTH by altering the muscle mass coupling distal or proximal to the hip. To test this hypothesis, this chapter describes simulations to study the effects of muscle tension on the risk and location of KTH injury from loading to the anterior surface of the flexed knee. Figure 5-1 illustrates the approach used in this study. Pairs of frontal knee impact simulations were performed using the LX FE Model described in Chapter 2 with and without the lower-extremity muscle forces for maximum one-foot braking reported in Chapter 4. These simulations included different knee-to-knee-bolster loading conditions in which a stationary whole-body model was impacted by different combinations of impact interface stiffness and impact speed. In one set of simulations, the fracture functions were turned off and the risks of knee, femoral shaft, and hip injury were evaluated by applying the predicted peak knee and hip forces and femur bending moments to KTH injury risk formulations reported in the literature. These simulations allowed the model to predict high injury risks, since fracture of the model will affect force transmitted through the KTH and bending moment of the femur. In a second set of simulations, the fracture functions with Tsai-Wu fracture criterion were turned on in an attempt to estimate the effects of combined loading on cortical bone failure, which cannot be done with existing injury risk

curves that are based on a single mode of loading. Results of two sets of simulations are compared and discussed.

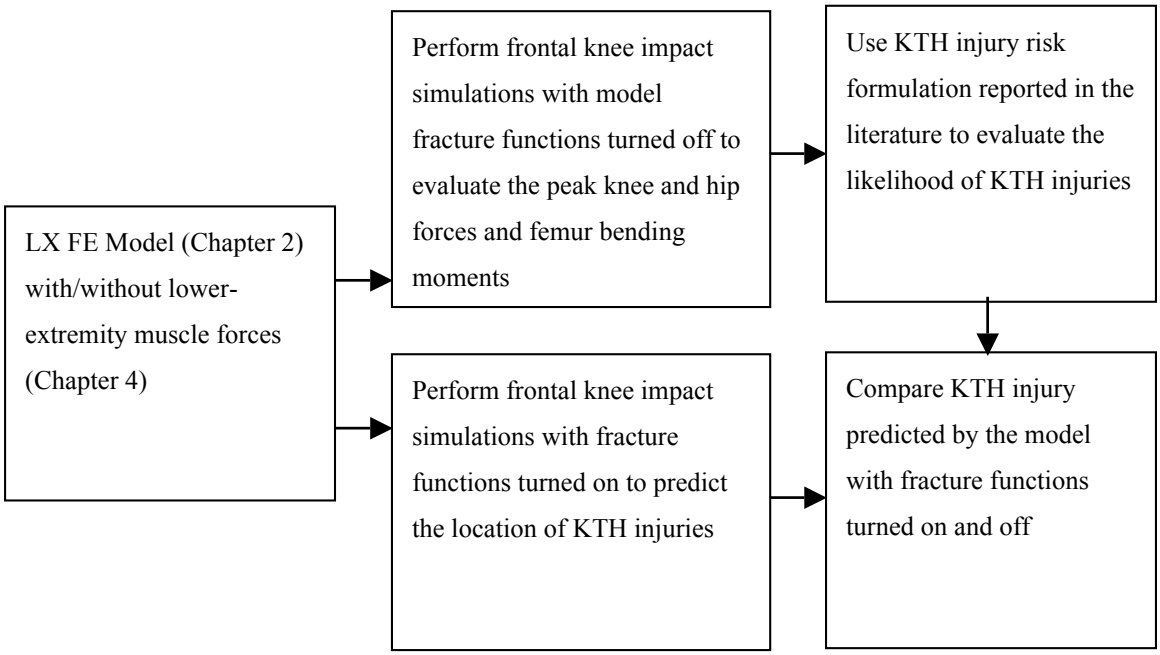

Figure 5-1. Approach used to study effects of muscle forces on KTH injuries.

5.2 METHODS

5.2.1 General Simulation Conditions

In all simulations, the knees of the LX FE Model were symmetrically impacted by a flat impactor with 100 mm of padded interface. This padding was modeled using a highly compressible low density foam material model (Material type 57, MAT_LOW_DENSITY_FOAM). In the simulations with muscle tension, muscle forces in the right hip and thigh from maximum one-foot braking (Table 4-4) were applied to both lower extremities since this condition simulates the largest possible effect of muscle tension on KTH injury. Identical muscle forces were applied to both lower extremities to prevent instability of the model responses due to the non-symmetric conditions. A 90˚ knee angle was used in all simulations based on estimates by Rupp et al. (2007) that this

represents the average knee angle at the time of knee-to-knee-bolster impact in frontal crashes.

Muscle activations were applied using a ramp function that increased muscle forces from zero to the target muscle activation level over a 30-ms time period prior to knee impact (Figure 5-2). This ramp function was used because it is more physiologically representative of the way muscle tension develops and because it reduces oscillations in bone stresses in the KTH compared to the oscillations that result when muscle forces are applied using a step function. The target muscle activation level was determined by dividing the input muscle force (i.e., individual muscle forces during maximum one-foot braking at knee angle of 90˚) by the individual muscle strength values in Appendix A. Muscle activations were maintained at the target level throughout knee loading.

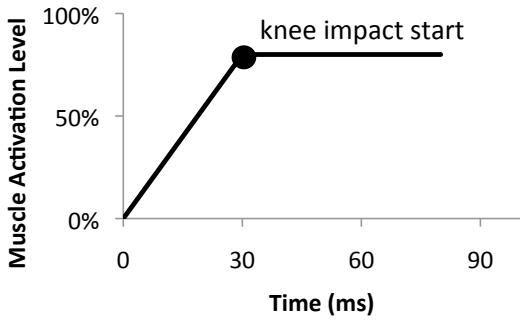

Figure 5-2. Muscle activation time profile.

5.2.2 Effects of Muscle Tension on KTH Injury Risk Based on Force Levels and Injury Risk Curves

In simulations to predict KTH injury risk, the fracture functions were turned off so that the relative risks of knee, femur, and hip injury could be predicted without being affected by element deletion. Simulations were performed for different combinations of impactor padding stiffness and impact velocity as listed in Table 5-1. These values were selected to produce knee, thigh, and hip injury risks that range from 5% to 95%. Peak

knee impact forces produced were between 5 and 18 kN and knee impact velocities ranged from 3 m/s to 9 m/s. Knee impact simulations in the range of these peak applied forces and loading rates are similar to those produced in FMVSS 208 and New Car Assessment Program (NCAP) frontal crash tests.

Table 5-1. Knee-Impact Conditions for the Simulations With and Without Muscle Tension

Impact Interface Modulus (MPa)	Impact Velocity (m/s)
6	3, 4, 5, 6, 7, 8, 9
8	3, 4, 5, 6, 7, 8, 9
10	3, 4, 5, 6, 7, 8
12	3, 4, 5, 6, 7, 8
14	3, 4, 5, 6, 7, 8
16	3, 4, 5, 6, 7, 8
18	3, 4, 5, 6, 7
20	3, 4, 5, 6, 7

To evaluate the risk of knee, thigh, and hip injuries in these simulations, the predicted peak knee and hip forces and peak femur bending moments from the simulations with and without muscle tension were applied to the knee injury risk curve (equation 5-1) reported by Rupp and Flannagan (2009), the hip injury risk curve reported by Rupp et al. (2008) (equations 5-2), and the femur injury risk curve reported by Kennedy et al. (2004) (equation 5-3). The predicted knee and hip force histories were calculated from the contact forces between impactor and knee, and femoral head and acetabulum, respectively. The predicted distal femur force and femur bending moment histories were determined by taking the net forces and bending moments at the cross sections of the femoral condyle and mid-shaft, respectively, that are perpendicular to the long axis of the femur.

$$Risk\ (knee\ injury) = 1 - Exp\left[-Exp\left[\frac{\ln(force) - 2.514}{0.2611}\right]\right] \quad \text{equation 5-1}$$

where, *force* is the peak knee impact force in kN.

Risk (hip fracture) =

$$\Phi\left[\frac{\ln(force) - (-0.2141 + 0.0114 \times stature) \times (1 - (flexion - abduction)/100)}{0.1991}\right]$$

equation 5-2

where, Φ is the cumulative distribution function of the standard normal distribution,

force is peak force transmitted to the hip in kN,

stature is the stature of the target population (178 cm for midsize males),

flexion is the hip flexion angle in degrees (15˚ for LX FE Model), and

abduction is the hip abduction angle in degrees (0˚ for LX FE Model).

$$Risk\ (femur\ fracture) = 1 - Exp\left[-Exp\left[9.3704 \times \ln(moment) - (46.3140 + 0.0216 \times area)\right]\right]$$

equation 5-3

where, *moment* is peak femoral shaft moment in Nm, and *area* is the cross-sectional area at the mid-shaft of the femur (467.26 mm^2 for midsize males).

5.2.3 Effects of Muscle Tension on KTH Injury Location Predicted Using Bone Fracture Models

Because KTH injury risk curves were developed using single loading mechanisms (e.g., pure compression or pure bending) and a single fixed occupant posture, they may not be valid for combined loading or for loading that occurs in conjunction with posture changes (e.g., hip compression combined with hip flexion caused by forward rotation of the torso during airbag ridedown). For these reasons, a second set of simulations was performed in which the fracture functions were turned on since the Tsai-Wu fracture model has the potential to account for the effects of combined loading on cortical bone failure (Gomez-Benito et al. 2005; Dejak et al. 2007). In these simulations, the knees of stationary whole-body model were symmetrically loaded using a 20-MPa flat impactor with 100-mm thick padded interface. Impact velocity was increased from 6.0 m/s in 0.1

m/s increments until the minimum velocity needed to produce a KTH fracture was identified. KTH fracture was assumed to occur when a contiguous group of elements at any location in the KTH was eliminated and a reduction in the force transmitted to the hip occurred. The threshold knee impact forces that produced KTH injuries in the simulations with and without muscle tension were recorded. Hip forces and femur bending moments at the time of KTH fracture were compared with the tolerance values reported in the literature.

5.3 RESULTS

5.3.1 Simulated KTH Impact Response With Muscle Tension

Figure 5-3 illustrates predicted force histories at the knee, femoral condyles, and hip, and the bending moment history at the femoral shaft from a simulation with muscle tension based on one-foot maximum braking at knee angle of 90˚ in which fracture functions were not used. As indicated, hip force and femur bending moment increase as muscle tension was applied between 0 and 30 ms prior to knee impact. At the time of knee contact with the knee bolster (~ 31 ms), muscle tension produced approximately 1.4 kN of force at the hip and a 54.4 Nm bending moment at the mid femoral shaft.

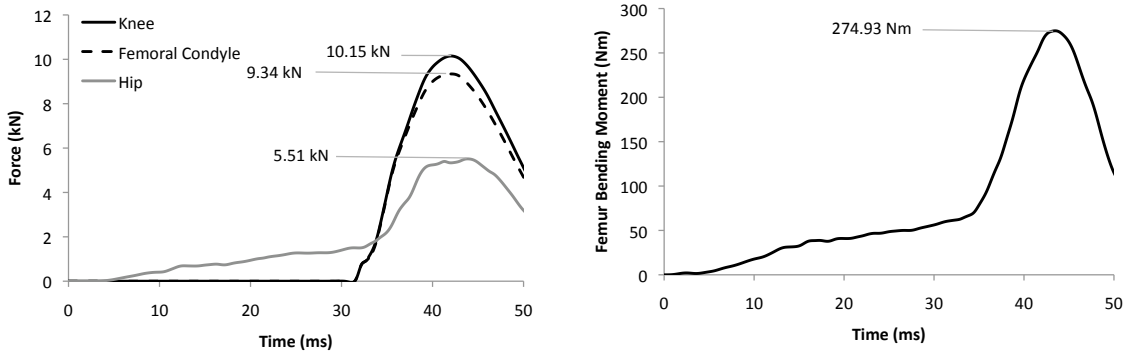

Figure 5-3. Histories of knee, distal femur, and hip forces (left) and femur bending moment (right) from a simulation with muscle tension during one-foot maximum braking at knee angle of 90˚.

5.3.2 Effects of Muscle Tensions on KTH Injury Risk

Figure 5-4 and 5-5 show peak knee, femoral condyle, and hip forces and femur bending moments from the simulations without and with muscle tension, where the muscle tensions are based on one-foot maximum braking at knee angle of 90˚. Peak knee, femoral condyle, and hip forces and femur bending moments from all simulations are contained in Appendix E. In general, peak knee, femoral condyle, and hip forces, and femur bending moments, increase linearly with increasing impact speed, and stiffer impactors produce higher knee-impact forces than softer impactors at the same impact velocities. The rates of increase in peak force greater in simulations with a stiffer knee impact interfaces.

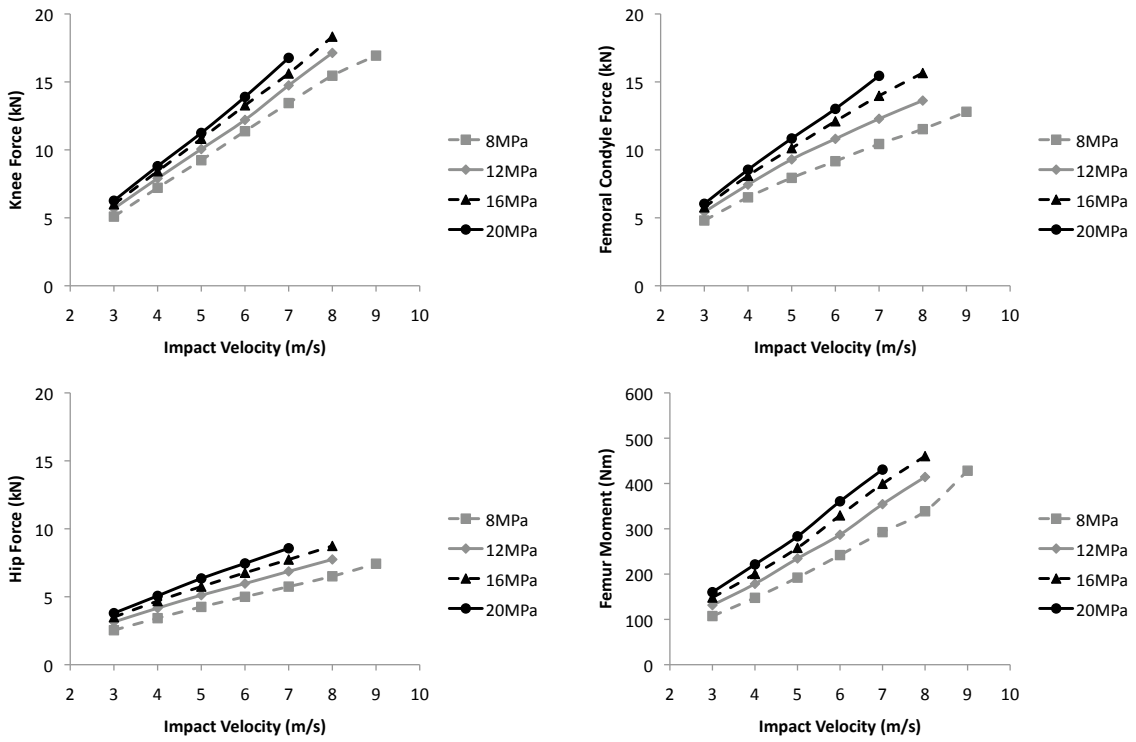

Figure 5-4. Peak knee, femoral condyle, and hip forces, and femur moments, from simulations WITHOUT muscle tension.

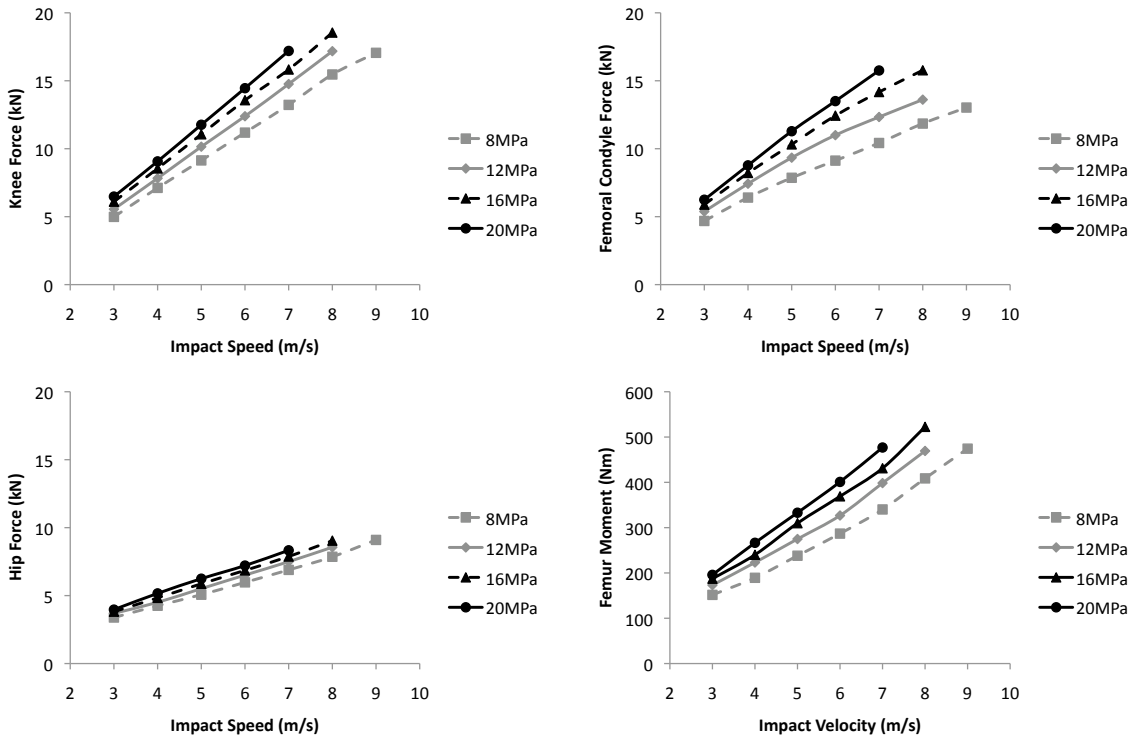

Figure 5-5. Peak knee, femoral condyle, and hip forces, and femur moments, from simulations WITH muscle tension.

In pairs of simulations using similar impact velocities and similar impact interface stiffness values, higher knee impact forces were produced in simulations with muscle tension than in simulations without muscle tension. In addition, peak femur bending moments are ~50 Nm greater in simulations with muscle tension than simulations without muscle tension. This value is similar to the 54 Nm bending moment produced by muscle tension prior to the knee impact in all simulations with muscle tension.

Figure 5-6 compares calculated knee, thigh, and hip injury risks from simulations with and without muscle tension. Tables of peak forces and moments from these simulations and the associated injury risk values are also contained in Appendix E. Risks of hip injury are greater than those of knee and thigh injury in all of the loading conditions, except for simulations with the softest knee impactor at 3 and 4 m/s impact velocities without muscle tension.

Muscle tension substantially increases the risk of femur injury. Predicted femur injury risk is approximately 20 to 40% higher in simulations with muscle tension than in simulations without muscle tension at different combinations of impactor stiffness and velocity. Muscle tension also increases the risk of hip injury, particularly in simulations with softer impactors.

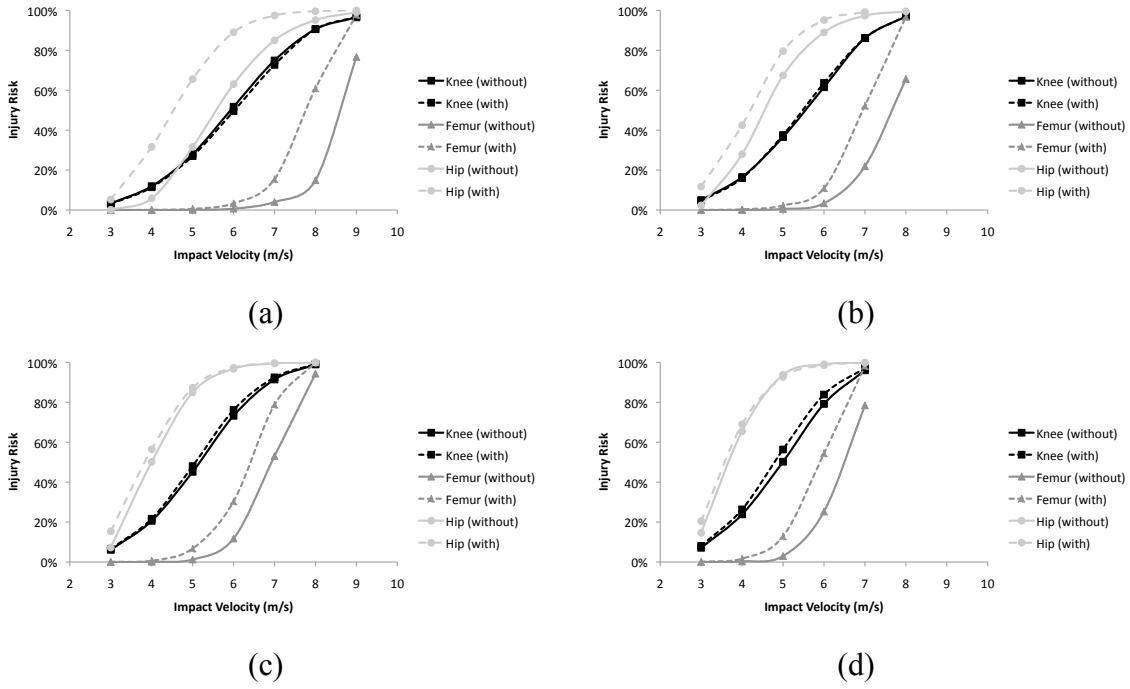

Figure 5-6. Injury risk from simulations with and without muscle tension with impactor stiffness values of (a) 8 MPa, (b) 12 MPa, (c) 16 MPa, and (d) 20 MPa.

5.3.3 Effects of Muscle Tension on Predicted KTH Fracture Location

Figure 5-7 shows the fracture locations and knee and hip force histories from simulations that produced threshold KTH injuries from the simulations without and with muscle tension that used bone fracture models. For simulations without muscle tension, a 7.0 m/s impact was required to produce KTH fracture, which occurred at the femoral neck. However, for simulations with muscle tension, the impact velocity required to

produce a KTH fracture decreased to 6.7 m/s and the fracture location shifted from the femoral neck to the mid-shaft of the femur.

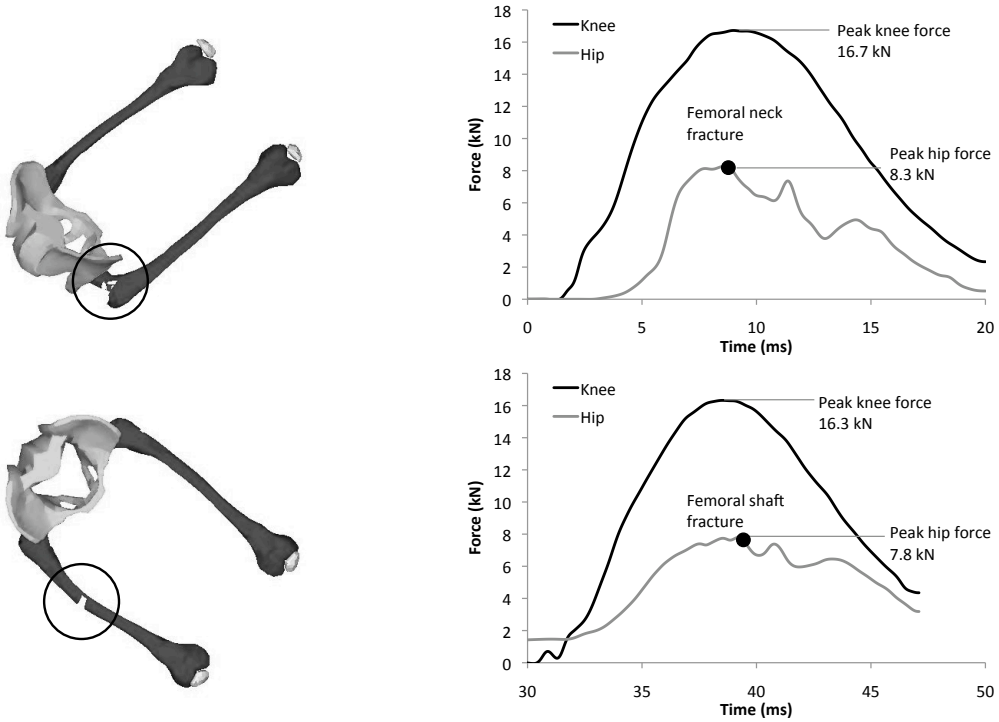

Figure 5-7. Locations of fractures and force histories at the knee and hip in threshold simulations of KTH fracture without muscle tension at 7.0 m/s impact velocity (top) and with muscle tension at 6.7 m/s impact velocity (bottom).

The peak knee impact forces associated with the first occurrence of KTH fracture are 16.7 kN and 16.3 kN for simulations without and with muscle tension, respectively. In the fracture-producing simulations without muscle tension, a femoral neck fracture occurred at a hip force of 8.3 kN. By comparison, peak force at the hip at the time of femoral shaft fracture in the simulation with muscle tension was 7.8 kN. In this same simulation, the femoral shaft fractured at 401.3 Nm.

5.4 SUMMARY AND DISCUSSION

Simulations of frontal knee impacts with and without muscle tension were performed to explore the effects of muscle tension on the risks of different types of KTH injury caused by knee bolster loading in frontal collisions. Simulations were performed with the bone fracture formulation turned "off" to explore the effects of muscle tension on KTH injury based on comparison of forces at the knee and hip and moments at the femoral shaft exceeding values in knee, thigh, and hip injury risk curves. Using this approach to predicting injury, simulation results showed that, for the same impact velocity and impact interface stiffness, the inclusion of muscle forces in the lower extremities associated with maximum braking increased the risk of mid-shaft femur fractures by approximately 20 to 40%, but had little effect on the probability of hip fracture. In addition, muscle tension increased the force at the knees by coupling muscle mass more tightly to the skeletal parts of the KTH.

A series of simulations was also performed in which the fracture model (i.e. Tsia-Wu fracture criterion) was used to determine the occurrence of fracture (i.e., with the fracture formulation turned "on"). In these simulations, lower extremity muscle tension slightly reduced the externally applied force at the knee required to cause KTH fracture, and shifted the predicted fracture location from the hip (femoral neck) to the mid shaft of the femur.

In the simulations with fracture model turned "on," femoral neck fracture occurred at a hip force of 8.3 kN in the condition without muscle tension, which is similar to the 8.1 kN femoral neck failure determined by Rupp et al. (2002) from the cadaver femur-tolerance tests. In contrast, in the simulations with muscle tension, the femoral shaft fractured at a bending moment of 401.3 Nm, which is in the range of 352 ± 83 Nm for femur shaft tolerance in M-L bending determined by Kennedy et al. (2004). In these simulations, acetabular fracture was not predicted despite the fact that force at the hip exceeded the reported 6.1 kN fracture tolerance of the acetabulum. This seemingly contradictory result is thought to occur because of pelvic rotation in these simulations that caused the femoral head to rotate in the acetabular socket. This rotation of the hip joint distributes strain energy over a larger area of the acetabulum during impact loading,

thereby reducing the strain energy in individual elements in the acetabulum and preventing the bone stresses and strains from reaching the levels associated with failure.

Figure 5-8 shows the percentage of force transmitted from the knee to the hip in the simulations with fracture formulations turned "off" for different impact speeds and impactor stiffness. In the simulation without muscle tension, a greater percentage of applied knee force was transmitted to the hip at lower impact speeds with a stiff impactor than for higher impactor speeds and softer impactors. However, in simulations with muscle tension, similar percentages of applied knee force were applied to the hip with different impactor stiffness. Approximately 45-60% and 50-65% of the force applied to the knee is applied to the hip in the simulations without and with muscle tension, respectively. These values compare favorably to the 56% decrease in force reported by Rupp et al. (2008) who used a one-dimensional mathematical spring-mass-damper model of a cadaver with knee loading speeds between 2 and 8 m/s to predict force at the knee and force at the hip.

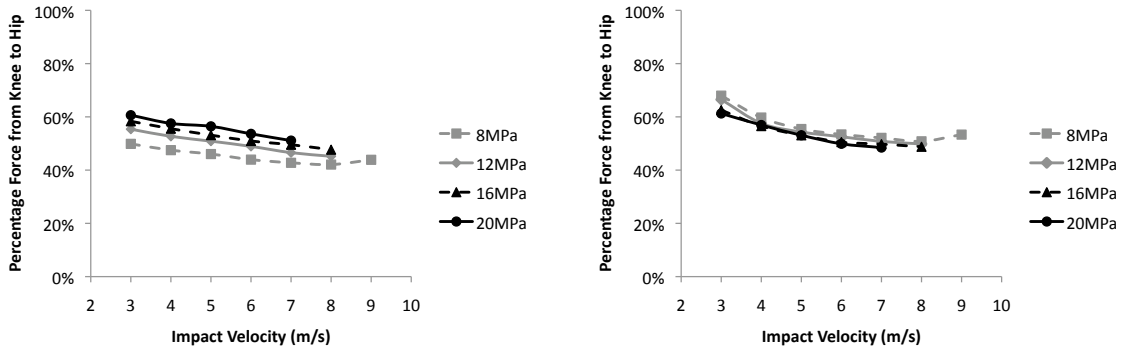

Figure 5-8. Percentage of force transmitted from the knee to the hip in the simulations without (left) and with (right) muscle tension.

There are several factors that might affect the percentage of force at the hip comparing with force at the knee in frontal impacts. One factor is the deformation of impactor. Greater deformation of the impactor (i.e., the knee bolster in production vehicle) is produced in the simulations at higher impact speeds with a softer impactor

surface. This greater deformation produces a larger contact area between the impactor surface and the knee, thereby allowing the impactor to directly contact and recruit more thigh flesh and reduce the percentage of force transmitted directly to the femoral condyles. This factor can be demonstrated using results of LX FE Model simulations by comparing the percentage of force transmitted from the knee to the femoral condyles as shown in Figure 5-9. Lower percentages of knee-impact forces are transmitted to the femoral condyles in the simulations at higher impact speeds and for softer impact interfaces because of some of the force is transmitted directly to the soft tissues surrounding the skeletal components.

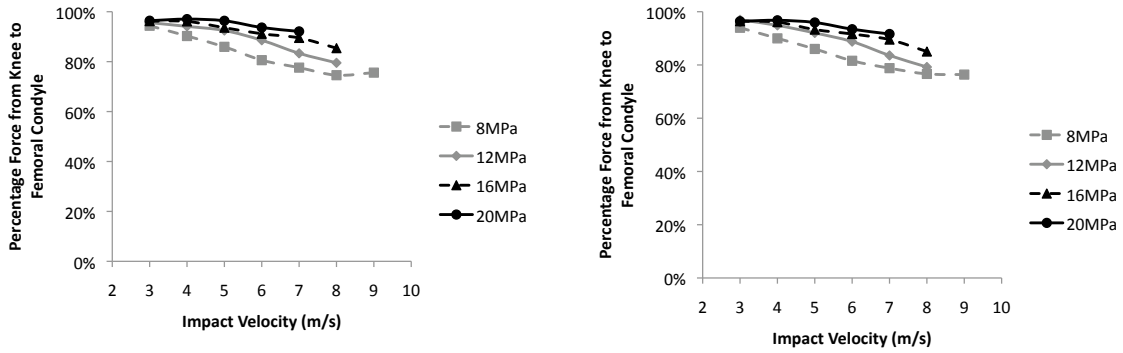

Figure 5-9. Percentage of force transmitted from the knee to the femoral condyles in the simulations without (left) and with (right) muscle tension.

Another factor is that muscle tension more tightly couples muscle mass distal to the hip, thereby increasing the decrease in force from the knee to the hip. As seen in Figure 5-10, when only considering force transmission through the femur (i.e., from femoral condyles to femoral head), in the simulations without muscle tension, the percentage of force at the femoral condyles that is transmitted to the hip is approximately 56% across different impactor stiffness and impact velocities. However, in the simulations with muscle tension, although the magnitude of force decrease from the femoral condyles to the hip is increased because of coupling of muscle mass distal to the hip, the magnitude of the force at the hip is similar in magnitude to the force at the hip

without muscle tension because of the additional force at the hip caused by muscle tension within the KTH complex and the higher force at the knee.

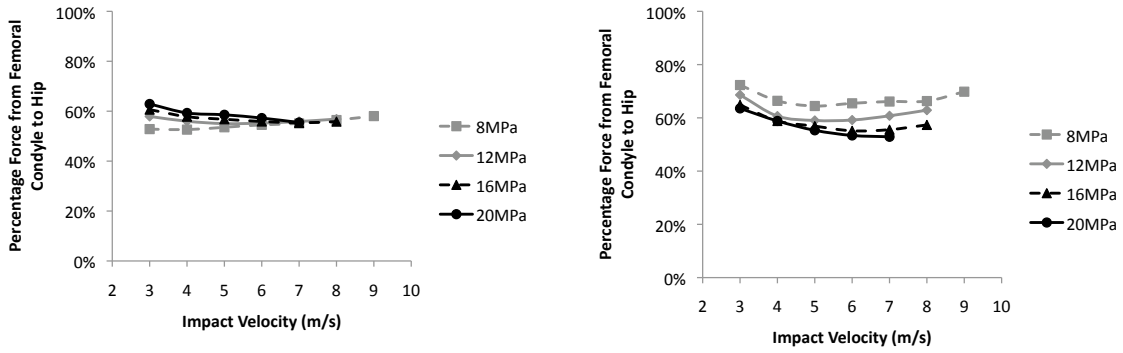

Figure 5-10. Percentage of force transmitted from the femoral condyle to the hip in the simulations without (left) and with (right) muscle tension.

CHAPTER 6
GENERAL DISCUSSION

This study uses computational modeling in conjunction with experimental testing with volunteer subjects to study the effects of muscle tension on knee-thigh-hip (KTH) injuries during simulated knee bolster loading in frontal crashes. Simulations of knee-to-knee-bolster loading were performed using a new lower-extremity finite element model (LX FE Model) with lower-extremity muscle activation levels from a commercial musculoskeletal model that was validated using EMG and reaction force data from subject one-foot braking and two-foot bracing tests in a laboratory seating buck. Simulation results confirm the original study hypothesis that muscle activation has the potential to affect force along the KTH and also shift fracture location from the hip to the shaft of the femur. However, these findings are subject to the limitations of the LX FE and musculoskeletal models and the limitations of the simulations used to assess the effects of muscle activation on KTH injury that are discussed below.

6.1 LIMITATIONS OF THE LX FE AND MUSCULOSKELETAL MODELS

6.1.1 Limitations of LX FE Model to Predicting Knee Fractures

The developed LX FE Model incorporates cortical bone with directionally dependent mechanical properties and Tsai-Wu failure criteria for better prediction of stress, strain, and fracture of the bone. Simulation results demonstrate that the LX FE Model can accurately predict the occurrence of fracture at the hip and femoral shaft. However, the model cannot directly predict the occurrence of knee fractures because fracture criteria were not included for the patella and femoral condyles for two reasons. First, the geometry and material characteristics of the knee (e.g., cortical bone thickness

at the patella and failure strength of the patellar cortical bone) are not well documented in the literature. Second, stress based failure criteria depend on the geometry and element size of the finite-element mesh. This is most evident in the patella where small variations in patellar cortical bone mesh density have a large effect on failure prediction.

Despite this shortcoming, the model can still be used to estimate the risk of knee injury using peak-force-based injury criteria. In addition, the inability of the model to simulate patella fracture based on bone stress is not considered to be a major limitation since the primary intent and use of the model is to predict KTH injuries due to knee loading by knee-bolster-like surfaces for which patellar fractures are unlikely (Atkinson et al. 1997; Rupp et al. 2007).

6.1.2 Limitations of LX FE Model Due to Single-Node Point Origins and Insertions of Muscles on Bone

The LX FE Model approximates three-dimensional muscle geometry using one-dimensional muscle elements and simplifies the connections between muscles and bones from areas to single nodes at the origin and insertion points. Therefore, muscle forces are currently applied at specific points on the bones rather than in a more anatomically correct distributed manner. This will tend to increase the local bone stresses at the origin and insertion points of muscle. In particular, original points of vastus lateralis, vastus medialis, and vastus intermedius are located in the femoral shaft. Forces from these muscles might increase local stresses in the femoral shaft and thereby initiate fracture at the origin points of these muscles during impacts. However, in this study, predicted forces of the vastus lateralis, vastus medialis, and vastus intermedius in simulations with the LX FE Model does not seem to have had a significant effect on the prediction of femoral shaft fracture. This is because the femoral shaft fractures were initiated at the lateral surface of the femur, which suggest that the fracture is primarily due to the bending of the curved femur and the location of the is some distance away from muscle origins of the three muscles that attach to the femoral shaft.

6.1.3 Limitations of Muscle Activation Levels Predicted by the AnyBody Model

The procedure that was used to validate the AnyBody Model involved comparing model predictions to EMG data collected from subjects performing simulated braking and bracing tasks in static postures, in which subjects produced primarily isometric contractions of the lower-extremity muscles. This is in contrast to the situation of panic braking and bracing in real-world crashes, for which different muscle activation patterns can be expected than those predicted by the AnyBody Model. In particular, the objective function that the AnyBody Model minimizes to solve the problem of indeterminate muscle activations assumes that muscles are activated to minimize muscle overall lower-extremity muscle activation, or fatigue. While such an approach is appropriate and physiologically reasonable for long-duration muscle activations such as those produce during lifting tasks, in short-duration panic braking and bracing where the primary objective is to stop the vehicle at all costs, the muscles are unlikely to be activated in a manner that attempts to minimize overall muscle fatigue. For example, because occupants who are braking and/or bracing in a manner to stop the vehicle at all costs while keeping the body from moving forward, it is likely that an objective function that maximizes joint stiffness is more appropriate for predicting muscle activation levels during panic braking in frontal crashes.

Results of simulations of isometric braking/bracing using the AnyBody Model in Chapter 4 indicate that the model reasonably predicts activation of agonistic muscles but generally fails to accurately predict activation of antagonistic muscles for these braking and bracing tasks. Many investigators have reported that optimization methods do not predict muscle co-contraction adequately (Crowninshield 1978; Hughes and Chaffin 1988; Brand et al. 1994; Collins 1995). To enforce co-contractions from the optimization solution, some researchers have added constraints to the optimization formulation, such as putting lower bounds on antagonistic muscle forces greater than allowing them to be zero, choosing negative signs for the weighting factors in the objective function, or including a shift parameter for the optimization criterion (Hughes et al. 1995; Raikova 1999; Forster et al. 2004). Unfortunately, these constraints cannot be applied in the

current version of the AnyBody Model since the AnyBody Model does not allow additional constraints to be added to the optimization formulation.

It should be noted that, if the AnyBody Model were improved to accurately predict activations of antagonistic muscle, activations of agonistic muscles would also increase to achieve the appropriate joint torques. This would increase compressive forces throughout the KTH complex and affect coupling of muscle mass in the KTH, thereby affecting KTH injury patterns and tolerance.

6.2 LIMITATIONS OF WHOLE-BODY KNEE-IMPACT SIMULATIONS WITH AND WITHOUT MUSCLE TENSION

6.2.1 LX FE Model Predictions Limited to Midsize Males

The whole-body frontal knee impact simulations with muscle tension were performed using the developed LX FE Model with lower-extremity muscle forces estimated from the AnyBody Model. The LX FE Model was developed using size, shape, material properties, and response data from male subjects who are approximately midsize (or 50%ile) in stature and weight for all U.S. men. The lower-extremity muscle forces during maximum braking were predicted by the AnyBody model configured to match the average lower-extremity dimensions and muscle strengths from the twelve midsize male subjects that participated in the simulated braking and bracing tests. As a result, the response and KTH injury patterns predicted by the LX FE Model only apply to people who are similar in size to midsize males.

The reason that this study has only focused on the KTH responses of midsize males is that there are currently no response validation data and bone and muscle characteristics (e.g., bone stiffness, cortical bone thickness, soft-tissue mass, and muscle force-length relationship) are not well documented for females and other sizes of occupants. Even though the developed LX FE Model can be scaled to fit the geometry of different sizes of occupants, the biofidelity of these scaled models would be very questionable.

6.2.2 Lack of Simulating Forced Stretching of Lower-Extremity Muscles Due to Occupant Dynamics in Frontal Crashes

In this study, simulations with the LX FE Model were performed by impacting the knees of a static whole-body occupant model in which lower-extremity muscle forces predicted from the musculoskeletal model were maintained at the same level throughout the impacts based on the predicted muscle activation patterns from the AnyBody Model. These simulations do not account for muscle forces generated during forced stretching of activated muscles, which result in changes (i.e., flexion) in lower-extremity joint angles during real-world frontal crashes due to inertial loading by the body. In particular, due to activated cross-bridged muscle fibers that act as a rate sensitive damper, forces in activated muscles can exceed twice the force generated from voluntary muscle activation during forced stretching of the muscle at high rates that can occur in frontal crashes. It can therefore be expected that these much higher muscle forces will dramatically affect the forces, bending moments, and stresses/strains within the KTH complex, and thereby affect KTH injury risk and location. The reason this type of simulation was not conducted in the current study is a lack of data on human impact response in whole-body deceleration tests to validate the model under these conditions. In particular, movements of the ankle, knee, and hip joints during whole-body decelerations are critical to the muscle forces generated during forced muscle stretching and these data are not yet available.

6.2.3 Effects of Upper Torso and Pelvis Restraint on Prediction of Hip Injuries

As discussed in the section above, simulations with and without muscle tension were performed by impacting the knees of the whole-body LX FE Model that was stationary prior to knee impact. These static-body simulations do not account for the effects of pelvis and torso restraint by the lap and shoulder belts, which are present in more than 80% of crashes (i.e., more than 80 percent of occupants use seatbelts), or for a driver bracing with the upper extremities against the steering wheel. These factors are likely to decrease the forward rotation of the pelvis during frontal impacts and could thereby increase the probability of hip injury by reducing the distribution of forces to a

larger area of the acetabulum. However, restraint of the torso and pelvis may also reduce upper body mass coupled proximal to the hip, thereby increasing the drop in force between the knee and the hip during knee bolster loading, and thereby decreasing the probability of hip injury. Thus, the effects of upper torso restraint by seatbelts and/or driver bracing in real-world crashes could increase or decrease hip injury risk, depending on which factor (reduction of area loaded in the acetablum or reduction in force at the hip) is more significant in a particular crash situation.

6.2.4 Effects of Muscle Activation Level

Muscle forces for use in simulations with the LX FE Model were estimated by simulating maximum one-foot braking using a version of the AnyBody Model in which the force generating capacities of muscles were set to match the average of those of the tuned subject-specific models. These results might over-predict injury risk for the case in which the driver is late in reacting to the threat of frontal collision or is just beginning to increase the brake pedal force when impact occurs. The reason that lower-extremity muscle forces predicted from maximum one-foot braking were used in this study was to represent worst-case muscle effects on KTH injuries. Since muscle activation level might not be proportional to the exerted braking/bracing forces, different combinations of lower-extremity muscle forces from different levels of braking/bracing force might result in different force, moment, and mass coupling in the KTH complex, and therefore produce different KTH injury pattern.

6.2.5 Lack of Equilibrium in Forces in the LX FE Model

Muscle forces used in this study were predicted from a musculoskeletal model that is separate from the LX FE Model used to investigate the effects of muscle tension on KTH injuries. Although these two numerical models have similar geometries, their geometries are not identical. As a result, forces predicted by the musculoskeletal model are not exactly in equilibrium in the LX FE Model prior to knee impacts. This causes

minor errors in bone segment movements, which has a small effect on the prediction of KTH injuries and response. Combining the LX FE Model and the musculoskeletal model would eliminate this problem. However, at the current time, no single numerical modeling system exists that can predict active muscle forces and perform finite-element simulations of occupant dynamics in crash environments.

6.3 MUSCLE ACTIVATIONS DURING ONE-FOOT BRAKING AND TWO-FOOT BRACING

It was found in the subject braking and bracing tests that, even though two-foot bracing was expected to produce twice the force on the foot plate as in one-foot braking, the average maximum two-foot bracing forces are only 27% greater than the average maximum one-foot braking forces. Also, even though subjects were asked to perform maximum exertion in all these tests, muscles were about 25-30% less activated during two-foot bracing than in one-foot braking. There might be several factors that cause subjects to produce lower muscle activation during maximum two-foot bracing than maximum one-foot braking. One of the factors might be due to the " bilateral deficit" which says that the central nervous system (CNS) is limited to produce bilateral maximum activation of a large number of muscles simultaneously (Howard and Enoka 1991; Koh et al. 1993; Schantz et al. 1989; Vandervoort et al. 1984; van Soest et al. 1985; Vint and Hinrichs 1996). Another factor might be the limitation of the test setup that reduces subjects' willingness to exert maximum efforts and/or to use different strategies to exert maximum forces in two-foot bracing compared with forces exerted during simulated one-foot braking. This limitation might be improved by performing panic braking/bracing tests instead of isometric braking/bracing tests, so that subjects are less able to adjust braking/bracing strategies during the test. In addition, if subjects perceived that they were starting to lift off the seat during two-foot bracing more than in one-foot braking, restraint of the pelvis and torso by seatbelts might prevent subjects from reducing efforts and/or changing strategies in two-foot bracing tests. Based on these issues and concerns, muscle activation levels measured from two-foot bracing tests are

considered questionable for use in simulating emergency two-foot bracing in real-world crashes.

6.4 SIMULATIONS OF KTH INJURIES DURING KNEE-IMPACT LOADING

6.4.1 Effects of Injury Prediction Method

This study conducted two sets of simulations to evaluate the effects of muscle tension on KTH injuries during frontal knee impacts: 1) simulations with fracture formulations turned "off," and 2) simulations with fracture formulations turned "on." In the simulations with fracture formulations turned off, the risks of knee, femoral shaft, and hip injury were evaluated by applying the predicted peak knee and hip forces, and peak femur bending moments, to KTH injury risk formulations reported in the biomechanical literature. In the simulations with fracture formulations turned on, the injuries were determined by the failure of bone elements predicted by a stress-based Tsai-Wu failure criterion. Both sets of simulations indicate that muscle tension has the potential to increase the risk of injury at the femoral shaft relative to the risk of hip fracture. However, it is difficult to determine which approach is more reliable in the prediction of KTH injuries since both methods have limitations and advantages as discussed below.

Simulations with the fracture formulation turned "on" most strongly support the hypothesis that muscle tension has the potential to shift injury location from the hip to the femoral mid-shaft. However, the major limitation of using the fracture model is that simulations with the fracture model can only be used to explore fracture location and the stress/strain and impact force associated with the occurrence of fracture—the fracture model cannot be used to estimate injury risk for any simulation that predicts a fracture. This is because the occurrence of this fracture will prevent force transmission along the KTH complex and thereby will effectively limit the forces/moments in the KTH complex to levels associated with the predicted fracture. The primarily advantage of using the stress-based fracture model is that predicts injury for combined loading, such as is produced when the femur is simultaneously compressed and bent by knee impact loading.

The primarily advantage of using peak-force-based or peak moment-based injury risk predictions in the simulations with fracture formulations turned "off" is that this approach allows injury prediction at different levels of risk based on the injury risk curves. However, the accuracy of this type of approach depends not only on the accuracy of peak force estimates at the knee and hip, and peak bending moment at the femoral shaft, but also on the manner in which the injury risk curves were determined. For example, risk predictions in the simulations with fracture formulations turned "off" described in Chapter 5 indicate that, even though muscle tension significantly increases femoral shaft injury risk, the femoral shaft still has a lower risk of injury than the knee and hip for all loading conditions. This is in contrast to real-world KTH injury data, which indicate that the risk of mid-shaft fractures is greater than the risk of knee injuries and similar to the risk of hip injuries.

One potential explanation for this discrepancy is that the injury risk curves used to evaluate the probabilities of femoral shaft fracture and knee fracture are not appropriate for the loading conditions that produce these injuries in frontal crashes. In particular, the femur injury risk curve was developed from pure three-point-bending tests but, in the simulations in the study and real-world frontal crashes, the femur fails during bending induced by axial compression of the curved femur. Also, the knee injury risk curve was developed using fracture force data from tests reported in the literature in which the cadaver knees were loaded by a rigid impactor. These loading conditions result in focal loading of the anterior patella (Atkinson et al. 1997), which significantly reduces the force required to produce knee fracture. By comparison, loading of the knees by padded impactors that simulate knee-bolster-like loading conditions significantly increases the force required to produce knee fracture by distributing the loads over a larger area of the patella and femoral condyles.

6.4.2 Effects of Compressive Forces, Bending Moments, and Mass Coupling of Soft Tissues Due to Muscle Activation on KTH Injuries

Lower-extremity muscle tension during braking/bracing not only increases forces within the KTH complex but also increases bending moments on the femoral shaft and

affects force transmission through the KTH by more tightly coupling muscle mass to bone. The specific KTH injury that results from a frontal impact may depend on the relative contributions of all of these factors.

Simulations with and without muscle tension indicate muscle tension has the potential to increase knee injury by increasing knee impact forces due to coupling muscle mass more tightly to the skeletal KTH. On the another hand, since bending of the femur due to axial compression of the curved femoral shaft is the primary mechanism for femoral shaft fractures during knee bolster loading, the additional bending moments on the femoral shaft due to active muscle tension and the increased knee loads due to tighter coupling of muscle mass to the bone may both contribute to increasing the risk of femoral shaft fractures. However, examination of the increased bending moments in the femoral shaft following muscle activations but prior to knee loading suggest that the effects of muscle tension alone on femoral shaft fractures are small.

Since hip injury during knee bolster loading is generally caused by contact between femoral head and acetabulum, which results in failure of the posterior acetabular wall, compressive force levels at the hip are critical for hip injuries. The factors that affect forces at the hip, and particularly at the acetabulum, include the additional compressive load from muscle tension, and the increase in muscle mass coupled distal proximal to the hip that affect transmission of force from the knee to the hip. This study showed that, because most of the increase in muscle mass coupling due to muscle tension is primarily distal to the hip, muscle tension results in an increase in the drop in force between the knee and the hip. However, this reduction in force at the hip relative to force at the knee may be offset by the increased force at the knee and the increased compressive forces at the hip due directly to muscle tension, thereby resulting in little effect of lower-extremity muscle tension on the risk of hip injuries.

6.5 FUTURE WORK

While this research provides new insights on KTH injury biomechanics in frontal crashes with regard to the potential contributions of lower-extremity muscle tension

during braking and/or bracing, like most studies, it raises many questions that require further research. Additional research is therefore needed before the factors that influence the types and risks of KTH injuries in frontal crashes can be fully understood, and before the findings from this study regarding the effects of lower-extremity muscle forces can be implemented with confidence in Injury Assessment Reference Values (IARVs) for use with measurements from instrumented crash-test dummies.

As discussed above, the current LX FE Model does not include fracture prediction for the patella based on bone stresses and strains. Additional data on the patellar cortical bone thickness and material properties (i.e., modulus, failure stress/strain) of patellar cortical and trabecular bone are needed before reliable fracture models can be applied to the knees of the LX FE Model. In addition, as noted previously, the current knee injury risk curve was developed using fracture force data from tests in which cadaver knees were loaded by rigid, or nearly rigid, impactors. Additional biomechanical tests in which the knees are loaded by softer knee-bolster-like impactors are needed to develop a knee injury risk curve that applies to loading by knee-bolster-like surfaces.

This study used the Kennedy et al. (2004) femoral shaft injury risk curve to predict injury risk to the femoral shaft in frontal knee impacts. However, this curve was developed using data from femur three-point-bending tests that are different from the femur bending induced by axial loading of the femur during impact to the anterior flexed knees, which is the primary mechanism of femur shaft fractures in real-world frontal crashes. Additional biomechanical tests that produce femur bending failures during axial loading are required to develop new femoral shaft injury risk curves that can be used with the knee and hip injury risk curves to more accurately predict the risk of knee, thigh, and hip injuries in frontal crashes.

Future research should also include sled-type simulations using the LX FE Model in which whole-body inertial effects result in forced stretching of activated joint extensor muscles. However, since posture change is critical to muscle lengthening and the muscle forces generated by forced stretching of muscle fibers, these simulations should be performed after the kinematics of LX FE Model in sled-type impacts have been validated, which will require the collection of additional whole-body response data.

Finally, federal regulatory vehicle crash testing uses IARVs that are associated with known probabilities of injuries to evaluate occupant protection systems based on measurements from instrumented anthropomorphic test devices (ATDs) representing particular segments of the occupant population. The results of this study suggest that muscle tension can significantly affect injury patterns and the body's tolerance to externally applied loads, and should therefore be incorporated in IARVs, especially for those used to predict lower-extremity injuries. To develop new KTH IARVs that account for the effects of muscle tension, relationships between forces at the knee and hip, as well as femur bending moments, from simulations of LX FE Model and the forces/moments measured by load cells at similar locations in ATDs, will need to be developed.

CHAPTER 7
CONCLUSIONS

This project used numerical simulations to investigate the potential role of muscle tension in the lower extremities during braking and bracing on KTH injuries, and particularly to see if muscle tension can partially explain why recent biomechanical testing using unembalmed cadavers and one-dimensional simulations of cadaver tests failed to produce any femoral shaft fractures, which occur frequently to front-seat occupants due to knee-to-knee-bolster loading in moderate to severe frontal collisions. Simulation results demonstrate that muscle activation in the lower extremities associated with maximum applied braking:

- increases the effective mass that resists knee impact by coupling muscle mass more tightly to the skeletal femur, thereby increasing knee impact forces compared to those that result without activation of lower extremity muscles,
- increases the bending moment in the curved shaft of the femur due to axial compression in the femur due to muscle tension but primarily because of increased loading at the knees, and
- produces a greater percentage decrease in force between the knee and the hip due to muscle mass coupling more tightly distal to the hip joint.

As a result of all of these factors, muscle tension was found to increase the likelihood of femoral shaft fractures by 20%-40%, but to have little effect on the risk of hip fractures.

In addition to these findings on the effects of muscle tension to KTH injuries, this research makes several other important contributions to the field of injury biomechanics. In particular, it provides the first finite-element model of the lower extremities that includes a complete set of lower-extremity muscles with associated mass and that can be used to simulate the effects of muscle tension on the decrease in force between the knee

and the hip. Results of subject testing to measure muscle activations in this study provide the first set of complete muscle activation data for midsize male subjects performing simulated maximum and sub-maximum braking and bracing in automotive seated postures.

APPENDICES

APPENDIX A

Table A1. Summary of Muscle Strength, PCSA, and Pennation Angle Reported by Delp et al. (1990), Friederich et al. (1990), and Wickiewicz et al. (1983).

Muscle	Strength (N)	PCSA (cm2)	Pennation angle (degree)
Soleus	2830	58.0	30.0
Gastrocnemius	1605	32.4	16.7
FlexorDigitorumLongus	310	5.1	6.7
FlexorHallucisLongus	320	5.3	10.0
TibialisPosterior	1270	20.8	11.7
PeroneusBrevis	350	5.7	5.0
TibialisAnterior	600	9.9	5.0
ExtensorDigitorumLongus	340	5.6	8.3
ExtensorHallucisLongus	110	1.8	6.0
Sartorius	104	1.7	0.0
Gracilis	108	1.8	3.3
VastusLateralis	1870	30.6	5.0
VastusMedialis	1295	21.1	5.0
VastusIntermedius	1235	22.3	3.3
RectusFemoris	780	12.7	5.0
Semitendinosus	330	5.4	5.0
Semimembranosus	1030	16.9	15.0
BicepsFemorisCaputLongum	720	12.8	0.0
BicepsFrmorisCaputBreve	400	12.8	0.0
Iliopsoas	800	23.3	6.5
AdductorLongus	420	6.8	6.0
AdducorMagnus1	345	25.5	5.0
AdducorMagnus2	310	18.4	2.5
AdducorMagnus3	445	17.0	5.0
GluteusMinimus1	180	6.79	10.5
GluteusMinimus2	190	8.2	0.0
GluteusMinimus3	215	12.0	21.0
GluteusMedius1	550	25.0	8.0
GluteusMedius2	380	16.2	0.0
GluteusMedius3	435	21.2	19.0
GluteusMaximus1	382	20.2	5.0
GluteusMaximus2	546	19.6	0.0
GluteusMaximus3	368	20.0	5.0
TensorFasciaeLatae	155	8.0	2.5
Piriformis	295	20.5	9.5

Table A2. Points Defining the Muscle Characteristics Reported by Delp (1990). Muscle strain is determined by divided the increase of muscle length by initial muscle length. The strain rate is determined by divided the increase rate of muscle length by initial muscle length. The normal force is determined by divided the muscle force by the muscle strength provided in Table A1.

Active Strain vs. Normal Force	Active Strain Rate vs. Normal Force	Passive Strain vs. Normal Force
(-5.00000,0.000000)	(-1.000000, 0.000000)	(-5.000, 0.000)
(0.000000,0.000000)	(-0.950000, 0.010417)	(0.998, 0.000)
(0.401000,0.000000)	(-0.900000,0.021739)	(0.999, 0.000)
(0.402000,0.000000)	(-0.850000,0.034091)	(1.000, 0.000)
(0.403500,0.000000)	(-0.800000,0.047619)	(1.100, 0.035)
(0.527250,0.226667)	(-0.750000,0.062500)	(1.200, 0.120)
(0.628750,0.636667)	(-0.700000,0.078947)	(1.300, 0.260)
(0.718750,0.856667)	(-0.650000,0.097222)	(1.400, 0.550)
(0.861250,0.950000)	(-0.600000,0.117647)	(1.500, 1.170)
(1.045000,0.993333)	(-0.550000,0.140625)	(1.600, 2.000)
(1.217500,0.770000)	(-0.500000,0.166667)	(1.601, 2.000)
(1.438750,0.246667)	(-0.450000,0.196429)	(1.602, 2.000)
(1.618750,0.000000)	(-0.400000,0.230769)	(5.000, 2.000)
(1.620000,0.000000)	(-0.350000,0.270833)	
(1.621000,0.000000)	(-0.300000,0.318182)	
(2.200000,0.000000)	(-0.250000,0.375000)	
(5.000000,0.000000)	(-0.200000,0.444444)	
	(-0.150000,0.531250)	
	(-0.100000,0.642857)	
	(-0.050000,0.791667)	
	(0.000000,1.000000)	
	(0.050000,1.482014)	
	(0.100000,1.601571)	
	(0.150000,1.655791)	
	(0.200000,1.686739)	
	(0.250000,1.706751)	
	(0.300000,1.720753)	
	(0.350000,1.731099)	
	(0.400000,1.739055)	
	(0.450000,1.745365)	
	(0.500000,1.750490)	
	(0.550000,1.754736)	
	(0.600000,1.758312)	
	(0.650000,1.761364)	
	(0.700000,1.763999)	
	(0.750000,1.766298)	
	(0.800000,1.768321)	
	(0.850000,1.770115)	
	(0.900000,1.771717)	
	(0.950000,1.773155)	
	(1.000000,1.774455)	

APPENDIX B

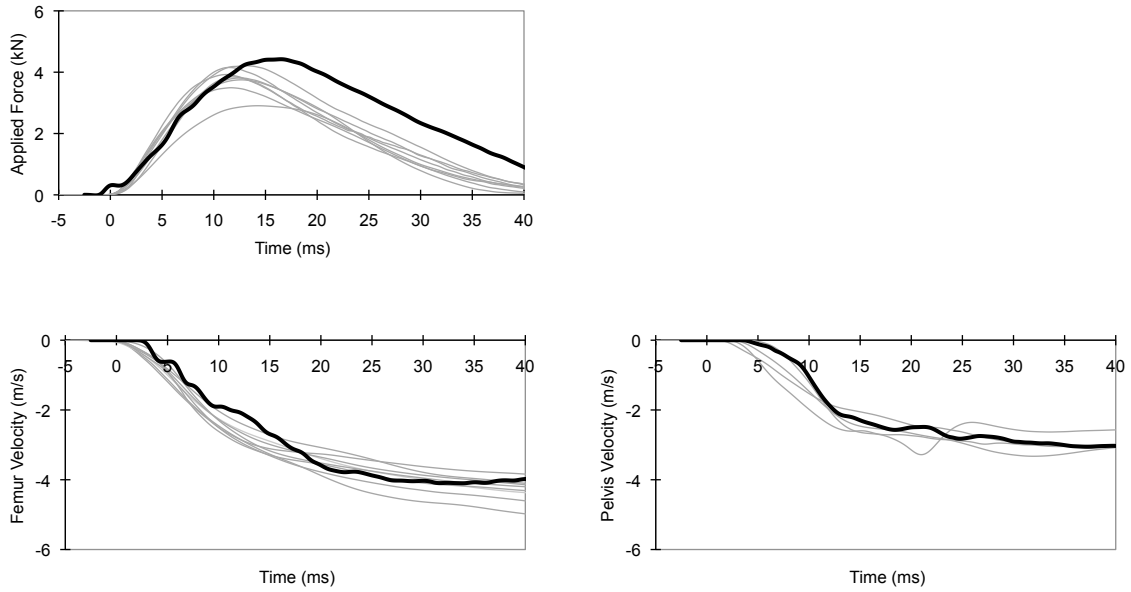

Figure B1. Comparison of applied force (top), femur velocity (bottom-left), and pelvis velocity (bottom-right) histories from experimental tests (gray lines) and KTH FE simulations (black lines) of whole-body 3.5 m/s tests.

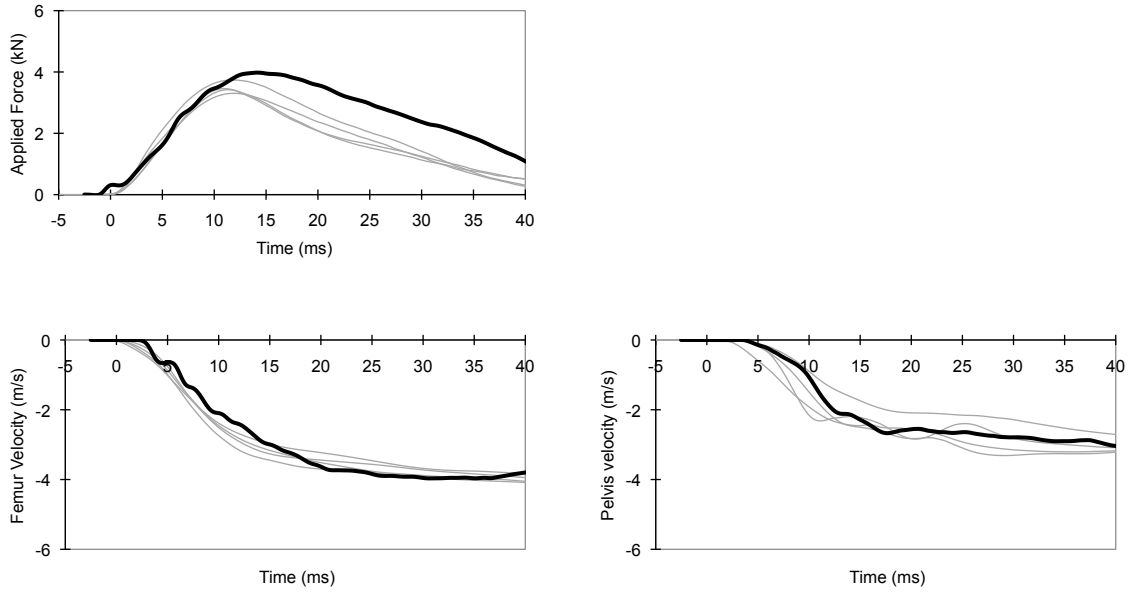

Figure B2. Comparison of applied force (top), femur velocity (bottom-left), and pelvis velocity (bottom-right) histories from experimental tests (gray lines) and KTH FE simulations (black lines) of thigh-flesh-cut 3.5 m/s tests.

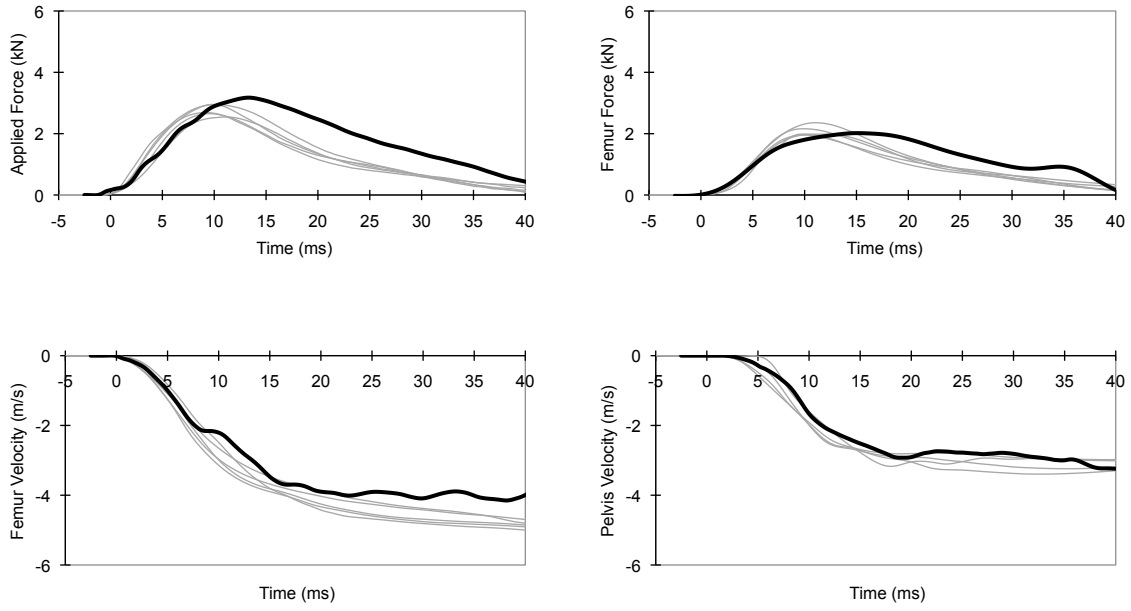

Figure B3. Comparison of applied force (top), femur velocity (bottom-left), and pelvis velocity (bottom-right) histories from experimental tests (gray lines) and KTH FE simulations (black lines) of thigh-flesh-removed 3.5 m/s tests.

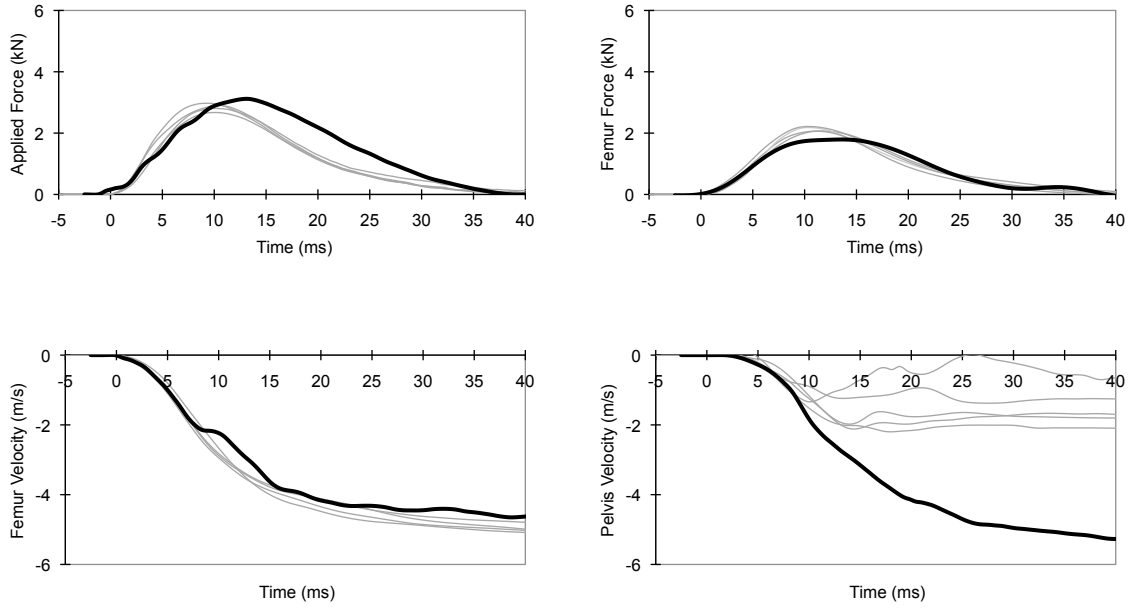

Figure B4. Comparison of applied force (top), femur velocity (bottom-left), and pelvis velocity (bottom-right) histories from experimental tests (gray lines) and KTH FE simulations (black lines) of torso-removed 3.5 m/s tests.

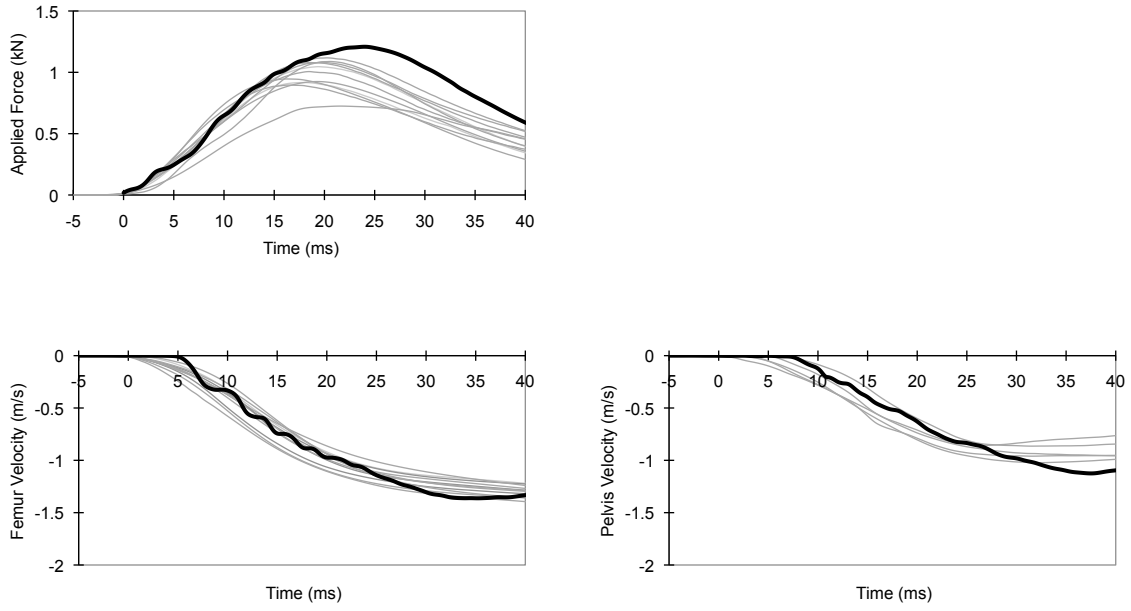

Figure B5. Comparison of applied force (top), femur velocity (bottom-left), and pelvis velocity (bottom-right) histories from experimental tests (gray lines) and KTH FE simulations (black lines) of whole-body 1.2 m/s tests.

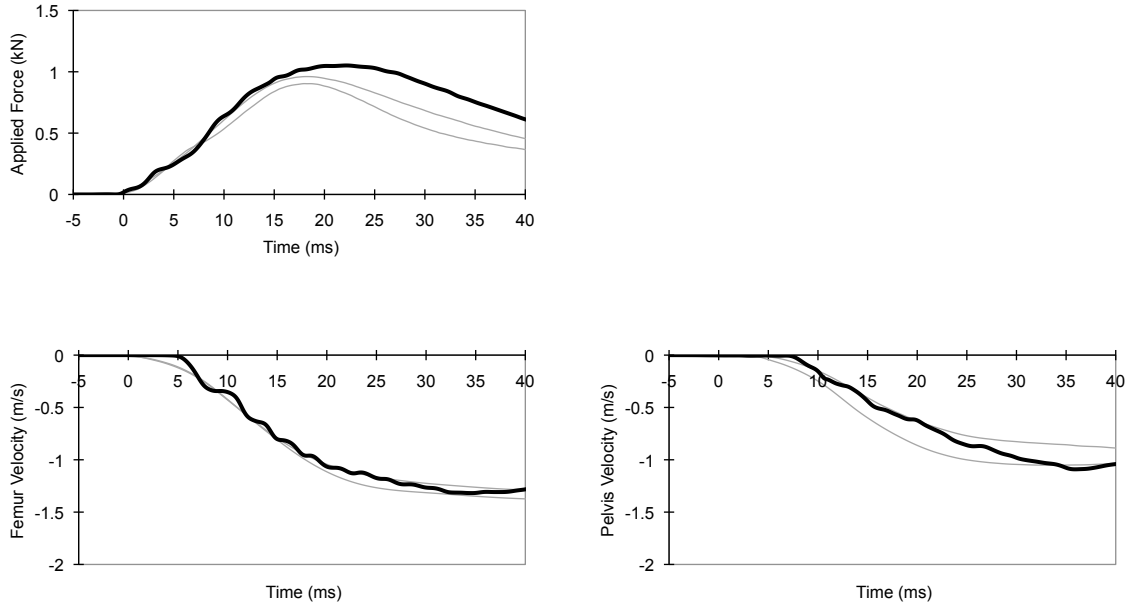

Figure B6. Comparison of applied force (top), femur velocity (bottom-left), and pelvis velocity (bottom-right) histories from experimental tests (gray lines) and KTH FE simulations (black lines) of thigh-flesh-cut 1.2 m/s tests.

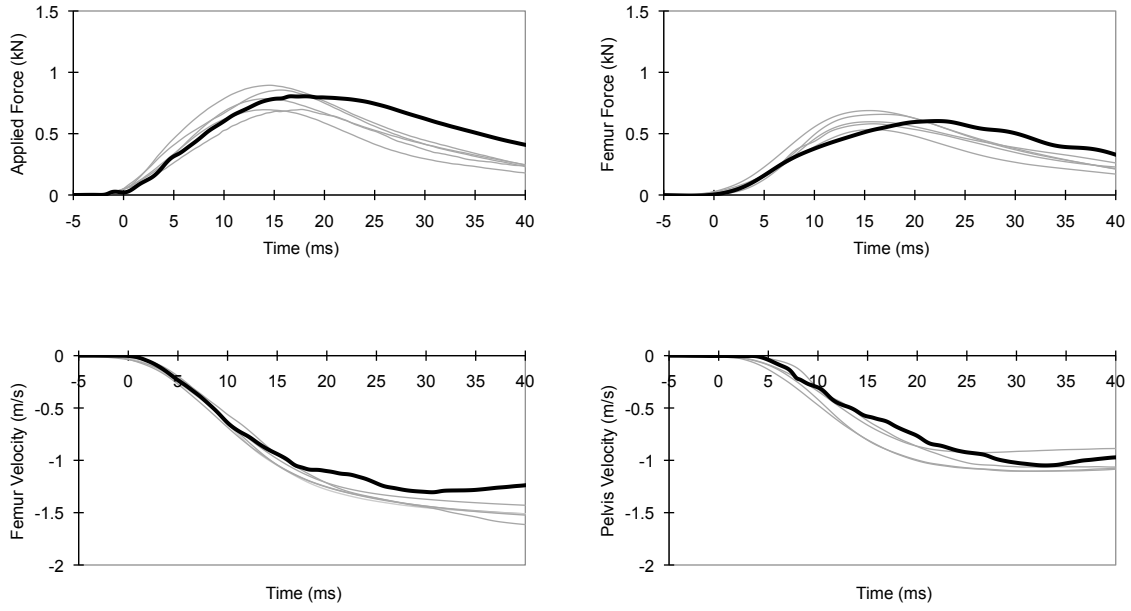

Figure B7. Comparison of applied force (top), femur velocity (bottom-left), and pelvis velocity (bottom-right) histories from experimental tests (gray lines) and KTH FE simulations (black lines) of thigh-flesh-removed 1.2 m/s tests.

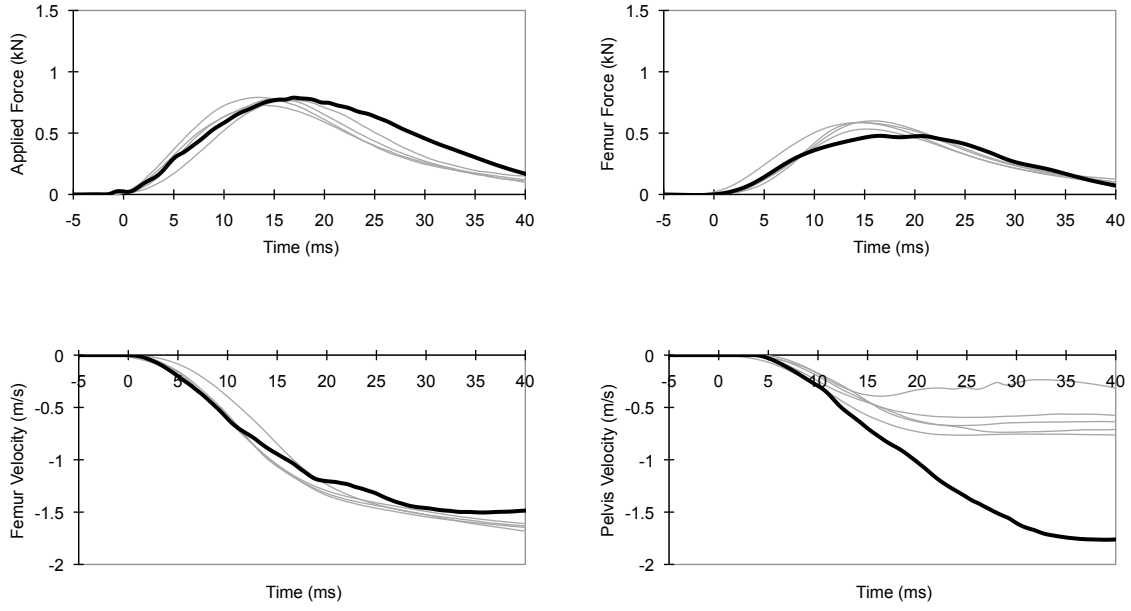

Figure B8. Comparison of applied force (top), femur velocity (bottom-left), and pelvis velocity (bottom-right) histories from experimental tests (gray lines) and KTH FE simulations (black lines) of torso-removed 1.2 m/s tests.

Table B1. Comparisons of Average (and Ranges) of Experimental and Simulation Results on Applied Force, Femur Force, Femur Velocity, and Pelvis Velocity at Time of Peak Applied Force of 3.5 m/s Tests

	Time of Peak Applied Force (ms)	Applied Force (kN)	Femur Force (kN)	Femur Velocity (m/s)	Pelvis Velocity (m/s)
Whole-Boby					
Experiment	12.3 (11.2 – 14.3)	3.76 (2.91 – 4.21)	NA	-2.77 (-2.40 - -3.00)	-2.13 (-1.87 - -2.46)
Simulation	16.5	4.42	NA	-2.96	-2.43
Error	34.15 %	17.55 %		6.86 %	14.08 %
Thigh-Flesh-Cut					
Experiment	11.5 (11.0 – 11.9)	3.48 (3.30 – 3.74)	NA	-2.81 (-2.62 - -3.07)	-1.94 (-1.24 - -2.31)
Simulation	14.2	3.98	NA	-2.91	-2.16
Error	23.48 %	14.37 %		3.56 %	11.34 %
Thigh-Flesh-Removed					
Experiment	10.0 (9.2 – 11.1)	2.76 (2.54 – 2.95)	2.07 (1.92 – 2.34)	-2.85 (-2.49 - -3.14)	-1.87 (-1.60 - -1.99)
Simulation	13.3	3.17	1.99	-3.01	-2.31
Error	33.00 %	14.86 %	3.86 %	5.61 %	23.53 %
Torso-Removed					
Experiment	10.1 (9.4 – 10.6)	2.84 (2.67 – 2.97)	2.10 (2.01 – 2.18)	-2.85 (-2.70 - -2.97)	-1.34 (-1.20 - -1.54)
Simulation	13.1	3.12	1.88	-3.05	-2.74
Error	29.70 %	9.86 %	10.48 %	7.02 %	104.48 %

Table B2. Comparisons of Average (and Ranges) of Experimental and Simulation Results on Applied Force, Femur Force, Femur Velocity, and Pelvis Velocity at Time of Peak Applied Force of 1.2 m/s Tests

	Time of Peak Applied Force (ms)	Applied Force (kN)	Femur Force (kN)	Femur Velocity (m/s)	Pelvis Velocity (m/s)
Whole-Boby					
Experiment	19.0 (16.2 – 21.6)	0.98 (0.72 – 1.12)	NA	-0.95 (-0.83 - -1.07)	-0.69 (-0.56 - -0.76)
Simulation	24.0	1.21	NA	-1.09	-0.83
Error	26.32 %	23.47 %		14.74 %	20.29 %
Thigh-Flesh-Cut					
Experiment	18.1 (18.0 – 18.2)	0.93 (0.90 – 0.96)	NA	-0.99 (-0.97 - -1.01)	-0.66 (-0.55 - -0.78)
Simulation	22.2	1.05	NA	-1.12	-0.73
Error	22.65 %	12.90 %		13.13 %	10.61 %
Thigh-Flesh-Removed					
Experiment	16.4 (15.5 – 17.1)	0.77 (0.68 – 0.88)	0.61 (0.53 – 0.69)	-1.10 (-1.07 - -1.14)	-0.80 (-0.70 - -0.88)
Simulation	16.7	0.80	0.60	-1.04	-0.62
Error	1.83 %	3.90 %	1.64 %	5.45 %	22.50 %
Torso-Removed					
Experiment	14.9 (13.5 – 17.2)	0.77 (0.73 – 0.79)	0.57 (0.53 – 0.59)	-1.01 (-0.93 - -1.06)	-0.48 (-0.44 - -0.57)
Simulation	17.0	0.79	0.49	-1.06	-0.83
Error	14.09 %	2.60 %	14.04 %	4.95 %	72.92 %

APPENDIX C

Maximum One-Foot Braking, Knee 120 degree

Table C1. Subject Force Exertions and Postures on Maximum One-Foot Braking Knee Angle 120 degree Test

Subject Number	Force in X-Axis (N)	Force in Y-Axis (N)	Torque in Z-Axis (Nm)	Hip Flex. Angle (degree)	Hip Abd. Angle (degree)	Knee Angle (degree)	Ankle Angle (degree)
1	747	399	79	125	83	159	97
2	715	369	36	121	89	157	97
3	374	256	-3	106	107	133	86
4	573	380	44	123	106	130	81
5	341	258	-1	124	99	132	80
6	258	185	-8	119	96	142	86
7	686	354	55	128	86	142	85
8	717	411	73	121	97	146	91
9	351	216	9	121	102	144	88
10	689	402	22	129	95	144	85
11	543	389	-5	118	85	141	89
12	1243	550	100	124	90	162	100

Table C2. Subject EMG data on Maximum One-Foot Braking Knee Angle 120 degree Test

Subject Number	Leg				Femur						Hip	
	MG	LG	SOL	TA	RF	VL	VM	AL	BFLH	BFSH	GMED	GMAX
1	0.54	0.56	0.94	0.73	0.14	0.48	0.15	0.09	0.04	0.22	0.27	0.07
2	0.64	0.86	0.68	0.06	0.39	0.40	0.41	0.05	0.08	0.24	0.82	0.05
3	0.34	0.32	0.28	0.10	0.70	0.93	0.53	0.27	0.05	0.19	0.42	0.17
4	0.45	0.20	0.95	0.90	0.33	0.59	0.78	0.08	0.02	0.22	0.78	0.21
5	0.15	0.13	0.41	0.11	0.69	1.00	0.68	0.11	0.21	0.17	0.57	0.11
6	0.09	0.03	0.10	0.02	0.61	0.50	0.43	0.04	0.04	0.46	0.36	0.56
7	0.29	0.28	1.00	0.34	0.81	0.74	0.74	0.06	0.04	0.14	0.27	0.07
8	0.58	1.00	1.00	0.22	0.44	0.68	0.85	0.11	0.11	0.63	0.61	0.03
9	0.73	0.59	0.36	0.70	0.28	0.63	0.51	0.08	0.09	0.22	0.11	1.00
10	0.57	0.17	0.84	0.58	0.47	0.69	0.61	0.16	0.06	0.38	0.67	0.41
11	0.37	0.31	0.21	0.22	0.66	0.80	0.87	0.00	0.22	0.51	0.67	0.00
12	0.35	0.29	1.00	0.68	0.59	0.96	0.89	0.00	0.02	0.02	0.44	0.12

Sub-Maximum One-Foot Braking, Knee 120 degree

Table C3. Subject Force Exertions and Postures on Sub-Maximum One-Foot Braking Knee Angle 120 degree Test

Subject Number	Force in X-Axis (N)	Force in Y-Axis (N)	Torque in Z-Axis (Nm)	Hip Flex. Angle (degree)	Hip Abd. Angle (degree)	Knee Angle (degree)	Ankle Angle (degree)
1	416	236	48	120	85	147	91
2	422	248	8	115	94	149	95
3	259	182	-5	102	107	132	85
4	346	223	25	120	108	125	79
5	204	165	-9	123	99	129	78
6	145	104	-6	118	96	139	85
7	388	204	21	126	91	138	84
8	416	231	36	120	99	142	88
9	204	117	10	119	101	142	87
10	330	286	-9	127	96	142	86
11	324	250	-1	117	84	136	86
12	653	352	22	120	95	151	93

Table C4. Subject EMG data on Sub-Maximum One-Foot Braking Knee Angle 120 degree Test

Subject Number	Leg				Femur						Hip	
	MG	LG	SOL	TA	RF	VL	VM	AL	BFLH	BFSH	GMED	GMAX
1	0.30	0.10	0.47	0.18	0.10	0.30	0.10	0.07	0.03	0.17	0.22	0.06
2	0.12	0.08	0.41	0.01	0.23	0.23	0.31	0.03	0.04	0.15	0.34	0.02
3	0.22	0.17	0.23	0.07	0.31	0.53	0.31	0.15	0.03	0.12	0.24	0.11
4	0.17	0.12	0.55	0.64	0.21	0.38	0.46	0.09	0.01	0.06	0.33	0.22
5	0.04	0.03	0.13	0.01	0.40	0.66	0.42	0.14	0.12	0.11	0.36	0.07
6	0.03	0.00	0.03	0.01	0.27	0.26	0.16	0.03	0.06	0.25	0.22	0.50
7	0.10	0.10	0.42	0.16	0.14	0.32	0.34	0.02	0.04	0.06	0.14	0.01
8	0.21	0.34	0.48	0.09	0.15	0.37	0.50	0.05	0.10	0.33	0.35	0.01
9	0.05	0.05	0.27	0.24	0.10	0.27	0.23	0.04	0.02	0.06	0.05	0.95
10	0.06	-0.01	0.05	0.23	0.21	0.34	0.42	0.05	0.03	0.20	0.33	0.36
11	0.23	0.07	0.07	0.02	0.26	0.45	0.52	0.00	0.12	0.31	0.36	0.26
12	0.12	0.05	0.36	0.33	0.26	0.74	0.49	0.00	0.01	0.03	0.18	0.06

Maximum Two-Foot Bracing, Knee 120 degree

Table C5. Subject Force Exertions and Postures on Maximum Two-Foot Bracing Knee Angle 120 degree Test

Subject Number	Force in X-Axis (N)	Force in Y-Axis (N)	Torque in Z-Axis (Nm)	Hip Flex. Angle (degree)	Hip Abd. Angle (degree)	Knee Angle (degree)	Ankle Angle (degree)
1	869	371	125	123	84	156	97
2	941	389	112	117	95	152	97
3	492	332	0	109	102	133	85
4	777	426	83	124	107	136	85
5	414	280	18	124	98	134	82
6	367	275	-6	119	98	138	84
7	748	381	75	126	94	137	83
8	1195	522	129	121	100	148	92
9	336	227	11	120	103	140	86
10	827	454	75	126	97	142	86
11	937	528	84	116	91	142	91
12	1477	594	155	122	98	155	96

Table C6. Subject EMG data on Maximum Two-Foot Bracing Knee Angle 120 degree Test

Subject Number	Leg				Femur						Hip	
	MG	LG	SOL	TA	RF	VL	VM	AL	BFLH	BFSH	GMED	GMAX
1	0.57	0.70	0.84	0.93	0.34	0.51	0.14	0.20	0.03	0.03	0.04	0.04
2	0.64	0.83	1.00	0.07	0.11	0.18	0.23	0.02	0.03	0.11	0.27	0.02
3	0.27	0.23	0.33	0.04	0.37	0.67	0.44	0.19	0.04	0.18	0.26	0.11
4	0.58	0.19	0.92	0.70	0.25	0.38	0.50	0.10	0.01	0.07	0.70	0.21
5	0.13	0.10	0.38	0.05	0.30	0.45	0.33	0.12	0.19	0.09	0.08	0.06
6	0.29	0.02	0.14	0.02	0.39	0.33	0.27	0.05	0.13	0.33	0.42	0.54
7	0.17	0.15	0.64	0.15	0.10	0.27	0.30	0.04	0.05	0.05	0.09	0.03
8	0.31	0.69	0.82	0.15	0.24	0.57	0.79	0.06	0.02	0.54	0.19	0.01
9	0.42	0.17	0.13	0.18	0.09	0.26	0.22	0.05	0.12	0.10	0.07	0.99
10	0.52	0.14	0.71	0.21	0.11	0.37	0.40	0.09	0.04	0.22	0.17	0.37
11	1.00	1.00	0.96	1.00	0.80	0.87	0.96	0.22	0.30	0.61	0.11	0.28
12	0.42	0.24	0.95	0.55	0.32	0.88	0.70	0.00	0.03	0.26	0.17	0.07

Sub-Maximum Two-Foot Bracing, Knee 120 degree

Table C7. Subject Force Exertions and Postures on Sub-Maximum Two-Foot Bracing Knee Angle 120 degree Test

Subject Number	Force in X-Axis (N)	Force in Y-Axis (N)	Torque in Z-Axis (Nm)	Hip Flex. Angle (degree)	Hip Abd. Angle (degree)	Knee Angle (degree)	Ankle Angle (degree)
1	505	254	79	120	86	148	92
2	520	277	17	116	96	148	94
3	297	207	5	105	105	131	84
4	445	273	55	119	105	125	79
5	259	188	0	122	98	129	79
6	220	172	-6	117	98	135	82
7	443	243	24	125	97	133	82
8	696	384	65	121	101	141	88
9	227	143	16	118	103	137	84
10	397	272	18	125	98	136	81
11	482	340	26	116	90	134	85
12	766	354	59	120	99	148	92

Table C8. Subject EMG data on Sub-Maximum Two-Foot Bracing Knee Angle 120 degree Test

Subject	Leg				Femur						Hip	
Number	MG	LG	SOL	TA	RF	VL	VM	AL	BFLH	BFSH	GMED	GMAX
1	0.24	0.12	0.54	0.50	0.01	0.19	0.07	0.14	0.03	0.08	0.07	0.05
2	0.18	0.13	0.34	0.01	0.11	0.14	0.22	0.02	0.03	0.10	0.10	0.02
3	0.36	0.34	0.49	0.03	0.10	0.30	0.21	0.10	0.02	0.12	0.10	0.10
4	0.18	0.10	0.64	0.44	0.15	0.15	0.27	0.07	0.00	0.03	0.20	0.22
5	0.07	0.05	0.20	0.02	0.20	0.32	0.22	0.08	0.10	0.06	0.08	0.06
6	0.04	0.02	0.16	0.00	0.17	0.16	0.12	0.05	0.07	0.16	0.10	0.52
7	0.07	0.07	0.34	0.07	0.06	0.18	0.25	0.02	0.04	0.03	0.06	0.02
8	0.14	0.27	0.41	0.02	0.11	0.31	0.32	0.10	0.02	0.27	0.02	0.00
9	0.03	0.02	0.17	0.06	0.03	0.10	0.09	0.03	0.02	0.03	0.03	0.93
10	0.30	0.06	0.36	0.03	0.05	0.20	0.30	0.08	0.02	0.11	0.15	0.40
11	0.20	0.11	0.11	0.03	0.17	0.36	0.39	0.08	0.10	0.27	0.06	0.25
12	0.31	0.06	0.44	0.31	0.08	0.57	0.35	0.03	0.01	0.02	0.10	0.06

Maximum One-Foot Braking, Knee 105 degree

Table C9. Subject Force Exertions and Postures on Maximum One-Foot Braking Knee Angle 105 degree Test

Subject Number	Force in X-Axis (N)	Force in Y-Axis (N)	Torque in Z-Axis (Nm)	Hip Flex. Angle (degree)	Hip Abd. Angle (degree)	Knee Angle (degree)	Ankle Angle (degree)
1	633	389	68	110	80	122	75
2	593	373	46	107	89	119	75
3	308	221	1	100	106	119	75
4	514	384	28	120	103	119	73
5	303	242	2	122	103	121	73
6	250	208	-8	113	97	124	74
7	636	360	41	123	88	126	74
8	691	403	57	117	93	134	81
9	381	254	13	117	111	131	79
10	755	544	56	126	95	133	79
11	576	439	-2	112	89	123	76
12	1136	589	97	117	87	141	86

Table C10. Subject EMG data on Maximum One-Foot Braking Knee Angle 105 degree Test

Subject	Leg				Femur						Hip	
Number	MG	LG	SOL	TA	RF	VL	VM	AL	BFLH	BFSH	GMED	GMAX
1	0.17	0.21	0.84	0.21	0.45	0.66	0.36	0.14	0.03	0.29	0.21	0.09
2	0.25	0.31	0.70	0.06	0.76	0.99	0.94	0.02	0.11	0.47	0.64	0.11
3	0.56	0.77	0.55	0.49	0.76	1.00	0.78	0.04	0.07	0.22	0.33	0.26
4	0.25	0.17	0.89	0.84	0.60	0.83	0.89	0.06	0.01	0.13	0.62	0.21
5	0.13	0.12	0.36	0.10	0.70	0.99	0.61	0.21	0.11	0.17	0.28	0.14
6	0.06	0.03	0.12	0.06	0.77	0.89	0.84	0.00	0.04	0.77	0.36	0.55
7	0.27	0.23	0.83	0.44	0.97	0.93	0.95	0.09	0.05	0.19	0.78	0.11
8	0.27	0.69	0.77	0.53	0.75	0.82	0.92	0.20	0.04	0.80	0.48	0.05
9	0.76	0.56	0.48	1.00	0.79	0.67	0.78	0.00	0.08	0.29	0.09	0.68
10	0.69	0.21	1.00	0.69	0.73	0.94	0.88	0.07	0.09	0.60	0.62	1.00
11	0.16	0.24	0.20	0.57	1.00	1.00	1.00	0.07	0.10	0.88	0.86	0.02
12	0.22	0.21	0.92	0.88	0.95	1.00	1.00	0.00	0.00	0.03	0.44	0.13

Sub-Maximum One-Foot Braking, Knee 105 degree

Table C11. Subject Force Exertions and Postures on Sub-Maximum One-Foot Braking Knee Angle 105 degree Test

Subject Number	Force in X-Axis (N)	Force in Y-Axis (N)	Torque in Z-Axis (Nm)	Hip Flex. Angle (degree)	Hip Abd. Angle (degree)	Knee Angle (degree)	Ankle Angle (degree)
1	347	238	33	107	84	117	72
2	310	223	8	104	95	115	73
3	223	163	-1	95	104	116	74
4	305	230	21	117	108	113	70
5	201	166	3	120	101	120	72
6	146	123	-7	113	97	122	73
7	437	253	20	121	92	123	73
8	388	246	32	117	95	128	78
9	233	159	8	116	106	129	77
10	366	287	4	123	96	126	75
11	289	244	1	109	88	118	74
12	584	333	37	113	87	134	82

Table C12. Subject EMG data on Sub-Maximum One-Foot Braking Knee Angle 105 degree Test

Subject	Leg				Femur						Hip	
Number	MG	LG	SOL	TA	RF	VL	VM	AL	BFLH	BFSH	GMED	GMAX
1	0.12	0.10	0.37	0.05	0.12	0.40	0.21	0.09	0.03	0.19	0.13	0.06
2	0.15	0.10	0.33	0.01	0.37	0.59	0.51	0.06	0.05	0.25	0.44	0.03
3	0.34	0.34	0.36	0.25	0.68	0.79	0.58	0.17	0.05	0.16	0.24	0.14
4	0.20	0.12	0.64	0.50	0.26	0.48	0.50	0.10	0.01	0.07	0.42	0.21
5	0.07	0.06	0.23	0.07	0.38	0.57	0.42	0.13	0.06	0.11	0.16	0.06
6	0.02	0.01	0.03	0.00	0.42	0.43	0.34	0.04	0.02	0.35	0.20	0.50
7	0.15	0.12	0.54	0.22	0.48	0.57	0.68	0.05	0.05	0.12	0.46	0.06
8	0.14	0.29	0.41	0.08	0.17	0.43	0.56	0.15	0.03	0.37	0.33	0.02
9	0.18	0.14	0.24	0.20	0.15	0.36	0.49	0.06	0.04	0.12	0.05	0.61
10	0.26	0.06	0.32	0.07	0.30	0.48	0.52	0.16	0.04	0.28	0.34	0.37
11	0.17	0.10	0.08	0.14	0.49	0.53	0.64	0.00	0.08	0.42	0.38	0.24
12	0.12	0.11	0.57	0.83	0.55	0.90	0.78	0.00	0.00	0.03	0.19	0.07

Maximum Two-Foot Bracing, Knee 105 degree

Table C13. Subject Force Exertions and Postures on Maximum Two-Foot Bracing Knee Angle 105 degree Test

Subject Number	Force in X-Axis (N)	Force in Y-Axis (N)	Torque in Z-Axis (Nm)	Hip Flex. Angle (degree)	Hip Abd. Angle (degree)	Knee Angle (degree)	Ankle Angle (degree)
1	806	490	91	113	91	124	76
2	742	428	81	108	97	117	74
3	472	334	8	103	108	117	74
4	731	524	57	121	106	113	69
5	403	307	2	121	105	123	74
6	318	288	-16	112	96	123	73
7	861	454	93	120	98	123	74
8	1174	533	130	116	100	129	79
9	432	294	23	117	105	129	77
10	843	513	74	124	100	131	78
11	612	439	21	111	92	118	74
12	1411	670	142	115	98	135	83

Table C14. Subject EMG data on Maximum Two-Foot Bracing Knee Angle 105 degree Test

Subject	Leg				Femur						Hip	
Number	MG	LG	SOL	TA	RF	VL	VM	AL	BFLH	BFSH	GMED	GMAX
1	0.44	0.49	0.71	0.85	0.66	0.58	0.30	0.25	0.04	0.28	0.09	0.07
2	0.22	0.21	0.68	0.05	0.41	0.69	0.61	0.10	0.11	0.34	0.19	0.03
3	0.46	0.63	0.50	0.17	0.72	0.89	0.63	0.24	0.06	0.19	0.15	0.18
4	0.29	0.20	0.91	1.00	0.42	0.76	0.80	0.18	0.01	0.12	0.45	0.21
5	0.04	0.03	0.14	0.01	0.31	0.58	0.36	0.17	0.12	0.10	0.06	0.07
6	0.03	0.01	0.02	0.02	0.57	0.52	0.39	0.06	0.04	0.50	0.84	0.60
7	0.21	0.18	0.69	0.44	0.64	0.63	0.68	0.05	0.05	0.11	0.21	0.05
8	0.23	0.51	0.66	0.28	0.61	0.79	0.95	0.09	0.04	0.79	0.16	0.02
9	0.68	0.46	0.32	0.55	0.15	0.40	0.52	0.08	0.14	0.19	0.05	0.89
10	0.51	0.14	0.69	0.34	0.43	0.55	0.59	0.16	0.05	0.36	0.21	0.38
11	0.47	0.23	0.18	0.37	0.74	0.79	0.88	0.04	0.21	0.69	0.14	0.25
12	0.20	0.20	0.92	0.87	0.83	0.98	0.94	0.00	0.03	0.03	0.24	0.07

Sub-Maximum Two-Foot Bracing, Knee 105 degree

Table C15. Subject Force Exertions and Postures on Sub-Maximum Two-Foot Bracing Knee Angle 105 degree Test

Subject Number	Force in X-Axis (N)	Force in Y-Axis (N)	Torque in Z-Axis (Nm)	Hip Flex. Angle (degree)	Hip Abd. Angle (degree)	Knee Angle (degree)	Ankle Angle (degree)
1	446	300	55	110	91	117	72
2	405	278	24	106	97	114	72
3	273	205	6	95	108	114	73
4	422	285	40	118	111	114	70
5	226	179	-1	120	104	117	70
6	127	113	-7	111	95	121	72
7	478	271	34	120	100	120	72
8	633	354	65	116	100	128	78
9	266	173	16	115	106	126	76
10	459	297	29	124	100	127	74
11	325	260	1	110	92	116	72
12	752	407	55	113	101	130	80

Table C16. Subject EMG data on Sub-Maximum Two-Foot Bracing Knee Angle 105 degree Test

Subject	Leg				Femur						Hip	
Number	MG	LG	SOL	TA	RF	VL	VM	AL	BFLH	BFSH	GMED	GMAX
1	0.13	0.09	0.35	0.06	0.08	0.25	0.13	0.12	0.03	0.14	0.13	0.06
2	0.17	0.06	0.32	0.01	0.27	0.49	0.33	0.06	0.08	0.18	0.14	0.02
3	0.38	0.36	0.48	0.05	0.17	0.35	0.25	0.10	0.02	0.08	0.05	0.12
4	0.15	0.10	0.55	0.53	0.24	0.35	0.41	0.09	0.01	0.04	0.14	0.22
5	0.05	0.03	0.13	0.01	0.23	0.32	0.24	0.07	0.11	0.06	0.03	0.06
6	0.01	0.00	0.01	0.00	0.18	0.20	0.10	0.03	0.02	0.16	0.08	0.34
7	0.10	0.10	0.45	0.18	0.25	0.32	0.32	0.03	0.05	0.05	0.07	0.03
8	0.16	0.27	0.38	0.05	0.14	0.45	0.54	0.09	0.03	0.35	0.03	0.00
9	0.05	0.04	0.24	0.04	0.08	0.23	0.27	0.04	0.02	0.07	0.04	0.61
10	0.31	0.06	0.36	0.03	0.09	0.34	0.47	0.06	0.03	0.18	0.13	0.36
11	0.18	0.07	0.05	0.02	0.19	0.41	0.52	0.00	0.08	0.34	0.08	0.24
12	0.11	0.07	0.50	0.57	0.25	0.71	0.50	0.00	0.00	0.03	0.09	0.06

Maximum One-Foot Braking, Knee 90 degree

Table C17. Subject Force Exertions and Postures on Maximum One-Foot Braking Knee Angle 90 degree Test

Subject Number	Force in X-Axis (N)	Force in Y-Axis (N)	Torque in Z-Axis (Nm)	Hip Flex. Angle (degree)	Hip Abd. Angle (degree)	Knee Angle (degree)	Ankle Angle (degree)
1	607	410	64	106	83	109	65
2	548	376	49	100	92	99	60
3	333	248	24	92	105	103	66
4	408	355	25	118	100	100	58
5	241	209	6	121	106	108	62
6	228	221	-1	110	97	111	65
7	619	432	36	122	85	114	64
8	795	524	59	118	93	122	70
9	270	218	6	113	105	112	64
10	539	412	36	120	95	119	68
11	474	385	19	108	90	106	64
12	678	484	15	110	90	115	67

Table C18. Subject EMG data on Maximum One-Foot Braking Knee Angle 90 degree Test

Subject	Leg				Femur						Hip	
Number	MG	LG	SOL	TA	RF	VL	VM	AL	BFLH	BFSH	GMED	GMAX
1	0.17	0.22	0.80	0.40	0.75	0.76	0.46	0.26	0.04	0.33	0.24	0.15
2	0.19	0.28	0.70	0.12	1.00	1.00	1.00	0.05	0.11	0.55	0.45	0.12
3	1.00	1.00	1.00	0.88	1.00	0.87	1.00	0.10	0.10	0.24	0.39	0.55
4	0.30	0.19	1.00	0.79	0.83	1.00	1.00	0.01	0.02	0.16	0.71	0.22
5	0.12	0.11	0.34	0.22	0.70	0.93	0.66	0.13	0.07	0.18	0.12	0.12
6	0.08	0.03	0.19	0.04	1.00	1.00	1.00	0.00	0.05	0.85	0.29	0.55
7	0.34	0.30	0.98	1.00	0.97	1.00	1.00	0.14	0.07	0.23	0.97	0.49
8	0.33	0.91	0.96	0.86	1.00	1.00	1.00	0.48	0.04	1.00	0.61	0.45
9	0.58	0.48	0.39	0.84	0.59	1.00	1.00	0.00	0.07	0.30	0.10	0.69
10	0.68	0.21	0.97	1.00	1.00	1.00	1.00	0.06	0.10	0.74	0.62	0.86
11	0.22	0.33	0.27	0.79	0.94	0.96	0.99	0.11	0.07	1.00	0.75	0.18
12	0.17	0.15	0.64	1.00	1.00	0.96	0.98	0.01	0.00	0.03	0.29	0.15

Sub-Maximum One-Foot Braking, Knee 90 degree

Table C19. Subject Force Exertions and Postures on Sub-Maximum One-Foot Braking Knee Angle 90 degree Test

Subject Number	Force in X-Axis (N)	Force in Y-Axis (N)	Torque in Z-Axis (Nm)	Hip Flex. Angle (degree)	Hip Abd. Angle (degree)	Knee Angle (degree)	Ankle Angle (degree)
1	323	232	33	104	84	105	63
2	323	251	20	99	96	96	58
3	220	167	16	90	105	100	66
4	250	196	24	115	104	98	58
5	136	122	1	118	105	105	60
6	159	155	-1	109	96	110	65
7	363	227	16	118	95	110	63
8	443	328	36	115	97	117	68
9	173	143	0	111	104	110	63
10	315	221	21	119	97	116	67
11	267	246	2	106	90	103	62
12	393	300	20	111	94	111	65

Table C20. Subject EMG data on Sub-Maximum One-Foot Braking Knee Angle 90 degree Test

Subject Number	Leg				Femur						Hip	
	MG	LG	SOL	TA	RF	VL	VM	AL	BFLH	BFSH	GMED	GMAX
1	0.13	0.13	0.43	0.07	0.30	0.49	0.28	0.13	0.04	0.25	0.17	0.06
2	0.22	0.18	0.43	0.06	0.59	0.74	0.68	0.09	0.09	0.43	0.53	0.05
3	0.80	0.94	0.92	0.56	0.89	0.75	0.80	0.00	0.08	0.21	0.31	0.20
4	0.17	0.11	0.61	0.58	0.35	0.57	0.63	0.12	0.01	0.09	0.38	0.22
5	0.08	0.07	0.23	0.07	0.38	0.52	0.47	0.08	0.05	0.13	0.08	0.06
6	0.04	0.01	0.10	0.01	0.53	0.63	0.54	0.06	0.03	0.55	0.20	0.53
7	0.13	0.11	0.50	0.34	0.58	0.72	0.85	0.05	0.07	0.15	0.68	0.07
8	0.17	0.36	0.49	0.69	0.49	0.65	0.85	0.19	0.05	0.61	0.39	0.03
9	0.22	0.17	0.22	0.28	0.30	0.53	0.58	0.09	0.04	0.17	0.05	0.59
10	0.35	0.08	0.42	0.21	0.44	0.52	0.62	0.16	0.05	0.31	0.35	0.37
11	0.11	0.12	0.10	0.23	0.59	0.65	0.80	0.00	0.04	0.63	0.39	0.25
12	0.10	0.09	0.53	0.81	0.41	0.79	0.66	0.00	0.00	0.03	0.14	0.07

Maximum Two-Foot Bracing, Knee 90 degree

Table C21. Subject Force Exertions and Postures on Maximum Two-Foot Bracing Knee Angle 90 degree Test

Subject Number	Force in X-Axis (N)	Force in Y-Axis (N)	Torque in Z-Axis (Nm)	Hip Flex. Angle (degree)	Hip Abd. Angle (degree)	Knee Angle (degree)	Ankle Angle (degree)
1	728	493	79	107	91	105	63
2	628	411	71	101	97	97	59
3	449	339	27	95	106	101	66
4	647	533	49	118	107	103	60
5	350	303	-8	119	103	109	63
6	372	337	2	109	98	111	65
7	787	455	68	119	96	111	64
8	1018	525	102	114	101	118	70
9	375	301	5	112	105	112	64
10	819	407	75	120	100	119	69
11	647	480	32	106	95	103	63
12	817	505	58	109	102	113	67

Table C22. Subject EMG data on Maximum Two-Foot Bracing Knee Angle 90 degree Test

Subject	Leg				Femur						Hip	
Number	MG	LG	SOL	TA	RF	VL	VM	AL	BFLH	BFSH	GMED	GMAX
1	0.13	0.13	0.47	0.06	0.42	0.52	0.29	0.22	0.04	0.26	0.11	0.07
2	0.19	0.23	0.52	0.05	0.71	0.89	0.85	0.05	0.10	0.50	0.19	0.03
3	0.60	0.66	0.48	1.00	0.88	0.80	0.78	0.05	0.07	0.20	0.15	0.21
4	0.24	0.18	0.95	0.58	0.56	0.84	0.85	0.12	0.01	0.13	0.15	0.22
5	0.06	0.05	0.20	0.05	0.75	0.89	0.67	0.10	0.12	0.18	0.03	0.07
6	0.06	0.02	0.16	0.02	0.80	0.95	0.87	0.00	0.05	0.81	0.68	0.59
7	0.21	0.19	0.76	0.52	0.61	0.77	0.82	0.06	0.06	0.15	0.29	0.06
8	0.19	0.43	0.56	1.00	0.68	0.82	0.94	0.13	0.03	0.79	0.09	0.03
9	0.73	0.39	0.41	0.89	0.28	0.57	0.58	0.10	0.10	0.22	0.05	0.68
10	0.53	0.14	0.67	0.41	0.52	0.60	0.66	0.08	0.05	0.37	0.16	0.39
11	0.37	0.36	0.29	0.59	0.69	0.76	0.88	0.00	0.06	0.76	0.10	0.25
12	0.14	0.14	0.69	0.96	0.95	0.95	0.94	0.00	0.00	0.03	0.18	0.07

Sub-Maximum Two-Foot Bracing, Knee 90 degree

Table C23. Subject Force Exertions and Postures on Sub-Maximum Two-Foot Bracing Knee Angle 90 degree Test

Subject Number	Force in X-Axis (N)	Force in Y-Axis (N)	Torque in Z-Axis (Nm)	Hip Flex. Angle (degree)	Hip Abd. Angle (degree)	Knee Angle (degree)	Ankle Angle (degree)
1	400	312	38	107	92	103	62
2	368	290	18	100	99	95	58
3	274	229	15	94	109	98	65
4	362	290	32	114	107	96	58
5	216	195	4	120	107	105	60
6	239	215	3	108	97	109	65
7	433	262	25	118	97	108	62
8	546	386	42	115	98	115	67
9	225	197	-4	111	107	109	63
10	439	308	16	119	101	117	67
11	364	342	1	106	94	100	61
12	502	353	21	108	102	110	65

Table C24. Subject EMG data on Sub-Maximum Two-Foot Bracing Knee Angle 90 degree Test

Subject	Leg				Femur						Hip	
Number	MG	LG	SOL	TA	RF	VL	VM	AL	BFLH	BFSH	GMED	GMAX
1	0.11	0.08	0.27	0.08	0.09	0.34	0.16	0.10	0.04	0.16	0.07	0.06
2	0.10	0.06	0.26	0.02	0.36	0.62	0.56	0.06	0.06	0.30	0.13	0.02
3	0.37	0.36	0.41	0.19	0.34	0.40	0.41	0.14	0.04	0.11	0.07	0.14
4	0.17	0.10	0.61	0.33	0.26	0.45	0.52	0.10	0.01	0.07	0.04	0.23
5	0.07	0.05	0.20	0.04	0.28	0.49	0.36	0.08	0.06	0.10	0.02	0.06
6	0.09	0.04	0.24	0.00	0.37	0.39	0.29	0.05	0.02	0.31	0.17	0.51
7	0.11	0.10	0.49	0.17	0.29	0.40	0.44	0.04	0.06	0.07	0.11	0.04
8	0.17	0.24	0.33	0.07	0.21	0.51	0.64	0.13	0.01	0.42	0.03	0.01
9	0.04	0.03	0.14	0.00	0.11	0.32	0.32	0.05	0.02	0.08	0.02	0.59
10	0.23	0.05	0.26	0.05	0.25	0.38	0.49	0.08	0.03	0.21	0.16	0.35
11	0.07	0.08	0.07	0.03	0.39	0.44	0.67	0.00	0.04	0.47	0.10	0.25
12	0.08	0.06	0.40	0.69	0.38	0.70	0.54	0.00	0.00	0.03	0.08	0.06

APPENDIX D

Table D1. Comparison of Experimental and Predicted Muscle Activations for Strength Adjustment for Subject01

	Subject	Model	Model/Subject	Trial
RF	1.00	1.25	1.25	knee extension
VL	1.00	1.25	1.25	knee extension
VM	1.00	1.25	1.25	knee extension
AL	0.92	0.62	0.68	hip adduction
BFLH	1.00	1.18	1.18	knee flexion
BFSH	1.00	1.18	1.18	knee flexion
GMED	1.00	0.62	0.62	hip abduction
GMAX	0.96	0.67	0.70	hip extension

Table D2. Comparison of Experimental and Predicted Muscle Activations for Strength Adjustment for Subject02

	Subject	Model	Model/Subject	Trial
RF	1.00	0.76	0.76	knee extension
VL	1.00	0.77	0.77	knee 90 Max. (one-foot)
VM	1.00	0.77	0.77	knee 90 Max. (one-foot)
AL	1.00	0.76	0.76	hip adduction
BFLH	1.00	0.54	0.54	knee flexion
BFSH	1.00	0.54	0.54	knee flexion
GMED	1.00	0.76	0.76	hip abduction
GMAX	1.00	0.62	0.62	hip abduction

Table D3. Comparison of Experimental and Predicted Muscle Activations for Strength Adjustment for Subject03

	Subject	Model	Model/Subject	Trial
RF	1.00	0.41	0.41	knee 90 Max (one-foot)
VL	1.00	0.30	0.30	knee 105 Max (one-foot)
VM	1.00	0.41	0.41	knee 90 Max. (one-foot)
AL	1.00	0.53	0.53	hip adduction
BFLH	1.00	0.37	0.37	knee flexion
BFSH	1.00	0.37	0.37	knee flexion
GMED	1.00	0.53	0.53	hip abduction
GMAX	1.00	0.43	0.43	hip abduction

Table D4. Comparison of Experimental and Predicted Muscle Activations for Strength Adjustment for Subject04

	Subject	Model	Model/Subject	Trial
RF	1.00	0.52	0.52	knee extension
VL	1.00	0.61	0.61	knee 90 Max (one-foot)
VM	1.00	0.61	0.61	knee 90 Max. (one-foot)
AL	1.00	0.51	0.51	hip adduction
BFLH	1.00	0.51	0.51	knee flexion
BFSH	1.00	0.51	0.51	knee flexion
GMED	1.00	0.51	0.51	hip extension
GMAX	1.00	0.36	0.36	hip extension

Table D5. Comparison of Experimental and Predicted Muscle Activations for Strength Adjustment for Subject05

	Subject	Model	Model/Subject	Trial
RF	1.00	0.44	0.44	knee extension
VL	0.92	0.44	0.47	knee extension
VM	1.00	0.44	0.44	knee extension
AL	0.77	0.24	0.31	hip adduction
BFLH	1.00	0.23	0.23	knee flexion
BFSH	1.00	0.23	0.23	knee flexion
GMED	1.00	0.24	0.24	hip abduction
GMAX	1.00	0.32	0.32	hip abduction

Table D6. Comparison of Experimental and Predicted Muscle Activations for Strength Adjustment for Subject06

	Subject	Model	Model/Subject	Trial
RF	1.00	0.23	0.23	knee 90 Max. (braking)
VL	1.00	0.23	0.23	knee 90 Max. (braking)
VM	1.00	0.23	0.23	knee 90 Max. (braking)
AL	1.00	0.35	0.35	knee flexion
BFLH	1.00	0.31	0.31	knee flexion
BFSH	1.00	0.31	0.31	hip flexion
GMED	1.00	0.35	0.35	hip abduction
GMAX	1.00	0.33	0.33	hip abduction

Table D7. Comparison of Experimental and Predicted Muscle Activations for Strength Adjustment for Subject07

	Subject	Model	Model/Subject	Trial
RF	1.00	0.66	0.66	knee extension
VL	1.00	0.71	0.71	knee 90 Max (braking)
VM	1.00	0.71	0.71	knee 90 Max (braking)
AL	1.00	0.81	0.81	hip adduction
BFLH	1.00	0.68	0.68	knee flexion
BFSH	1.00	0.68	0.68	knee flexion
GMED	1.00	0.81	0.81	knee extension
GMAX	1.00	0.73	0.73	hip extension

Table D8. Comparison of Experimental and Predicted Muscle Activations for Strength Adjustment for Subject08

	Subject	Model	Model/Subject	Trial
RF	1.00	0.65	0.65	knee 90 Max. (braking)
VL	1.00	0.65	0.65	knee 90 Max. (braking)
VM	1.00	0.65	0.65	knee 90 Max. (braking)
AL	1.00	0.88	0.88	hip adduction
BFLH	1.00	0.82	0.82	knee flexion
BFSH	1.00	0.82	0.82	knee flexion
GMED	1.00	0.88	0.88	hip abduction
GMAX	1.00	0.55	0.55	hip abduction

Table D9. Comparison of Experimental and Predicted Muscle Activations for Strength Adjustment for Subject09

	Subject	Model	Model/Subject	Trial
RF	1.00	0.41	0.41	knee extension
VL	1.00	0.28	0.28	knee 90 Max. (braking)
VM	1.00	0.28	0.28	knee 90 Max. (braking)
AL	1.00	0.34	0.34	knee flexion
BFLH	1.00	0.60	0.60	knee flexion
BFSH	1.00	0.60	0.60	knee flexion
GMED	1.00	0.34	0.34	hip abduction
GMAX	1.00	0.37	0.37	hip abduction

Table D10. Comparison of Experimental and Predicted Muscle Activations for Strength Adjustment for Subject10

	Subject	Model	Model/Subject	Trial
RF	1.00	0.45	0.45	knee 90 Max. (braking)
VL	1.00	0.45	0.45	knee 90 Max. (braking)
VM	1.00	0.45	0.45	knee 90 Max. (braking)
AL	1.00	0.59	0.59	knee flexion
BFLH	1.00	0.61	0.61	knee flexion
BFSH	1.00	0.61	0.61	knee flexion
GMED	1.00	0.59	0.59	hip abduction
GMAX	1.00	0.50	0.50	knee 105 Max. (braking)

Table D11. Comparison of Experimental and Predicted Muscle Activations for Strength Adjustment for Subject11

	Subject	Model	Model/Subject	Trial
RF	1.00	0.50	0.50	knee 105 Max. (braking)
VL	1.00	0.50	0.50	knee 105 Max. (braking)
VM	1.00	0.50	0.50	knee 105 Max. (braking)
AL	0.96	0.45	0.47	hip adduction
BFLH	1.00	0.49	0.49	knee flexion
BFSH	0.89	0.49	0.54	knee flexion
GMED	1.00	0.45	0.45	hip abduction
GMAX	1.00	0.49	0.49	hip abduction

Table D12. Comparison of Experimental and Predicted Muscle Activations for Strength Adjustment for Subject12

	Subject	Model	Model/Subject	Trial
RF	1.00	0.65	0.65	knee 90 Max. (braking)
VL	1.00	0.37	0.37	knee 105 Max. (braking)
VM	1.00	0.37	0.37	knee 105 Max. (braking)
AL	0.95	0.85	0.89	hip adduction
BFLH	1.00	1.10	1.10	knee flexion
BFSH	1.00	1.10	1.10	knee flexion
GMED	1.00	0.85	0.85	hip abduction
GMAX	1.00	0.97	0.97	hip abduction

APPENDIX E

Table E1. Summary of Results from Frontal Knee Impact Simulations without Muscle Tension in Different Loading Conditions

Impactor Stiffness (MPa)	Impact Velocity (m/s)	Peak Knee Force (kN)	Peak Femoral Condyle Force (kN)	Peak Femur Bending Moment (Nm)	Peak Hip Force (kN)	Knee Injury Risk	Femur Injury Risk	Hip Injury Risk	Impactor Deform. (mm)
6	3	4.7	4.3	99.5	2.1	2.4%	0.0%	0.0%	23.6
6	4	6.5	5.7	140.0	2.9	8.0%	0.0%	0.9%	30.4
6	5	8.4	6.8	182.8	3.8	20.0%	0.1%	13.4%	36.8
6	6	10.2	8.0	233.6	4.3	38.5%	0.5%	32.4%	42.9
6	7	12.0	9.0	280.2	5.0	59.2%	2.7%	63.0%	48.6
6	8	13.7	10.4	325.0	5.9	77.6%	10.4%	87.7%	54.7
6	9	15.6	11.8	376.7	6.7	91.1%	35.4%	96.4%	60.6
6	10	16.8	12.9	425.8	7.5	96.0%	74.8%	99.1%	67.2
8	3	5.1	4.8	107.4	2.5	3.3%	0.0%	0.1%	20.4
8	4	7.2	6.5	147.7	3.4	11.9%	0.0%	5.9%	26.1
8	5	9.2	7.9	192.3	4.3	28.0%	0.1%	31.6%	31.7
8	6	11.4	9.2	242.0	5.0	51.7%	0.7%	63.0%	37.0
8	7	13.4	10.4	292.6	5.8	74.9%	4.0%	85.0%	42.2
8	8	15.5	11.5	338.7	6.5	90.5%	14.9%	95.1%	46.6
8	9	16.9	12.8	428.2	7.4	96.5%	76.6%	99.0%	51.2
10	3	5.4	5.1	117.9	2.9	4.2%	0.0%	0.7%	18.7
10	4	7.6	7.0	163.6	3.8	14.3%	0.0%	13.3%	23.8
10	5	9.7	8.6	214.8	4.6	33.1%	0.2%	46.2%	28.6
10	6	12.0	9.9	268.9	5.5	59.4%	1.8%	78.8%	33.0
10	7	14.2	11.2	320.0	6.4	81.5%	9.1%	93.8%	37.8
10	8	16.3	12.5	379.1	7.1	94.4%	37.1%	98.2%	42.2
12	3	5.7	5.4	131.4	3.1	5.0%	0.0%	2.3%	16.8
12	4	7.9	7.4	178.5	4.2	16.5%	0.0%	27.9%	21.4
12	5	10.1	9.3	234.5	5.1	36.5%	0.5%	67.4%	25.7
12	6	12.2	10.8	287.0	6.0	61.5%	3.4%	89.0%	29.7
12	7	14.7	12.3	354.4	6.9	86.0%	21.9%	97.3%	34.1
12	8	17.1	13.6	414.3	7.8	97.0%	65.6%	99.4%	38.4
14	3	5.8	5.6	140.6	3.3	5.4%	0.0%	3.9%	15.4
14	4	8.2	7.8	187.6	4.4	18.5%	0.1%	39.1%	19.7
14	5	10.4	9.6	244.7	5.4	40.1%	0.8%	74.9%	23.6
14	6	12.9	11.5	302.7	6.3	68.8%	5.5%	93.7%	27.4
14	7	15.5	13.2	378.0	7.3	90.5%	36.3%	98.8%	31.3
14	8	18.1	14.6	443.4	8.3	98.6%	86.7%	99.8%	35.0
16	3	6.0	5.8	148.3	3.5	6.1%	0.0%	7.2%	14.2
16	4	8.4	8.1	200.4	4.7	20.6%	0.1%	50.2%	18.3
16	5	10.8	10.1	257.9	5.8	45.2%	1.3%	85.0%	22.0
16	6	13.3	12.1	329.6	6.8	73.2%	11.8%	96.8%	25.2
16	7	15.6	14.0	399.3	7.7	91.4%	53.0%	99.4%	27.9
16	8	18.3	15.7	460.4	8.7	98.9%	94.3%	99.9%	31.7
18	3	6.1	5.9	153.6	3.6	6.6%	0.0%	10.5%	13.3
18	4	8.6	8.3	213.2	4.8	22.0%	0.2%	55.9%	17.2
18	5	11.0	10.5	274.0	6.1	47.7%	2.2%	90.7%	20.5
18	6	13.5	12.7	342.5	7.2	75.9%	16.4%	98.3%	23.9
18	7	16.3	14.7	415.8	8.2	94.5%	66.8%	99.8%	27.2
20	3	6.3	6.0	160.1	3.8	7.1%	0.0%	14.6%	12.5
20	4	8.8	8.5	221.3	5.1	23.9%	0.3%	65.5%	16.1
20	5	11.3	10.8	283.3	6.4	50.2%	3.0%	93.7%	19.3
20	6	13.9	13.0	360.7	7.5	79.2%	25.3%	99.0%	22.6
20	7	16.8	15.5	430.7	8.6	96.0%	78.4%	99.9%	25.7

Table E2. Summary of Results from Frontal Knee Impact Simulations with Muscle Tension in Different Loading Conditions

Impactor Stiffness (MPa)	Impact Velocity (m/s)	Peak Knee Force (kN)	Peak Femoral Condyle Force (kN)	Peak Femur Bending Moment (Nm)	Peak Hip Force (kN)	Knee Injury Risk	Femur Injury Risk	Hip Injury Risk	Impactor Deform. (mm)
6	3	4.7	4.2	142.0	3.2	2.3%	0.0%	2.4%	23.5
6	4	6.5	5.6	175.0	4.0	8.2%	0.0%	22.8%	30.1
6	5	8.4	6.8	208.9	4.7	20.4%	0.2%	51.5%	36.7
6	6	10.4	8.0	253.6	5.5	39.9%	1.1%	79.3%	42.8
6	7	12.1	9.3	304.8	6.3	60.4%	5.8%	93.2%	48.7
6	8	14.0	10.3	353.1	7.2	79.8%	21.2%	98.4%	54.2
6	9	15.5	11.5	402.5	8.0	90.7%	55.7%	99.6%	61.0
6	10	16.8	12.7	434.9	8.7	96.0%	81.4%	99.9%	66.1
8	3	5.0	4.7	151.6	3.4	3.0%	0.0%	5.3%	20.1
8	4	7.1	6.4	189.3	4.3	11.4%	0.1%	31.6%	26.0
8	5	9.1	7.9	238.1	5.1	27.0%	0.6%	65.6%	31.6
8	6	11.2	9.1	286.9	6.0	49.5%	3.4%	89.0%	36.8
8	7	13.2	10.4	340.2	6.9	72.7%	15.5%	97.4%	41.9
8	8	15.5	11.9	408.7	7.9	90.6%	60.9%	99.5%	46.7
8	9	17.1	13.0	474.4	9.1	96.8%	97.8%	100.0%	51.3
10	3	5.3	5.1	163.5	3.6	3.8%	0.0%	8.4%	18.2
10	4	7.5	7.0	207.8	4.3	13.5%	0.2%	35.1%	23.4
10	5	9.6	8.6	255.2	5.3	31.2%	1.1%	71.9%	28.3
10	6	11.8	9.9	307.0	6.2	56.4%	6.2%	92.6%	33.3
10	7	14.0	11.2	367.2	7.2	80.1%	29.1%	98.4%	37.4
10	8	16.2	12.4	434.0	8.2	94.2%	80.8%	99.8%	41.8
12	3	5.6	5.4	173.2	3.7	4.6%	0.0%	11.7%	16.6
12	4	7.8	7.4	223.1	4.5	16.0%	0.3%	42.5%	21.3
12	5	10.2	9.3	274.9	5.5	37.6%	2.3%	79.5%	25.8
12	6	12.4	11.0	326.8	6.5	63.6%	10.9%	95.2%	30.1
12	7	14.8	12.3	398.4	7.5	86.1%	52.2%	99.1%	33.8
12	8	17.2	13.6	469.3	8.6	97.1%	96.8%	99.9%	37.7
14	3	5.9	5.6	176.6	3.8	5.6%	0.0%	13.5%	15.5
14	4	8.2	7.8	229.3	4.7	18.9%	0.4%	48.8%	20.0
14	5	10.7	9.9	295.0	5.8	43.5%	4.3%	85.2%	24.0
14	6	13.1	11.6	352.4	6.7	71.1%	20.9%	96.4%	27.8
14	7	15.6	13.1	419.7	7.8	91.4%	70.0%	99.5%	31.6
14	8	18.1	14.7	497.4	8.8	98.7%	99.7%	99.9%	35.2
16	3	6.1	5.9	187.3	3.8	6.5%	0.1%	15.4%	14.5
16	4	8.6	8.2	240.1	4.8	21.7%	0.6%	56.5%	18.6
16	5	11.1	10.3	309.8	5.9	48.0%	6.8%	87.3%	22.4
16	6	13.6	12.4	369.2	6.9	76.1%	30.4%	97.3%	26.0
16	7	15.8	14.2	431.2	7.9	92.5%	78.8%	99.6%	28.6
16	8	18.6	15.8	522.5	9.0	99.1%	100.0%	100.0%	32.4
18	3	6.3	6.1	193.3	3.9	7.3%	0.1%	18.0%	13.6
18	4	8.8	8.5	257.1	5.0	24.0%	1.2%	63.4%	17.5
18	5	11.5	10.8	310.6	6.0	52.7%	6.9%	90.0%	21.0
18	6	14.1	13.1	385.8	7.2	80.8%	42.1%	98.4%	24.4
18	7	16.7	15.0	456.0	8.0	95.9%	92.7%	99.7%	27.7
20	3	6.5	6.3	195.8	4.0	8.1%	0.1%	20.5%	12.9
20	4	9.1	8.8	266.6	5.2	26.4%	1.7%	69.0%	16.5
20	5	11.8	11.3	333.0	6.2	56.3%	12.9%	92.7%	19.9
20	6	14.5	13.5	401.0	7.2	83.9%	54.4%	98.5%	23.1
20	7	17.2	15.8	476.9	8.3	97.1%	98.2%	99.8%	26.2

REFERENCES

Anderson, A. E., Peters, C. L., Tuttle, B. D., & Weiss, J. A. (2005). Subject-specific finite element model of the pelvis: development, validation and sensitivity studies. Journal of Biomechanical Engineering , 127, 364-373.

Ashman, R. B., Cowin, S. C., Burskirk, W. C., & Rice, J. C. (1984). A continuous wave technique for the measurement of the elastic properties of cortical bone. Journal of Biomechanics , 17, 349-361.

Athanasiou, K. A., Agarwal, A., Muffoletto, A., Dzida, F. J., Constsntinides, G., & Clem, M. (1995). Biomechanical properties of hip cartilage in experimental animal models. Clinical Orthopaedics and Related Research , 316, 254-266.

Athanasiou, K. A., Zhu, C. F., Lanctot, D. R., Agrawal, C. M., & Wang, X. (2000). Fundamentals of biomechanics in tissue engineering of bone. Tissue Engineering , 6, 361-381.

Atkinson, P. J., Garcia, J. J., Altiero, N. J., & Haut, R. C. (1997). The influence of impact interface on human knee injury: Implications for instrument panel design and the lower extremity injury criterion. Proceedings of the 41st Stapp Car Crash Conference (pp. 167-180). Warrendale, PA: Society of Automotiv Engineers.

Atkinson, P. J., Newberry, W. N., Atkinson, T. S., & Haut, R. C. (1998). A Method to increase the sensitivity range of pressure sensitive film. Journal of Biomechanics , 31 (9), 855-859.

Behr, M., Arnoux, P. J., Serre, T., Bidal, S., Kang, H. S., Thollon, L., et al. (2003). A Human model for road safety: from geometrical acquisition to model validation with Radioss. Computer Methods in Biomechanics and Biomechanical Engineering , 6 (4), 263-273.

Beillas, P., Begeman, P. C., Yang, K. H., King, A. I., Arnoux, P. J., Kang, H. S., et al. (2001). Lower limb: advanced FE model and new experimental data. Stapp Car Crash Journal , 469-493.

Bigland, B. (1981). EMG force relationship and fatigue of human voluntary contractions. Exercise and Sport Science Reviews , 9, 75-117.

Bigland, B., & Lippold, O. (1954). The relation between force, velocity and integrated EMG. Journal of Physiology , 123, 214-224.

Bogey, R. A., Perry, J., & Gitter, A. J. (2005). An EMG-to-force processing approach for determining ankle muscle forces during normal human gait. IEEE Transactions on Neural Systems and Rehabilitation Engineering , 13, 302-310.

Brand, R. A., Pedersen, D. R., Davy, D. T., Kotzar, G. M., Heiple, K. G., & Goldberg, V. M. (1994). Comparison of hip force calculations and measurements in the same patient. Journal of Arthroplasty , 9 (1), 45-51.

Chancey, V. C., Nightingale, R. W., Van Ee, C. A., Knaub, K. E., & Myers, B. S. (2003). Improved estimation of human neck tensile tolerance: reducing the range of reported tolerance using anthropometrically correct muscle and optimized physiologic initial conditions. Stapp Car Crash Journal , 47.

Cheng, R., Yang, K. H., Levine, R. S., & King, A. I. (1984). Dynamic Impact loading of the femur under passive restrained condition. Proceedings of the Twenty-Eight Stapp Car Crash Conference (pp. 101-118). Warrendale, PA: Society of Automotive Engineering.

Choi, H. Y., Sah, S. J., Lee, B., Cho, H. S., Kang, S. J., Mun, M. S., et al. (2005). Experimental and numerical studies of muscular activations of bracing occupant. International Harmonized Research Activities.

Ciarlet, P. G. (1990). Handbook of numerical analysis (Vol. 12).

Cohen, Z. A., McCarthy, D. M., Kwak, S. D., Legrand, P., Fogarasi, F., Ciaccio, E. J., et al. (1999). Knee cartilage topography, thickness, and contact areas from MRI: in-vitro calibration and in-vivo measurement. Osteoarthritis and Cartilage , 7, 95-109.

Collins, J. J. (1995). The redundant nature of locomotor optimization laws. Journal of Biomechanics , 28 (3), 251-267.

Cowin, S. C. (2001). Bone mechanics handbook (2nd ed.). Boca Raton, FL: CRC Press.

Cram, J. R., & Kasman, G. S. (1998). Introduction to surface electromyography. Gaithersburg, MD, USA: Aspen Publishers.

Crowninshield, R. D. (1978). Use of optimization techniques to preict muscle forces. Journal of Biomechanical Engineering , 100, 88-92.

Crowninshield, R. D., & Brand, R. A. (1981). A physiologically based criterion of muscle force prediction in locomotion. Journal of Biomechanics , 14, 793-801.

Dalstra, M., Huiskes, R., Odgaard, A., & van Erning, L. (1993). Mechanical and textural properties of pelvic trabecular bone. Journal of Biomechanics , 26 (4), 523-535.

Dejak, B., Mlotkowski, A., & Romanowicz, M. (2007). Strength estimation of different design of ceramic inlays and onlays in molars based on the Tsai-Wu failure criterion. Journal of Prosthetic Dentistry , 98 (2), 89-100.

Delagi, E. F., Perotto, A., & Iazzetti, J. (1975). Anatomic guide for the electromyographer: the limbs. Springfield, IL, USA: Charles C Thomas.

Delp, S. L. (1990). Surgery simulation: a computer graphics system to analyze and design musculoskeletal reconstructions of the lower limb. Dissertation, Stanford University.

Donnelly, B. R., & Roberts, D. P. Comparison of cadaver and Hybrid III dummy response to axial impacts of the femur. Proceedings of the Thirty-First Stapp Car Crash Conference (pp. 105-116). Warrendale, PA: Society of Automotive Engineers.

Dul, J., Johnson, G. E., Shiavi, R., & Townsend, M. A. (1984). Muscular synergism-ii. A minimum-fatigue criterion for load sharing between synergistic muscles. Journal of Biomechanics , 17 (9), 675-684.

Faber, S. C., Eckstein, F., Lukasz, S., Muhlbauer, R., Hohe, J., & Englmeier, K. H. (2001). Gender difference in knee joint cartilage thickness, volume and articular surface areas: assessment with quantitative here-dimensional MR imaging. Skeletal Radiology , 30 (3), 144-150.

Ferguson, S. J., Bryant, J. T., Ganz, R., & Ito, K. (2000). The influence of the acetabular labrum on hip joint cartilage consolidation: a poroelastic finite element model. Journal of Biomechanics , 33, 953-960.

Forster, E., Simon, U., Augat, P., & Claes, L. (2004). Extension of a state-of-the-art optimization criterion to predict co-contraction. Journal of Biomechanics , 37, 577-581.

Friederich, J. A., & Brand, R. A. (1990). Muscle fiber architecture in the human lower limb. Journal of Biomechanics , 23, 91-95.

Funk, J. R., Crandall, J. R., Tourret, L. J., MacMahon, C. B., Bass, C. R., Patrie, J. T., et al. (2002). The axial injury tolerance of the human foot/ankle complex and the effect of achilles tension. Journal of Biomechanical Engineering , 124, 705-757.

Glitsch, U., & Baumann, W. (1997). The three-dimensional determination o internal loads in the lower extremity. Journal of Biomechanics , 30, 1123-1131.

Goldstein, S. A. (1987). The mechanical properties of trabecular bone: dependence on anatomic location and function. Journal of Biomechanics , 20, 1055-1332.

Gomberg, B. R., Saha, P. K., & Wehrli, F. W. (2005). Method for cortical bone structural analysis from magnetic resonance images. Academic Radiology , 12 (10), 1320-1332.

Gomez-Benito, M. J., Garcia-Aznar, J. M., & Doblare, M. (2005). Finite element prediction of proximal femoral fracture patterns under different loads. Journal of Biomechanical Engineering , 127, 9-14.

Hagg, G. M., Luttmann, A., & Jager, M. (2000). Methodologies for evaluating electromyographic field data in ergonomics. Journal of Electromyography and Kinesiology , 10, 301-312.

Hardin, E. C., Su, A., & van den Bogert, A. J. (2004). Foot and ankle forces during an automobile collision: the influence of muscles. Journal of Biomechanics , 37, 637-644.

Hayashi, S., Choi, H. Y., Levine, R. S., Yang, K. H., & King, A. I. (1996). Experimental and analytical study of knee fracture mechanisms in a frontal knee impact. Proceedings of the 40th Stapp Car Crash Conference. Society of Automotive Engineers.

Hof, A. (1984). EMG and muscle force: An introduction. Human Movement Science , 3, 119-153.

Hogler, W., Blimkie, C. J., Cowell, C. T., Kemp, A. F., Briody, J., Wiebe, P., et al. (2003). A comparison of bone geometry and cortical density at the mid-femur between prepuberty and young adulthood using magnetic resonance imaging. Bone , 33, 771-778.

Howard, J. D., & Enoka, R. M. (1991). Maximum bilateral contractions are modified by neurally mediated interlimb effecs. Journal of Applied Physiology , 70, 306-316.

Hudelmaier, M., Glaser, C., Hohe, J., Englmeier, K. H., Reiser, M., Putz, R., et al. (2001). Age-related changes in the morphology and deformational behavior of knee joint cartilage. Arthritis and Rheumatism , 44 (11), 2556-2561.

Hughes, R. E., & Chaffin, D. B. (1988). Conditions under which optimization models will not predict coactivation of antagonis muscles. 12th Meeting of the American Society of Biomechanics, (pp. 155-156). Urbana Champaign, IL.

Hughes, R. E., Bean, J. C., & Chaffin, D. B. (1995). Evaluating the effect of co-contraction in optimization models. Journal of Biomechanics , 28, 875-878.

Iwamoto, M., Miki, K., & Tanaka, E. (2005). Ankle skeletal injury predictions using anisotropic inelastic constitutive model of cortical bone taking into account damage evolution. Stapp Car Crash Journal , 49, 133-156.

Iwamoto, M., Tamura, A., Furusu, K., Chiharu, K., Miki, K., Hasegawa, J., et al. (2000). Development of a finite element model of the human lower extremity for analyses of automotive crash injuries. SAE Paper No. 2000-01-0621 .

Janssen, I., Heymsfield, S. B., Wang, Z., & Ross, R. (2000). Skeletal muscle mass and distribution in 468 men and women aged 18-88 yr. Journal of Applied Physiology , 89, 81-88.

Joyce, G. C., Rack, P. M., & Westbury, D. R. (1969). The mechanical properties of cat soleus muscle during controlled lengthening and shortening movements. Journal of Physiology , 204, 461-474.

Karlsson, S., & Gerdle, B. (2001). Mean frequency and signal amplitude of the surface EMG of the quadriceps muscles increase with increasing torque – a study using the continuous wavelet transform. Journal of Electromyography and Kinesiology , 11, 131-140.

Kennedy, E. A., Hurst, W. J., Stitzel, J. D., Cormier, J. M., Hansen, G. A., Smith, E. P., et al. (2004). Lateral and posterior dynamic bending of the mid-shaft femur: fracture risk curves for the adult population. Stapp Car Crash Journal , 48, 27-51.

Kim, Y. S., Choi, H. H., Cho, Y. N., Park, Y. J., Lee, J. B., Yang, K. H., et al. (2005). Numerical investigations of interactions between the knee-thigh-hip complex with vehicle interior structures. Stapp Car Crash Journal , 85-115.

Kitagawa, Y., Ichikawa, H., Pal, C., King, A. I., & Levine, R. S. (1998). Lower leg injuries caused by dynamic axial loading and muscle tensing. Proceedings to the 16th International Technical Conference on Experimental Safety Vehicles. II, pp. 1597-1607. Washington, DC: NHTSA.

Koh, T. J., Grabiner, M. D., & Clough, C. A. (1993). Bilateral deficit is larger for step than for ramp isometric contractions. Journal of Applied Physiology , 74, 1200-1205.

Komi, P. V., & Buskirk, E. (1970). Reproducibility of electromyographic measurements with inserted wire electrodes and surface electrodes. Electromyography , 10, 357-367.

Kuppa, S., & Fessahaie, O. (2003). An overview of knee-thigh-hip injuries in frontal crashes in the United States. 18th International Technical Conference on the Enhanced Safety of Vehicles. Nagoya.

Lee, J. B., & Yang, K. H. (2001). Development of a finite element model of he human abdomen. Stapp Car Crash Journal , 45, 79-100.

Leis, A. A., & Trapani, V. C. (2000). Atlas of electromyography. Oxford, NY, USA: Oxford University Press.

Leung, Y. C., Hue, B., Fayon, A., Tarriere, C., Harmon, H., Got, C., et al. (1983). Study of "knee-thigh-hip" protection criterion. Proceedings of the Twenty-Seven Stapp Car Crash Conference (pp. 351-364). Warrendale, PA: Society of Automotive Engineers.

Lindahl, O. (1976). Mechanical properties of dried defatted spongy bone. Acta Orthopaedica Scandinavia , 47, 11-19.

Looker, A. C., & Beck, T. J. (2004). Maternal history of osteoporosis and femur geometry. Calcified Tissue International , 75, 277-285.

Magnussen, R. A., Guilak, F., & Vail, T. P. (2005). Cartilage degeneration in post-collapse cases of osteonecrosis of the human femoral head: Altered mechanical properties in tension, compression, and shear. Journal of Orthopaedic Research , 23, 576-583.

Manning, P., Wallace, A., Owen, C., Roberts, A., Oakley, C., & Lowne, R. (1998). Dynamic response and injury mechanism in the human foot and ankle and an analysis of dummy biofidelity. Proceedings of the 16th International Technical Conference on the Enhanced Safety of Vehicles, (pp. 1960-1998). Windsor, Ontario.

McConville, J. T., Churchill, T. D., Kaleps, I., Clauser, C. E., & Cuzzi, J. (1980). Anthropometric relationships of body and body segment moments of inertia. Wright Patterson Air Force Base, Aerospace Medical Research Laboratorirs, OH.

Melvin, J. W., & Nusholtz, G. S. (1980). Tolerance and response of the knee-femur-pelvis complex to axial impacts-Impact sled tests. The University of Michigan, Highway Safety Research Institute, Ann Arbor, MI.

Melvin, J. W., & Stalnaker, R. L. (1976). Tolerance and response of the knee-femur-pelvis complex to axial impact. The University of Michigan, Highway Safety Research Institute, Ann Arbor, MI.

Melvin, J. W., Stalnaker, R. L., Alem, N. M., Benson, J. B., & Mohan, D. (1975). Impact response and tolerance of the lower extremities. Proceedings of the Nineteenth Stapp Car Crash Conference (pp. 543-559). Warrendale, PA: Society of Automotive Engineers.

Meyer, E. G., & Haut, R. C. (2003). The effect of impact angle on knee tolerance to rigid impacts. Stapp Car Crash Journal , 47, 1-9.

National Highway Traffic Safety Administration (NHTSA) (2008). CFR 49, Part 571.208: Federal Motor Vehicle Safety Standard 208. National Highway Traffic Safety Administration, Washington, DC.

Oi, N., & Pandy, M. G. (2004). Variation of neck muscle strength along the human cervical spine. Stapp Car Crash Journal , 48, 397-417.

Partick, L. M., Kroell, C. K., & Mertz, H. M. (1965). Forces on the human body in simulated crashes. Proceeding of the Ninth Stapp Car Crash Conference (pp. 237-260). Warrendale, PA: Society of Automotive Engineers.

Partick, L. M., Mertz, H. M., & Kroell, C. K. (1967). Cadaver knee, chest, and head impact loads. Proceedings of the Eleventh Stapp Car Crash Conference (pp. 168-182). Warrendale, PA: Society of Automotove Engineering.

Patriarco, A. G., Mann, R. W., Simon, S. R., & Mansour, J. M. (1981). An evaluation of the approaches of optimization models in the prediction of muscle forces during human gait. Journal of Biomechanics , 14, 513-525.

Peacock, M., Liu, G., Carey, M., Ambrosius, W., Turner, C. H., Hui, S., et al. (1998). Bone mass and structure at the hip in men and women over the age of 60 years. Osteoporosis International , 8, 231-239.

Pedersen, D. R., Brand, R. A., Cheng, C. K., & Arora, J. S. (1987). Direct comparison of muscle force predictions using linear and non-linear programming. Journal of Biomechanical Engineering , 109, 192-199.

Powell, W. R., Advani, S. H., Clark, R. N., Ojala, S. J., & Holt, D. J. (1974). Investigation of Femur Response to Longitudinal Impact. Proceedings of the Eighteenth Stapp Car Crash Conference (pp. 539-556). Warrendale, PA: Society of Automotive Engineers.

Powell, W. R., Ojala, S. J., Advani, S. H., & Martin, R. B. (1975). Cadaver femur responses to longitudinal impacts. Proceedings of the Nineteenth Stapp Car Crash Conference (pp. 561-579). Warrendale, PA: Society of Automotive Engineers.

Press, W. H., Teukolsky, S. A., Vettering, W. T., & Flannery, B. P. (2002). Numerical recipes in C++. Cambridge, NY, USA: Cambridge University Press.

Raikova, R. (1999). About weight factors in the non-linear objective functions used for solving indeterminate problems in biomechanics. Journal of Biomechanics , 32 (7), 689-694.

Rasmussen, J., Damsgaard, M., & Voigt, M. (2001). Muscle recruitment by the min/max criterion-a comparative numerical study. Journal of Biomechanics , 34 (3), 409-415.

Reed, M. P., Manary, M. A., & Schneider, L. W. (1999). Methods for measuring and representing automobile occupant posture. SAE.

Reynolds, H. M., Snow, C. C., & Young, J. (1981). Spatial geometry of the human pelvis. Federal Aviation Administration Memorandum .

Riggs, B. L., Melton, L. J., Robb, R. A., Camp, J. J., Atkinson, E. J., Peterson, J. M., et al. (2004). Population-based study of age and sex differences in bone volumetric density, size, geometry and structure at different skeletal sites. Journal of Bone and Mineral Research , 19, 1945-1953.

Robin, S. (2001). HUMOS: Human model for safety – a joint effort towards the development of refined human-like car occupant models. 17th International Technical Conference on the Enhanced Safety of Vehicles.

Rupp, J.D. & Flannagan, C.A. (2009) Development of new risk curves for the knee/distal amd hip for use in frontal impact. Report No. UMTRI-2009-08. University of Michigan Transportation Research Institute, Ann Arbor.

Rupp, J. D. (2006). Biomechanics of hip injuries in frontal motor-vehicle crashes. Ann Arbor: The University of Michigan.

Rupp, J. D., Miller, C. S., Reed, M. P., Madura, N. H., Klinich, K. D., & Schneider, L. W. (2008). Characterization of knee-thigh-hip response in frontal impact using biomechanical testing and computational simulations. Stapp Car Crash Journal , 52, 421-474.

Rupp, J. D., Miller, C. S., Reed, M. P., Mandura, N. H., Ritchie, N. L., & Schneider, L. W. (2007). Characterization of knee impacts in frontal crashes. Proceedings of the 20th International Technical Conference on Experimental Safety Vehicles.

Rupp, J. D., Reed, M. P., Jeffreys, T. J., & Schneider, L. W. (2003). Effects of hip posture on the frontal impact tolerance of the human hip joint. Stapp Car Crash Journal , 47, 21-33.

Rupp, J. D., Reed, M. P., Van Ee, C. A., Kuppa, S., Wang, S. C., Goulet, J. A., et al. (2002). The tolerance of the human hip to dynamic knee loading. Stapp Car Crash Journal , 46, 211-228.

Schantz, P. G., Moritani, T., Karlson, E., Johansson, E., & Lundh, A. (1989). Maximal voluntary force of bilateral and unilateral leg extension. Acta Physiologica Scandinavica , 136, 185-192.

Schneider, L. W., Robbins, D. H., Pflug, M. A., & Snyder, R. G. (1983). Anthropometry of motor vehicle occupants, Vol. 2. National Highway Traffic Safety Administration, Washington, DC.

Schuster, P. J., Chou, C. C., Prasad, P., & Jayaraman, G. (2000). Development and validation of a pedestrian lower limb non-linear 3-D finite element model. Stapp Car Crash Journal , 44, 315-334.

Shah, C. S., Lee, J. B., Hardy, W. N., & Yang, K. H. (2004). A partially validated finite element whole-body human model for organ level injury prediction. Proceedings of the 2004 ASME International Mechanical Engineering Congress. Detroit, MI.

Shah, C. S., Yang, K. H., Hardy, W., Wang, H. K., & King, A. I. (2001). Development of computer model to predict aortic rupture due to impact loading. Stapp Car Crash Journal , 45, 161-182.

Snedeker, J. G., Muser, M. H., & Walz, F. H. (2003). Assessment of pelvis and upper leg injur risk in car-pedestrian collisions: comparison of accident statistics, impactor tests and a human body finite element model. 47, 437-457.

Takahashi, Y., Kikuchi, Y., Konosu, Y., & Ishikawa, H. (2000). Development and validation of the finite element model for the human lower limb of pedestrians. Stapp Car Crash Journal , 44, 335-355.

Tsai, S. W., & Wu, E. M. (1971). A general theory of strength for anisotropic materials. Journal of Composite Materials , 5, 58-80.

Untaroiu, C., Kurosh, D., Crandall, J., Deng, B., & Wang, J. T. (2005). A finite element model of the lower limb for simulating pedestrian impacts. 49, 157-181.

Van Ee, C. A., Nightingale, R. W., Camacho, D. L., Chancey, V. C., Knaub, K. E., Sun, E. A., et al. (2000). Tensile properties of the human muscular and ligamentous cervical spine. Stapp Car Crash Journal , 44, 85-102.

van Soest, A. J., Roebroeck, M. E., Bobbert, M. E., Huijing, P. A., & van Ingen Schenau, G. J. (1985). A comparison of one-legged and two-legged countermovement jumps. Medicine and Science in Sports and Exercise , 17, 635-639.

Vandervoort, A. A., Sale, D. G., & Moroz, J. (1984). Comparison of motor unit activity during unilateral and bilateral leg extension. Journal of Applied Physiology , 56, 46-51.

Viano, D. C., & Stalnaker, R. L. (1980). Mechanisms of femoral fracture. Journal of Biomechanics , 13, 701-715.

Vint, P. F., & Hinrichs, R. N. (1996). Differences between one-foot and two-foot vertical jump performances. Journal of Applied Biomechanics , 12, 338-358.

Wickiewicz, T. L., Roy, R. R., Powell, P. L., & Edgerton, V. R. (1983). Muscle architecture of the human lower limb. Clinical Orthopaedics and Related Research , 179, 275-283.

Wyler, A., Bousson, V., Bergot, C., Polivka, M., Leveque, E., Vicaut, E., et al. (2007). Hyaline cartilage thickness in radiographically normal cadaveric hips: comparison of spiral CT arthrographic and macroscopic measurements. Radiology , 242, 441-449.

Yamada, M. Y. (1970). Strength of biological materials. Baltimore: Williams & Wilkins Co.

Yaszemski, M. Y., Payne, R. G., Hayes, W. C., Langer, R., & Mikos, A. G. (1996). Evolution of bone transplantation: molecular, cellular and tissue strategies to engineer human bone. Biomaterials , 17, 175-185.